

UNIVERSITY OF OKLAHOMA

GRADUATE COLLEGE

LONG TERM EXPERIMENTAL INVESTIGATION FOR LEAKAGE AND PERMEABILITY  
OF THE CEMENT-CASING MICROANNULUS

A DISSERTATION

SUBMITTED TO THE GRADUATE FACULTY

in partial fulfillment of the requirements for the

Degree of

DOCTOR OF PHILOSOPHY

By

HUSSAIN AL RAMIS

Norman, Oklahoma

2021

LONG TERM EXPERIMENTAL INVESTIGATION FOR LEAKAGE AND PERMEABILITY  
OF THE CEMENT-CASING MICROANNULUS

A DISSERTATION APPROVED FOR THE  
MEWBOURNE SCHOOL OF PETROLEUM AND GEOLOGICAL ENGINEERING

BY THE COMMITTEE CONSISTING OF

Dr. Catalin Teodoriu (Chair)

Dr. Jeffrey Harwell

Dr. Mahmood Amani

Dr. Mashhad Fahs

Dr. Ramadan Ahmed

Dr. Saeed Salehi

© Copyright by HUSSAIN AL RAMIS 2021

All Rights Reserved.

To my lovely wife and daughter

## Acknowledgements

Countless people have made my journey towards this moment of completing my Ph.D. a very special one.

The extent of the supports and mentorship that Dr. Catalin Teodoriu has provided me and my gratitude for it cannot be expressed in words. His knowledge, experience, and passion for our shared subject is shaping the present and the future of the field. I would also like to thank each and every member of my committee—I am forever in their debt.

I would like to acknowledge the support of my teammates in our research group, especially Dr. Opeyemi Bello and my colleagues at the Well Integrity Lab.

I would like to acknowledge the ever-present support system created by my friends and colleagues who have provided me with so much technical advice, particularly Mr. Hassan Al Hussain, Dr. Hussain Al Bahrani, and Dr. Murtada Al-Jawad. I also extend my heartfelt thanks to all my friends in Norman who have become a family away from my family.

I am deeply grateful to my family: My mother, who has always kept me in her prayers and encouraged me through tough times; my role model, my father, who supported me without me ever having to ask him; my sister, whose heart is big enough to care for an entire village and who has always believed in me; and my two brothers whom I hope will be proud of me for this work.

Finally, I would like to thank the beacon that lit my way even at times when light did not seem to exist: My little family, my little Rihana, and my dear wife, Zahrah—the essence of joy and my support from the beginning, guiding us to the brightest shared future.

# Table of Contents

Acknowledgements .....	v
Table of Contents .....	vi
List of Figures .....	xii
List of Tables .....	xix
Abstract .....	xxii
Chapter 1: Introduction .....	1
1.1 Background .....	1
1.2 Motivation and Problem Statement .....	7
1.3 Research Objective .....	8
1.4 Research Scope .....	9
1.5 Dissertation Outline .....	9
Chapter 2: Barriers in Plug and Abandonment .....	11
2.1 Well Integrity Basics .....	11
2.2 Well Barriers .....	11
2.2.1 Well Barrier Definition .....	12
2.3 Level of Abandonment .....	13
2.4 Types of Barriers .....	18

2.5 Country-Based Barrier Requirements .....	19
2.6 Gas Leakage Evaluation .....	20
Chapter 3: Cement Overview .....	22
3.1 Cement Purpose.....	22
3.2 Cement Composition .....	22
3.3 Cement in Oil and Gas Operations.....	26
3.3.1 Cement Plug .....	32
3.3.2 Cement Plug Usage.....	34
Chapter 4: Background on Cement Experimental Research .....	36
4.1 Need for Further Experimental Work.....	36
4.2 Experimental Literature Review .....	37
4.3 Limitations of Research on the Microannulus .....	42
Chapter 5: Experimental Procedure and Methodology.....	44
5.1 Introduction.....	44
5.2 Experimental Setup and Procedures.....	46
5.2.1 Cement properties.....	46
5.2.2 Steel Properties .....	46
5.2.3 Cement Mixing and Curing Procedures.....	47

5.2.4 Cement Strength Measurements .....	49
5.2.5 Pressure Decline Measurement .....	51
5.3 Data Process for Lab Experiments .....	57
Chapter 6: Results and Analysis .....	58
6.1 Introduction.....	58
6.2 Data and Analysis.....	59
6.2.1 Pressure Decline Analysis for Various Lengths .....	59
6.3 System Permeability Calculation .....	64
6.3.1 Darcy’s Law .....	64
6.3.1.5.1 Klingenberg Effect.....	68
6.3.2 Brace Method (Pulse Decay).....	72
6.4 Selected System Permeability Method .....	74
6.4.1 Sample Length Variation Effect on System Permeability .....	78
6.4.2 Sample Age Variation Effect on Cement System Permeability.....	79
6.5 Cement Gap and Behavior .....	82
6.5.1 Sample Length Variation Effect on the Microannulus .....	87
6.5.2 Measured Gap Versus Literature Equation .....	89
6.6 System Permeability Relationship with the Microannulus Measured.....	90

6.7 Effect of Application of Pressure Before Complete Hardening .....	93
6.8 Non-Wetted Cement Effect on Gap (Shrinkage) .....	95
6.9 Statistical Analysis .....	98
6.9.1 General Data Statistics .....	98
6.9.2 Statistical Prediction of the Gap for the 6-inch Pipe .....	101
6.9.3 Statistical Prediction of the Gap for All specimens.....	102
Chapter 7: Numerical Validation .....	104
7.1 Decline Curve Analysis Basics .....	104
7.1.1 Model Equations .....	105
7.1.2 Modeling Construction .....	107
7.1.3 Modeling Results .....	111
Chapter 8: Summary and Conclusions .....	120
8.1 Summary .....	120
8.2 Recommendations .....	122
8.3 Conclusions.....	123
8.4 Future Work .....	125
Nomenclature.....	126
References .....	129

Appendix A: Cement Field Evaluation .....	147
A.1 Barrier Evaluation Review .....	147
A. 1.1 Acoustic Logging .....	147
A.1.2 Spectral Noise Logging (SNL) .....	148
A.1.3 Annulus Verification Tool (AVT) .....	149
A.1.4 Temperature Logging .....	149
A.1.5 Hydraulic Pressure Testing .....	150
Appendix B: Cement Bond Overview .....	151
B.1 Introduction .....	151
B.2 Bonding .....	152
B.3 Cement Failure .....	154
B.3.1 Tensile Strength .....	156
B.3.2 Mechanical Property Failure .....	156
B.3.3 Radial and Hoop Stress Failure .....	157
B.3.4 Shrinkage .....	157
B.3.5 Shear Failure .....	158
B.3.5 Cyclic Pressure and Temperature Variation Failure .....	159
B.3.6 Hydraulic Bond Failure .....	160

Appendix C: Numerical Modeling of Cement Debonding ..... 161

    C.1 Introduction ..... 161

    C.2 Model Assumption..... 161

    C.3 Model Construction ..... 162

    C.4 Model Results ..... 166

## List of Figures

Fig. 1-1—Global wells drilled 2019-2025 (ENERGY 2021 after Rystad Energy).....	1
Fig. 1-2—Estimated abandonment cost and other operations in the North Sea (OGUK 2020).....	5
Fig. 1-3—Plug and abandonment pressure and regulatory monitoring framework (Ruivo and Morooka 2001). .....	6
Fig. 3-1—Cement hydration and bond initiation a) SEM of dry cement grain b-d) hydration at t=1 hr, 3hr, 4hr of time respectively at the different magnitude top and bottom (Varshney et al. 2017).....	23
Fig. 3-2—Cement composition: raw materials (Aïtcin 2016a). .....	25
Fig. 3-3—Measurement of the hydration level for different categories of class H cement; H-P on the left is premium class H ( C <sub>3</sub> S composition 47.9 by mass) and H-I on the right is regular standard class H ( C <sub>3</sub> S composition 66.5-70.3 by mass) by mass( Xueyu P.et al. 2013). .....	26
Fig. 3-4—Casing design sketch. ....	28
Fig. 3-5—Cement pumping unit with well sketch (IADC 2015). .....	31
Fig. 3-6—Sketch of a cement plug. ....	32
Fig. 4-1—Wellbore system leak pathways (Gasda et al. 2004). .....	36

Fig. 4-2—Microannulus width equivalent to permeability (Boukhelifa et al. 2005). .....	38
Fig. 4-3— Scan of the void before and after the thermal cycle (Albawi et al. 2014).....	39
Fig. 5-1—Flow chart representing the research methodology. ....	45
Fig. 5-2—Measuring cup for cement and water. ....	47
Fig. 5-3—Cement mixer.....	48
Fig. 5-4—Cement molds with cement. ....	48
Fig. 5-5—Ultrasonic measurement at the center of the cement cube. ....	49
Fig. 5-6—Cement cube crushing. ....	50
Fig. 5-7—UCS data trend for class H cement tested. ....	50
Fig. 5-8—Specimen before testing. ....	51
Fig. 5-9—Upstream setup for the experiment. ....	52
Fig. 5-10—Hydraulic (pneumatic) cement casing permeability setup. ....	53
Fig. 5-11—Upstream and downstream experiment sketch. ....	53
Fig. 5-12—Control temperature bath for the experiment.....	53

Fig. 5-13—Specimen cut into 1-inch section .....	54
Fig. 5-14—Specimen prepared for mechanical cutting. ....	54
Fig. 5-15—Specimen 1-inch × 1-inch after polishing. ....	55
Fig. 5-16—Angular positions for the microscopic measurement.....	55
Fig. 5-17—High-resolution optical microscope. ....	56
Fig. 5-18—Microscope attached to a high-resolution camera.....	56
Fig. 5-19—Microscopic sample gap measure (20 micron-scale).....	56
Fig. 5-20—Summarizes the data journey across research steps.....	57
Fig. 6-1—Pressure behavior decline vs time for 6-inch specimen at (1, 2, 3, and 9 months) cement age (5% error).....	60
Fig. 6-2—Pressure behavior decline with time for 9-inch pipe at 1- and 2-month cement age (5% error).....	61
Fig. 6-3—Pressure behavior decline with time for 4-inch specimen at 1- and 2-month cement age (5% error). ....	62
Fig. 6-4—Pressure behavior decline with time for 4-, 6-, and 9-inch-length specimens at 1- month age. ....	63

Fig. 6-5—Pressure behavior decline with time for 4-, 6-, and 9-inch-length specimens at 2-month age. ....63

Fig. 6-6—Darcy’s permeability correction (Klingenberg).....69

Fig. 6-7—Darcy’s permeability correction (Forchheimer’s) ( $m^2$ ).....71

Fig. 6-8—Darcy’s permeability correction (Forchheimer’s) steady state ( $m^2$ ).....72

Fig. 6-9—Pulse decay (Brace method) pressure with time. ....74

Fig. 6-11—System permeability calculations for 4-, 6-, and 9-inch- specimen at 1- and 2-month cement age. ....77

Fig. 6-10—Permeability calculations for 4-, 6-, and 9-inch-length specimen at 1-month cement age. ....77

Fig. 6-12—Comparison of system permeability with two methods for 6- and 9-inch-length pipes. ....79

Fig. 6-13—Comparison of system permeability with two methods at 1- and 2-month cement age. ....80

Fig. 6-14—Comparison of system permeability at one- and two-months’ age and length of 4, 6, and 9 inches. ....80

Fig. 6-15— Specimen6-inch pipe system permeability calculation at different cement ages (1, 2, and 9 months). .....81

Fig. 6-16—Cement-casing gap (20-micrometer scale) (Al Ramis et al. 2020).....82

Fig. 6-17—Gap measurement across the specimen. ....83

Fig. 6-18—Pipe length of 4-inch and 6-inch gap measurement across the points of measurement. ....84

Fig. 6-19—Sketch of the points of measurement. ....85

Fig. 6-20—Gap representation of 0-20 microns. ....87

Fig. 6-21—Effective length of gas flow across the sample.....88

Fig. 6-22—Comparison of pipe length (4-, 6-, and 9-inches) across system permeability and gap. ....91

Fig. 6-23—Comparison between the measured gap and the calculated gap for 4-, 6-, and 9-inch-length pipes at 1-month cement age.....92

Fig. 6-24—System permeability calculated with the gap measured for 4-, 6-, and 9-inch-length pipes. ....93

Fig. 6-25—Bubbles appear in the cement surface after cured if tested before hardening. ....94

Fig. 6-26—System permeability increment for cement is tested while curing with gap measurement.....	94
Fig. 6-27—Gap measured with system permeability values calculated. ....	95
Fig. 6-28—Plot of gap increase after dry-out (2 months-1 year) .....	97
Fig. 6-29—Gap distribution for all samples tested.....	99
Fig. 6-30—Gap count (less than 30 micrometers) for all the pipes with age and length.....	100
Fig. 7-1—Initial conditions for Saphir software.....	110
Fig. 7-2 —Properties for the initial conditions in Saphir software.....	110
Fig. 7-3—Drawdown pressure for the 6-inch-length pipe at 2-month (wet) cement age. ....	112
Fig. 7-4—Pressure derivative of the 6-inch-length pipe at 2-month cement age.....	113
Fig. 7-5—Derivative match for the 6-inch-length pipe at 2-month cement age. ....	114
Fig. 7-6—Derivative match for the 6-inch-length pipe at 2-month cement age with different skin factors.....	115
Fig. 7-7—Permeability match for the 6-inch-length pipe at 2-month cement age.....	115
Fig. 7-8—Permeability fitted for the 6-inch-length pipe at 2-month cement age. ....	116

Fig. 7-9—Drawdown pressure for 6-inch-length pipe at 1-month (dry) cement age. .... 117

Fig. 7-10—Derivative pressure of the 9-inch-length pipe at 2-month cement age. .... 118

Fig. 7-11—Derivative match wellbore storage fitting of the 9-inch-length pipe at 2-month  
cement age. .... 118

Fig. 7-12—Permeability fitted for the 9-inch-length pipe at 2-month cement age with wellbore  
storage. .... 119

## List of Tables

Table 2-1—Permanent well abandonment as specified by the Bureau of Safety and Environmental Enforcement (BSEE) (30 CFR) .....	15
Table 2-2—Reservoir plugging requirements (after IOGP 2017). .....	20
Table 2-3 —Allowable leakage rate with different international entities. ....	21
Table 3-1—Casing types and purposes.....	28
Table 3-2—Cement types and their usage (API 10 A). ....	30
Table 5-1—Class H cement composition (Central Plain Cement Company). ....	46
Table 5-2—Steel properties used in the experiments .....	46
Table 6-1—Experimental data initial conditions .....	59
Table 6-2—Summary of system permeability calculations by different methods for the specimens. ....	75
Table 6-3—Pulse decay system permeability method (research-based method). ....	75
Table 6-4—Comparison of 6- and 9-inch-specimen at one- and two-months cement age.....	78

Table 6-5—Comparison of system permeability (md) at one- and two-month cement age. ....	81
Table 6-6—Summary of the gap measure across the specimen cut. ....	85
Table 6-7— Effect length range calculated. ....	88
Table 6-8—Summary of the gap calculated by flow rate (Darcy, ave. pressure, ave. density). ...	90
Table 6-9 Summarize some points of measurement for 6-inch-length pipe two months (wet) and one year (dry).....	96
Table 6-10—Summary of the statistical gap results. ....	99
Table 6-11—Confidence intervals of all gaps. ....	100
Table 6-12—Pearson correlation for all gaps measured. ....	101
Table 6-13—Mean confidence interval for all pipes tested (4-, 6-inch, and 9-inch length). ....	101
Table 6-14—Effect of pipe length on the cement gap for the 6-inch-length pipe.....	102
Table 6-15—Effect of pipe length on the cement gap for the 6-inch-length pipe.....	102
Table 6-16—Dependency of length, cement age, and system permeability on the gap. ....	103
Table 6-17—Predicted mean value of gap across all pipes with the selected pipe. ....	103

Table C-1—List of mechanical properties used for modeling cement behavior (Bosma et al. 1999; James and Boukhelifa 2008).....163

## **Abstract**

The oil and gas industry is the primary provider of energy globally. Energy extraction from wells takes place through several stages, such as exploration, drilling and production, and then plugging and abandonment. The ISO, API, and NORSOK standards require oil and gas wells to be isolated such that any fluid leakage or pressure does not reach the surface. This isolation is achieved by using well barriers composed principally of cement plugs.

The integrity of the cement used to isolate the wells, however, is repeatedly compromised by preventable gas leaks. In the long term, this unwanted flow constitutes a safety hazard and is detrimental to the environment.

The objective of the present quantitative research study is to experimentally identify and understand the fluid flow path that causes leakage in the cement. This study is conducted in two stages. First, the system permeability of internally cemented pipe (specimen) is determined using pressure decline experiments. The specimens were subjected to an air pressure of 50 psig at the inlet and atmospheric pressure at the outlet. After closing the air supply valve, the inlet pressure was measured and recorded as a function of time. System permeability is calculated using various estimation methodologies, including the pulse decay method. Second, the data collected are used to understand the behavior and direction of the microannulus. A new method is developed to measure the gap between cement and casing. This technique visually measures the gap (microannulus) and relates the measurements to the flow rate through the specimen. The main test variables were the hydration time and specimen length. The results show that system permeability is more affected by hydration time than the specimen length. Thus, cement age is more indicative of the gap size than cement-pipe contact length.

# Chapter 1: Introduction

## 1.1 Background

Energy consumption both in the US and internationally continues to increase as the population grows and industrialization advances globally. Further, due to the lockdowns in many countries to slow the spread of COVID-19, 2020 turned out to be a volatile year in the oil and gas industry in terms of energy consumption figures and industrial activities worldwide.

According to Rystad Energy (2021), the number of wells drilled worldwide last year was very low as compared to the number for 2019. Drilling, though is expected to recover over the next two years (Fig. 1-1).

Jul 14th, 2020

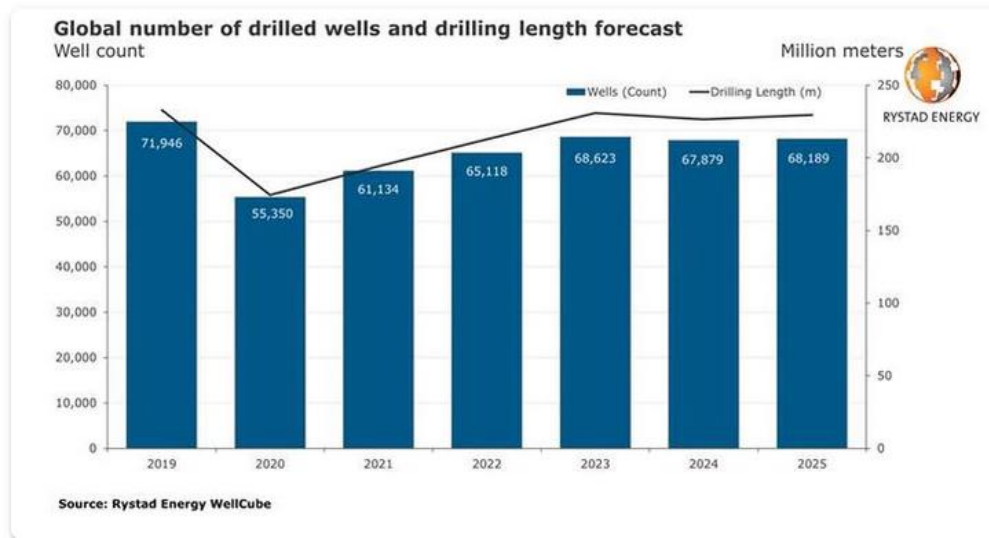


Fig. 1-1—Global wells drilled 2019-2025 (ENERGY 2021 after Rystad Energy).

Also, even as interest in renewable energy increases, the petroleum industry will remain the most economically viable producer of and thus the primary source of energy in coming years.

Petroleum (oil and gas) discovery occurs through a specific kind of evaluation and management. The first step involves a feasibility study in which the topography of the area with potential hydrocarbon is researched. In this critical exploration step, numerous processes are initiated and completed, including a seismic survey, rock sampling, and formation lithology building.

In the exploration stage, a lot of information is gathered with the overarching goal of fully assessing the location; therefore, considerable investment and justification for proceeding are needed from the company's senior management. Geological data and any nearby fields are subjected to a comprehensive investigation before a decision to drill is taken. Significant costs are associated with extensive logs for most of the formations, coring, and safety equipment for drilling across an area that may not turn to be productive.

Then the first well must be drilled as a basis for examining all the assumptions and results from the geologists and geophysicists scientists to design a drilling program. The drilling program is designed to target the deepest exploration formation and develop a contingency plan. During this stage, the unknown is vast, and the risk to reward is high. Therefore, multiple fundamentally important safety and well integrity issues should be examined and implemented to ensure safety and well integrity. Drilling requires intensive planning and logistical preparations to gain a complete and robust understanding of the well schematic. The logistic required fluid, casing, cement, and equipment needed to be forecasted before drilling. The rig selection is usually chosen based on the horsepower and pumping capacity needed. Then the evaluation and confirmation are studied while the well is drilled by taking several logs and cores across the formation (reservoir).

The company's management must then decide whether to drill more wells to build the reservoir boundaries. The wells are then completed and opened for production. In the appraisal stage, more wells are drilled (delineation wells) in order to gain the information needed to decide on the reservoir size and confirm production capability. It is also advisable to perform extensive well testing to confirm the hydrocarbon quality and establish whether it is economically viable to safely produce the discovered hydrocarbons.

After the exploration and appraisal stages, the management can decide to go forward to the development stage or start plug and abandonment for the drilled wells. If the decision to commence with plug and abandonment is taken, the company will lose its investment in the operational costs involved in the first two stages.

After all the data collected from the previous wells are analyzed in the development stage, a long-term plan for field production is developed. The number of wells to drill, the period over which the field will be economically profitable, and any enhanced oil recovery needed are all taken into account in establishing production and goals.

In the production stage, the well is completed with the last tubing (if not already installed), and the rate of production is decided with the ultimate control of the reservoir pressure. Additionally, any stimulation or artificial lift required should be planned at this stage. The reservoir engineer will be involved in deciding whether any enhanced recovery technique is necessary.

In the plug and abandonment stage, the field is considered partially or completely dead because of negative cash flow, the company's economic situation more generally, or because the well is not productive or has a severe leak. A decision at this stage should either suspend drilling at the well

or to abandon it for good. The plug and abandonment procedures require running plugs at the reservoir level with mechanical or hydraulic barriers. In offshore fields, decommissioning is required for wells by removing the well structure and cleaning the location.

The cost of decommissioning wells globally for the period of 2019 to 2029 has been calculated as approximately or even exceeding \$85 billion—a figure that has motivated researchers to develop new plugging materials and methodologies according to Oil & Gas Industry Association Limited UK (OGUK 2019, 2020). For example, Plug and Abandonment (P&A) operations in offshore Norway account for roughly 25% of the total spent on drilling and exploration wells (Khalifeh & Saasen 2013). Further, in 53% of all deepwater P&A operations, cement is used as the plugging material, which has raised more concerns about P&A failures in the past (Bogaerts et al.). The tendency of cement to shrink and crack is also a drawback for its use in the context of isolating wells (Rassenfoss et al. 2014). Barriers used in P&A operations should be designed to bear all the stress, including high temperatures and high pressure, to which it will be exposed. However, the fact remains that fractures or tectonic stress can cause barriers to fail (Khalifeh & Saasen 2013).

This risk of failure must be understood in the context of the significant costs associated with plug and abandonment, which must be executed following established industry standards and government regulations. In 2018, for example, the estimated cost of decommissioning and plugging wells in the North Sea was \$2.1–2.8 billion per year over five years (Fig. 1-2).

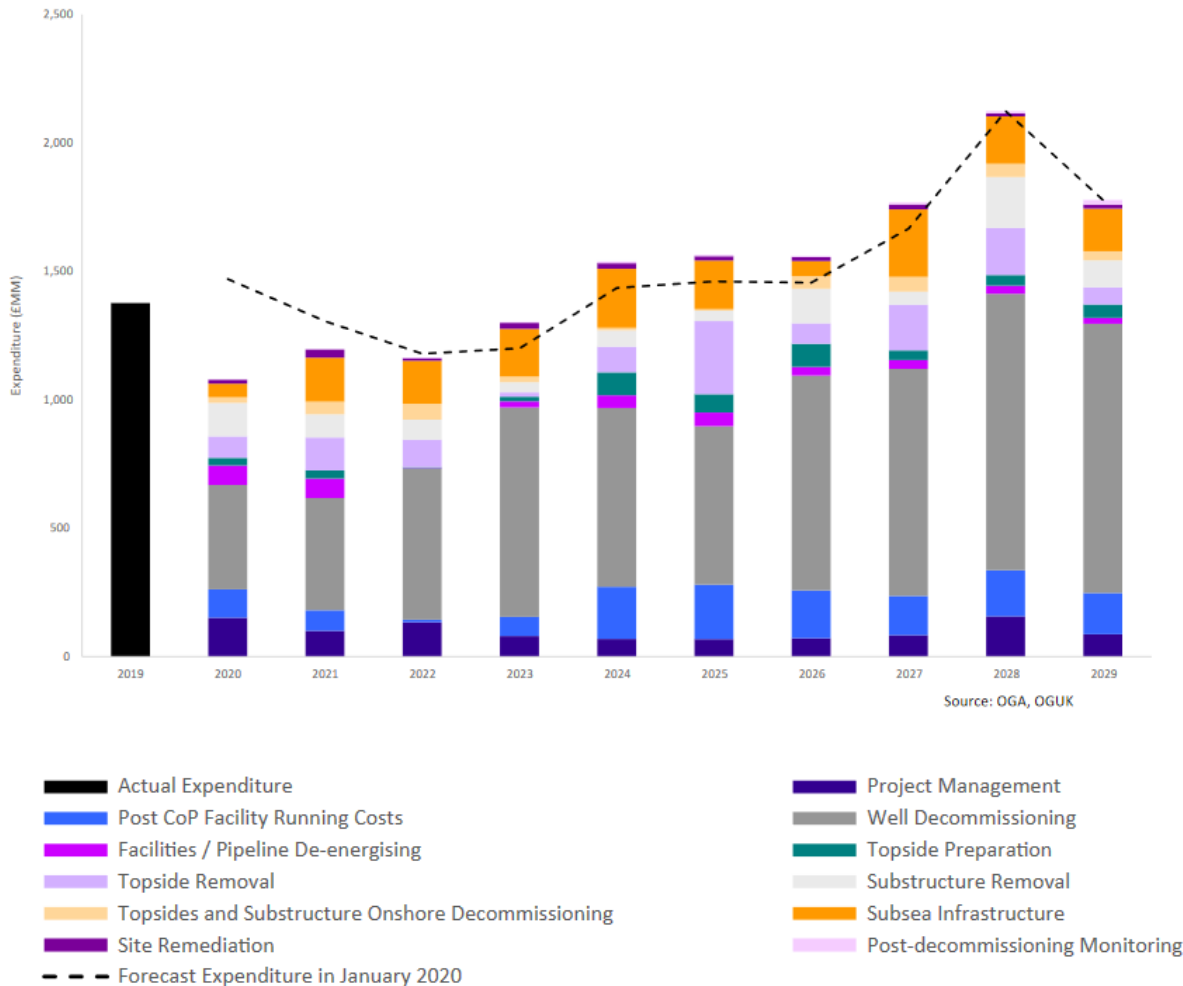


**Fig. 1-2—Estimated abandonment cost and other operations in the North Sea (OGUK 2020).**

Many factors must be reviewed and multiple measures implemented to ensure that plug and abandonment (the last stage in the lifecycle of all wells) is executed in the safest way possible in line with the regulatory point of view and industry standards. Plugging and abandonment should prevent freshwater table contamination and environmental pollution, which are both important considerations, and among the zones that must be secured is the high hydrocarbon pressure reservoir. Wellbore integrity failures usually occur at the loss-circulation zone and arise from unsuccessful cement job, insufficient hanger and packer seals, or damaged casing areas. These

well locations are all at high risk for well leakage, which can, in turn, result in a disaster if the cause is not addressed fully and promptly. Fig. 1-3 presents the plug and abandonment pressure and regulatory monitoring framework and its relationship with public perceptions of P&A.

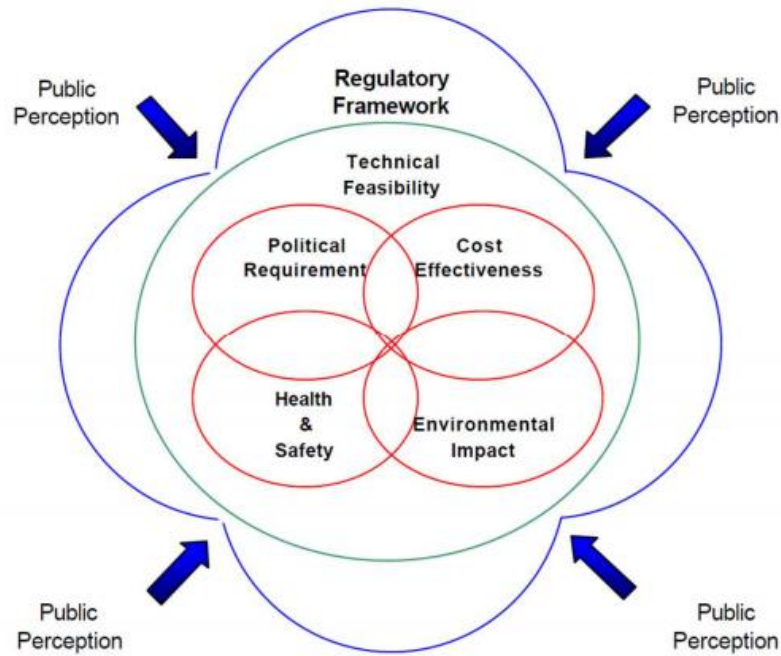


**Fig. 1-3—Plug and abandonment pressure and regulatory monitoring framework (Ruivo and Morooka 2001).**

Significant research literatures have developed in the last twenty years in response to the growing number of well integrity issues (Bauer et al. 2005; Kermani et al. 2006; Backes et al. 1999; Feng et al. 2015; Aas et al. 2016; Chen et al. 2017; Eijden et al. 2017; Khalifeh et al. 2017; De Andrade et al. 2019; and Gardner et al. 2019). One of the reasons for these issues is that more new wells have been drilled using fracturing technology to increase production from the tight zone, which is especially the case in shale reservoir production. Also, the rise of greenhouse sequestration (CO<sub>2</sub>) proposal projects has become an important area of research interest in relation to efforts to reduce

pollution. In terms of specific incidents that have brought research interest to this area, the Macondo oil spill—a failure of great magnitude—opened more eyes to the importance of well integrity and the regulations and standards meant to ensure it.

## **1.2 Motivation and Problem Statement**

The oil and gas industry have sought the best isolation methods between the formation drilled and the wellbore from an early stage in its development. Well integrity is a major factor in sustaining the cycle of production safely and efficiently. Cement has been used as the main material for isolation and barrier methods and as a cohesive and adhesive material between the formation and the casing. Any problems in the cement body or the cement contact could lead to well integrity issues resulting in significant negative consequences. Critical hydrocarbon reservoirs with high pressure or aquifer, if not well-secured during well operations could lead to environmental damage and even give rise to life-threatening conditions.

Cement shrinkage, pressure, and temperature variance account for some of the shortcomings and failures of wells. Gas migration, well leakage, mud filter, casing roughness, and water contamination are among the problems associated with cement failure during well operations.

In P&A and decommission operations, cement is a widely used material. Given the high cost of well plugging and the decommission process overall, it is necessary to use plug materials to withstand extreme conditions over the long term. Standard practice is to pump a cement plug that is 250–500 ft long into the casing to plug the well. These plugs usually have a minimum pressure across them, as the well is secured with a range of casing levels. However, the plugs will play a significant role as the last defense if the well becomes pressurized or the casing is damaged. The

bond strength between the cement and the casing is a complex subject requiring research from many angles if the chemical mechanical and environmental paths are fully understood.

Flow through the cement is suspected as a major factor in initiating flow leakage in the wellbore especially at the casing cement microannulus. However, the flow-through cement and the microannulus measurement is not well defined, especially with cement age. Although some researches do include studies with a focus on the microannulus (Goodwin and Crook 1992; Teodoriu et al. 2010; Kosinowski and Teodoriu 2012; Albawi et al. 2014; Li et al. 2016; Kjølner et al. 2016; and Al Ramadan et al. 2019), overall there is a lack of reliable and comparable data, which makes it difficult to integrate these considerations into well integrity approaches. Hence, the present study was undertaken to explore this area more strategically and comprehensively to develop more effective and safer methodologies.

### **1.3 Research Objective**

Understanding how leakage occurs across the cement casing is crucial to identifying the cement integrity problem. The cement–casing gap (microannulus) is believed to be the main cause of the leakage in cement. In that context, this research study began with developing an experimental setup to measure the hydraulic permeability (system permeability) of the cement–casing system and to identify its leakage behavior over time. Further, a new concept of measuring the cement–casing gap based on digital-image correlation is introduced, and a new way to identify and quantify the contact gap over time across the cement circumferences is proposed. The main objectives of this study are as follows:

- Develop a methodology to test cement sheath permeability (hydraulic bond)

- Introduce a new concept as a basis for measuring the cement–casing microannulus
- Quantify the microannulus gap for cement age over the long term
- Observe the microannulus gap for cement age over the long term
- Formulate and critique new cement permeability calculation methods
- Evaluate the effect of cement shrinkage on the microannulus

#### **1.4 Research Scope**

In this experimental study, an investigation of API neat cement class H system permeability with pipes of different lengths was conducted. Neat cement is used in order to create a reference data set for future tests that might investigate the effect of additives in cement slurries. The condition for the experiments was under room temperature and a maximum pressure of 50 psig. The microannulus gap was then measured to identify the gap -permeability relation with cement hydration time and specimen length.

#### **1.5 Dissertation Outline**

The study is presented as eight chapters, each with a specific focus as follows:

- Chapter 1: Introduces some basic concepts and a roadmap to hydrocarbon exploration and development
- Chapter 2: Defines barriers and describes leakage in plug and abandonment wells and provides an account of the standards and regulatory bodies in the oil and gas industry
- Chapter 3: Describes the use of cement in the oil and gas industry

- Chapter 4: Summarizes the literature on permeability and microannulus analysis, identifies the gap in and indicates the limitations of the research
- Chapter 5: Presents the experiment setup and methodology procedure used to test cement
- Chapter 6: Highlights the results from all the experiments, including the statistical results, and provides an account of their implications for the field
- Chapter 7: Describes the validation of the experimental results by using the numerical solution
- Chapter 8: Summarizes the research findings with suggestions for future research directions

## **Chapter 2: Barriers in Plug and Abandonment**

### **2.1 Well Integrity Basics**

The term “well integrity” in the drilling and production stage refers to a system of barriers consisting of fluid hydrostatic pressure, cement, casing, and mechanical plugs. Several tools and plugs have been developed to form protection and isolation (barriers) between the main wellbore and the unstable zone. Functioning as an envelope around the well, the barriers have the purpose of preventing any flow to the surface. In the plug and abandonment stage, barriers are categorized as mechanical or hydraulic that might divide into fluid or equipment to avoid pressure and fluid from reaching the surface. Thus, well integrity is not a consideration at the end of a well’s life. Instead, well integrity should be secured process during all well design, drilling, completion, and production stages and processes.

### **2.2 Well Barriers**

Most countries have a regulatory authority that sets standards to ensure the security and integrity of wells. The Norwegian body, NORSOK D010, for example, defines well integrity as the “application of technical, operational, and organizational solutions to reduce risk of uncontrolled release of formation fluid throughout the life cycle of a well” (NORSOK 2004). All hazards and potential leakage should be identified during well construction. In addition, according to NORSOK, the barriers must constitute an envelope of multiple barriers to be effective in preventing flow.

Mechanical (Sub Surface Safety Valve (SSSV), packer) and hydraulic plug (cement, fluid) is the broad term used to refer to the barriers. Also, “normally open” or “normally closed” is how mechanical barriers intended to be permanent are classified. For example, the blow-out preventer (BOP) and the Sub Surface Safety Valve (SSSV) are considered to be open, whereas cement, casing, and packer are deemed to be closed (permanently). Further, an additional classification referred to as an “independent barrier” is used for mechanical plugs such as the flapper valve and dependent-like casing (Khalifeh and Saasen 2020).

In most cases, companies develop their standards and procedures for plugging wells, such that governmental regulations may constitute only the minimum requirements for this purpose. Some of the organizations that set standards in this sphere are as follows:

- The International Organization for Standardization (ISO) is one of the largest standard-setting organizations with over 18,500 international standards.
- The American Petroleum Institute (API) is a national trade association representing a group of oil and gas companies with technical expertise.
- The American Society of Mechanical Engineers (ASME) is a scientific association for engineers.

### **2.2.1 Well Barrier Definition**

Barriers are defined as an object or process that prevents uncontrolled fluid flow (gas or liquid) between two zones (API Bull E3 2019; ISO 2013). A barrier element, however, is part of an entire system that prevents flow from taking place. A single element cannot avoid flow between zones;

instead, several components or plugs are used together to form a barrier (NORSOK 2012; ISO 2013; API Bull E3 2019).

The primary well barrier—which is almost always required in the case of P&A (ISO 2013)—is the first defense against any source of possible flow or abnormal pressure around the wellbore. An object specifically designed to prevent hazards (NORSOK 2012; ISO 2013), the primary barrier can consist of one or a combination of any of the following: cap rock, hydrostatic fluids, cement, casing, packers, completions, SSSV, and tree master valves.

The secondary barrier is the second line of defense in preventing flow (API RP 90 1993; NORSOK 2012; ISO 2013). It can consist of one or a combination of sealing formation, hydrostatic pressure, cement, blow-out preventers, wellhead valves, and tubing with seals or master valves (ISO 2013). The pressure and leakage path of flow prevention must have at least two well barriers present at any moment of the life of the well. These barriers are subjected to pressure tests and verification procedures in order to establish that their reliability.

The purpose of installing barriers as per API BULL E3 is to protect the groundwater by isolating reservoir zones, including hydrocarbon and water (API BULL E3 2019). Isolating the hydrocarbon reservoir, shallow gas, tar, shallow aquifers, and injection fluid zones is the purpose stated by the International Organization for Standardization (ISO 2017). In the US environmental requirements, Sulphur-containing zones are also included (30 CFR § 250, Subpart Q 2015).

### **2.3 Level of Abandonment**

NORSOK, the API, and the BSEE standards stated the objective for abandonment as that of sealing off inflow from the fluid-bearing formation to other zones, including to the surface and the

freshwater table. It is necessary to calculate the future load of the well to design a barrier that can withstand the conditions expected over time. Pressure tests are also needed for verification purposes as per ISO 16350-1 (ISO 2013).

There are two main levels of abandonment: temporary (well suspension) and permanent, which is executed when the intention is never to use the wells again. ISO 16350 defines well abandonment in general as preventing communications between zones through verified well barriers (ISO 2017). NORSOK agrees with that definition, although it specifies that the intention is never to enter the well again (NORSOK 2012). Similarly, in the API's definition, permanent abandonment refers to wells that will not have any utility in the future (API BULL E3 2019).

NORSOK requires the cross-section of the well to be entirely sealed, which includes sealing annuli and all holes. All sections, whether horizontal or vertical, must be isolated. Accordingly, the permanent barriers should be sealed in a way that accounts for conditions in the long term such that (i) no permeability and no shrinkage occurs, (ii) the barriers can bear the anticipated mechanical load with ductility, (iii) the barriers bond to steel, and (iv) the plug resists H<sub>2</sub>S, CO<sub>2</sub>, oil, and gas (NORSOK 2004). NORSOK 2012 includes an additional requirement whereby it is necessary to place the barrier in an impermeable formation while maintaining the (high) quality of the steel tubular and elastomers used (NORSOK 2012).

On the other hand, compared with NORSOK and other relevant standard-setting organizations, the Bureau of Safety and Environmental Enforcement (BSEE) is more concerned with environmental impact. The BSEE, therefore, requires permanent abandonment when a well is unsafe and poses a threat to the environment and/or its production level is not sufficient to be economically viable (30 CFR 250, 2015). Table 2-1 presents the BSEE's requirements for permanent well abandonment.

**Table 2-1—Permanent well abandonment as specified by the Bureau of Safety and Environmental Enforcement (BSEE) (30 CFR)**

If you have . . .	Then you must use . . .
<p>1. Zone in open hole,</p> <p>2. Open hole below casing,</p> <p>3. A perforated zone that is currently open and not previously squeezed or isolated,</p> <p>4. A casing stub where the stub end is within the casing,</p>	<p>Cement plug(s) set from at least 100 feet below the bottom to 100 feet above the top of oil, gas, and fresh-water zones to isolate fluids in the strata.</p> <p>(i) A cement plug, set by the displacement method, at least 100 feet above and below deepest casing shoe;</p> <p>(ii) A cement retainer with effective back-pressure control set 50 to 100 feet above the casing shoe, and a cement plug that extends at least 100 feet below the casing shoe and at least 50 feet above the retainer; or</p> <p>(iii) A bridge plug set 50 feet to 100 feet above the shoe with 50 feet of cement on the top of cement plug for expected or known lost circulation condition</p> <p>(i) A method to squeeze cement to all perforations;</p> <p>(ii) A cement plug set by displacement method at least 100 feet above to 100 feet below the perforated interval or down to the casing plug whichever is less or</p> <p>(iii) If the perforated zones are isolated from the hole below, you may use any of the plugs specified in paragraphs (a)(3)(iii)(A) through (E) of this section. Instead of those specified in paragraphs (a)(3)(i) and (a)(3)(ii) of this section.</p> <p>(A) A cement retainer with effective back-pressure control set 50 to 100 feet above the top of the perforated interval, and a cement plug that extend at least 100 feet below the bottom of the perforated interval with at least 50 feet of cement above the retainer;</p> <p>(B) A bridge plug set 50 to 100 feet above the top of the perforated interval and at least 50 feet of cement on top of the bridge plug;</p> <p>(C ) A cement plug at least 200 feet in length, set by the displacement method, with the bottom of the plug no more that 100 feet above the perforated interval;</p> <p>(D) A through-tubing basket plug set no more that 100 feet above the perforated interval</p>

<p>5. A casing stub where the stub end is below the casing,</p> <p>6. An annular space that communicated with open hole and extends to the mud line,</p> <p>7. A subsea well with unsealed annulus,</p> <p>8. A well with casing,</p> <p>9. Fluid left in the hole,</p> <p>10. Permafrost areas,</p>	<p>with at least 50 feet of cement on top of the basket plug; or  (E) A tubing plug set no more that 100 feet above the perforated interval topped with a sufficient volume of cement so as to extend at least 100 feet above the uppermost packer in the wellbore and at least 300 feet of cement in the casing annulus immediately above the packer.</p> <p>(i) A cement plug set at least 100 feet above and below the stub end;</p> <p>(ii) A cement retainer or bridge plug set at least 50 to 100 feet above the stub end with at least 50 feet of cement on top of the retainer or bridge plug; or  (iii) A cement plug at least 200 feet long with the bottom of the plug set no more that 100 feet above the stub end.</p> <p>A plug as specified in paragraph (a)(1) or (a)(2) of this section, as applicable.</p> <p>A cement plug at least 200 feet long set in the annular space. For a well completed above ocean surface, you must pressure test each casing annulus to verify isolation.</p> <p>A cutter to sever the casing, and you must set a stub plug as specified in paragraphs (a)(4) and (a)(5) of this section.</p> <p>A cement surface plug at least 150 feet long set in the smallest casing that extends to the mud line with top of the plug no more than 150 feet below the mud line.</p> <p>A fluid in the intervals between the plugs that is dense enough to exert a hydrostatic pressure that is greater than formation pressures in the intervals.</p> <p>(i) A fluid to be left in the hole that has a freezing point below the temperature of the</p>
--	--

<p>11. Removed the barriers required in §250.420(b)(3) for the well to be completed</p>	<p>permafrost, and a treatment to inhibit corrosion; and  (ii) Cement plugs designed to set before freezing and have a low heat of hydration.</p> <p>Two independent barriers, one of which must be a mechanical barrier, in the center wellbore as described in §250.420(b)(3) once the well is to be placed in a permanent or temporary abandonment...</p>
---	--

Temporary abandonment is sometimes divided into two types: well suspension and temporary abandonment. For suspension, the well is intended to be reused. The downhole is isolated from the surface using a Christmas tree and other barriers, which is achieved as monitoring on the well continues (NORSOK 2012). In Norwegian standards, temporary abandonment does not include the well control equipment. However, the ISO standards do not differentiate between suspension and temporary abandonment and require two barriers in high pressure cases and one in cases of normal pressure (ISO 2017).

In Norway, the barriers must have the capacity to withstand pressure and possible leakage for double the amount of time of the planned suspension. Depending on the duration of the abandonment, a mechanical barrier could be acceptable (NORSOK 2012). Furthermore, NORSOK recommends subjecting the barriers to quality checks over a period longer than a year. Therefore, the well design must afford sufficient access for monitoring to take place. Continuous pressure testing of the equipment must be performed for the tubing hangers, the tubing, the packers, the downhole safety valves, and the Christmas tree valves (NORSOK 2012).

More information on the temporary abandonment of wells can be found in 30 CFR 250, subpart Q (US-based entity). The requirements for the temporary abandonment of wells are the same as those for permanently abandoned wells with the exception that in the latter case, the wellhead must be

removed and the location must be cleared (30 CFR § 250, Subpart Q 2015). However, whether the abandonment is temporary or permanent, both a cement plug and a bridge plug are required (Al Ramis H. and Teodoriu 2020).

## 2.4 Types of Barriers

The API divides the barriers used for abandonment purposes as plugs for (API BULL E3 2019):

- (i) Any exposed casing/liner shoe
- (ii) Open hole
- (iii) Above perforated intervals in a cased hole
- (iv) Casing no longer exists
- (v) Liner top
- (vi) Above and below the water table
- (vii) Hydrocarbon-bearing zone or other potential flow
- (viii) Surface or mud line

The ISO standards for barriers, however, are written differently: “hardware barriers (equipment which is designed, installed, and verified), operational barriers (monitoring equipment, practices, and procedures); human barriers (competencies, training); and administrative controls (assignment of roles, resource provision, auditing, reviews)” (ISO 2013).

NORSOK specifies that the barriers must:

- (i) Withstand differential pressure
- (ii) Prevent leakage
- (iii) Enable maintenance and repairs
- (iv) Tolerate the long-term surrounding environment

- (v) Have a determinable location
- (vi) Be subjected to continuous plug integrity tests

Consist of a primary and secondary barrier that are not dependent on each other

## **2.5 Country-Based Barrier Requirements**

In 2017, the International Association of Oil and Gas Producers (IOGP) released a report in which the international regulations of 32 countries are discussed. Some of these countries, Algeria, Egypt, Azerbaijan, Oman, Qatar, Myanmar, and Venezuela, have very few or even no regulations focused on plugging and abandonment in offshore operations. Other countries, that is, Italy, Kazakhstan, Angola, Equatorial Guinea, and the Republic of Guinea, require only an advanced plan for P&A activities with no other specifications or even guidance offered. However, some countries have extensive regulations, including Norway, Malaysia, India, Indonesia, the United Arab Emirates (Abu Dhabi), and the United States (and the Gulf of Mexico as a separate entity). In contrast, others, such as New Zealand, Argentina, and Trinidad and Tobago, have some standards in place, although these are not extensive (Table 2-2).

**Table 2-2—Reservoir plugging requirements (after IOGP 2017).**

Country	Reservoir plugging
Norway	Two barriers: Primary: 50 m above and below the reservoir Secondary: 50 m inside the casing or 30 m behind the casing
Malaysia	30 m above and below perforations
India	30 m above or below hydrocarbon and water
United States	100 ft above and below the perforated zone
United Kingdom	100 ft of high-quality cement Two barriers for hydrocarbon, water, or over-pressured reservoir and one barrier for all other zones
Canada	Cement plugs 100 m in open hole and 30 m in cased hole
Brazil	30 m cement plug top of the liner
Trinidad and Tobago	30 m above and below hydrocarbon and fresh water
Denmark	Cement: At least 50 m above and below the reservoir
Netherland	Minimum 100 m cement or a combination of a mechanical plug and 50 m cement
Abu Dhabi (United Arab Emirates)	One or two 150 ft cement above or below the reservoir
Indonesia	100 ft above and below the reservoir
Thailand	100 ft from TD to 100 ft above hydrocarbon reservoir
Russia	Dependent on type of well
Argentina	Two cement plugs with a 30-m retainer and another 50 m, of which 30 m must be below the casing shoe
New Zealand	100 m cement with 50 m above and 50 m below the source of flow

## 2.6 Gas Leakage Evaluation

Table 2-3 shows several standards for leakage between barriers. Leakage is defined as an unintended movement of the fluid in the wellbore (ISO 2013).

**Table 2-3 —Allowable leakage rate with different international entities.**

International Entity	Leakage Rate	Source	Remark
International Organization for Standardization (ISO)	24l/hr liquid 900 scf/hr gas	ISO 2013	No uncontrolled leak to the surface
American Petroleum Institute (API)	SSSV: 10 cc/min and 5 ft <sup>3</sup> /min SSCSV: 400 cc/min and 15 scfm USV: 400 cc/min and 15 scfm High-pressure valve: 0.27 ml/min	API 14A 2001 API 6DSS 2014	Every 6 months
Code of Federal Regulations (CFR) US	SSSV: 200 cc/min liquid and 5 SCFM SSV & USV: zero	Buckingham 1999	
Norwegian Shelf's Competitive Position NORSOK	Zero unless otherwise specified	ISO 2013 & Gardner, Volkov, and Greiss 2019	
Abu Dhabi Standard (United Arab Emirates)	Oil: 6.3 gallons/hr or 3.6 BPD Gas: 15 SCF/min, 21.6 MSCFD Water: 400 gals/hr or 229 BPD	Al-Tamimi et al. 2008	
UK Standard	Washout: 50 cc/min Liquid rate: 2/cc/min/inch	H&SE UK Report and Mineral Management System Report	
Air Barrier Association of America (ABAA)	0.2 L/S.m <sup>2</sup> at 75 Pa	Waite and O'Brien 2010	
Manufacturers Standardization Society (MSS)	10m/hr of liquid or 0.1 SCF/hr under specific conditions	VAVTECHNOLOGIES	
Others	Some operators: Gas: 0.012 kg/s or 1928 scf/hr Oil: 50.1 l/hr	Raj 2014	

## **Chapter 3: Cement Overview**

### **3.1 Cement Purpose**

Cement in the oil and gas industry is an important aid in securing open zones and addressing severe losses. In almost all wells, the casing–formation annulus is filled with cement as an adhesive agent as part of the well-integrity procedure. In this chapter, an overview of how cement is used for this purpose is provided.

### **3.2 Cement Composition**

The design and execution of drilling operations require cooperation between the cement services contractor company and the drilling company with the operational contractor. If placed correctly, cement should withstand the following:

- Axial load from hanging linear or BOP surface weight
- Thermal expansion arising from a drilling operation
- Stress-related to the formation and reservoirs

The cement is a dry mix that makes slurry when mixed with water. The properties of cement relating to thickening over time and solidification are of primary importance in terms of well barriers. The solidification of cement, referred to as “hydration,” results from the chemical reaction of the cement composition with water (Fig. 3-1).

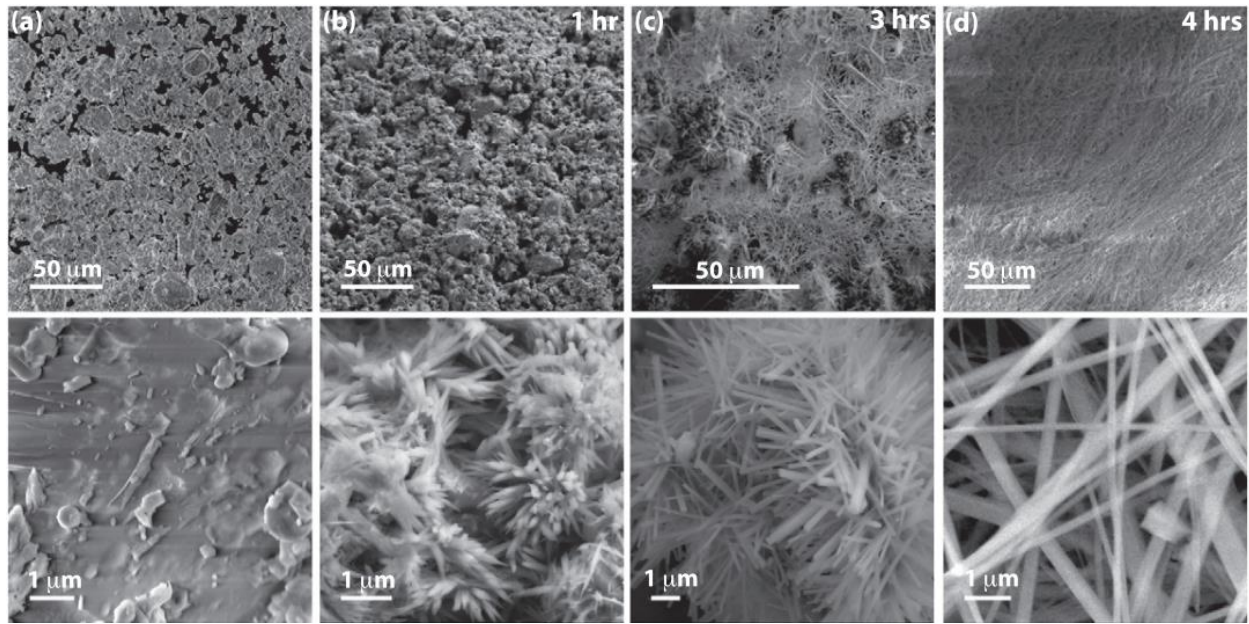


**Fig. 3-1—Cement hydration and bond initiation a) SEM of dry cement grain b-d) hydration at t=1 hr, 3hr, 4hr of time respectively at the different magnitude to and bottom (Varshney et al. 2017).**

A mixture of limestone, clay, and other materials is used to make Portland cement. The mixture is heated to produce clinker, which is mixed and ground up with a certain percentage of calcium sulfate to make gypsum. Calcium sulfates control the strength development of the resulting mixture. The clinker has a composition of almost 67% CaO, 22% SiO<sub>2</sub>, 5% Al<sub>2</sub>O<sub>3</sub>, 3% Fe<sub>2</sub>O<sub>3</sub>, and 3% other materials. Cement hardening occurs because of the chemical reaction between the water and the major materials. The most important clinker combustion is tricalcium silicate (Ca<sub>3</sub>SiO<sub>5</sub>). The cement chemical ratio is exothermal. The coarser the cement, the slower the heat evolution (Chatterji and Rawat 1965).

The raw material for Portland cement is a composite of calcareous rock, including lime and other industrial products, clay, a silica-alumina, and iron oxide (Michaux 2012).

When hydration is measured or described, it usually refers to the development of the mechanical bond, the exothermal reaction, and the shrinkage of the cement. The drying of cement could be a result of a different stage:

- Chemical shrinkage happens because the water reacts with the cement
- Plastic shrinkage on the surface refers to fresh concrete water evaporation
- Autogenous shrinkage refers to the cement paste hydrate at a low water-cement ratio
- Drying shrinkage refers to hardening cement evaporation

The first two stages can be avoided using an external source of water for the cement (Aïtcin 2016a; 2016b). Fig. 3-2 shows the raw materials used in the composition of cement.

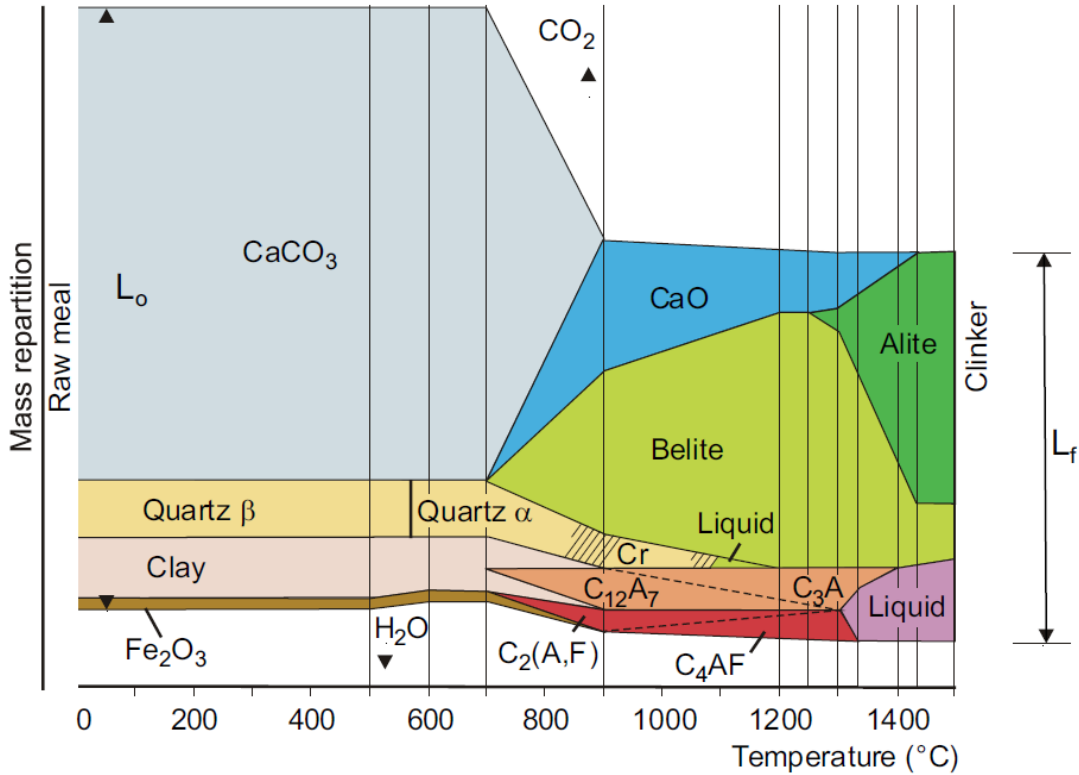
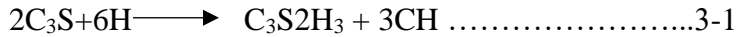


Fig. 3-2—Cement composition: raw materials (Aïtcin 2016a).

The major hydration of cement occurs because of the calcium silicate (Double and Hellawell 1976)

(Eq. 3-1 and Eq. 3-2):



The majority of the particles distribution for class H has a size of 20–40 μm (Aïtcin 2016a).

According to the ASTM (C1608 standard), to measure the chemical shrinkage of cement, a large amount of water should be added to test cement (< 10 mm) for saturation, which affects the test result. Surface water has been found to increase the chemical shrinkage reaction with cement in the first period (Fernandez 2008). In another study, researchers found that cement shrinkage at a

later stage in the first 15 h may decrease as the thickness of the cement sample increases (Sant et al. 2006).

The shrinkage mechanism depends on the humidity of the cement. There are three main kinds of shrinkage: capillary depression, surface tension, and the disjoining effect. Thus, with cement at 80% humidity or higher, capillary shrinkage is dominant. The study results may be attributable to the reduction in cement permeability and the surface cement dilution calorimetry (Fig. 3-3) (Sasaki et al. 2018 and Xueyu P.et al. 2013).

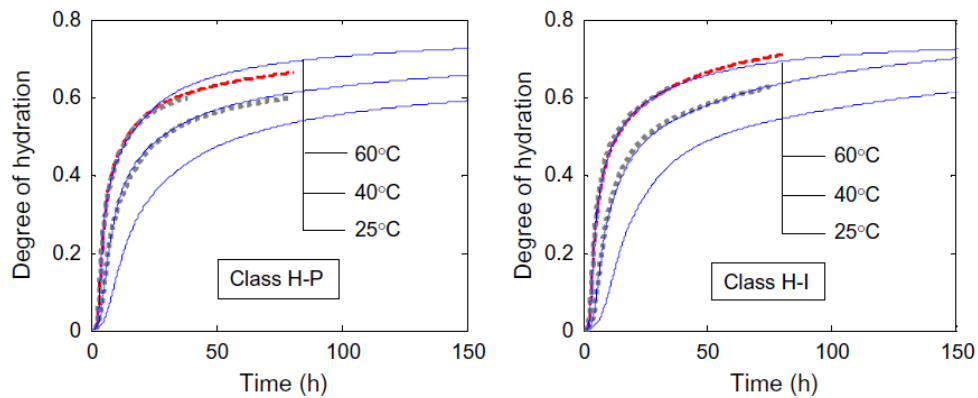


**Fig. 3-3—Measurement of the hydration level for different categories of class H cement; H-P on the left is premium class H (  $C_3S$  composition 47.9 by mass) and H-I on the right is regular standard class H (  $C_3S$  composition 66.5-70.3 by mass) by mass( Xueyu P.et al. 2013).**

### 3.3 Cement in Oil and Gas Operations

Cement is considered the main barrier for any P&A wellbore and the principal support for any barriers installed in P&A wells. In this section, how cement is used in the oil and gas industry are reviewed. For producing wells, cement acts as a secondary barrier together with casing strings.

The selection of cement in the oil and gas well is subject to the well depth and conditions. The temperature of a well might range from 150 to 500 °F depending on the depth and formation. The

first design property considered after the cement weight has been established is the thickening or pumping time—which is a measure of the time during which the cement is in the liquid phase before it has thickened. Usually, additives are used to control the pace of the thickening time: accelerator to reduce the thickening time or retarder to increase it. These additives are added depending on the cement volume and the time required to pump the cement across the length of the well (wellbore). The second important property is the cement’s development of compressive strength over a certain period, which will determine the extent to which it withstands the effects of operations and pore pressure. Further, the volume of the cement required for the operation must be determined by calculating the number of cement sacks through the cement yield and the water requirement. Usually, cement is pumped in two stages for large cement quantities—lead and tail which differ in terms of the cement density required. For any remedial job squeeze, the cement operation is performed in certain zones. API-RP-10B provides recommendations to the industry for testing the cement.

The objectives of using cement during well operations can be summarized as follows (IADC 2000):

- Support the casing and the bond with the formation
- Isolate the production zone
- Prevent unconsolidated sand from caving in onto the casing
- Serve as a well control aid to prevent leakage
- Support and protect the casing from corrosion from the reservoir fluid

Cement is pumped to the bottom of the well across the hole through the drill pipe, casing, and/or tubing. The main casing categories are shown in Table 3-1 and Fig. 3-4.

**Table 3-1—Casing types and purposes**

Casing Type	Purpose
<b>Conductor</b>	Prevent unconsolidated sand from caving in and provide support to the rig structure
<b>Surface</b>	Prevent fluid contamination with the water table zone and serve as a media to install the BOP
<b>Intermediate</b>	Support formation and isolation
<b>Production</b>	Set across the reservoir or production zone to complete the well

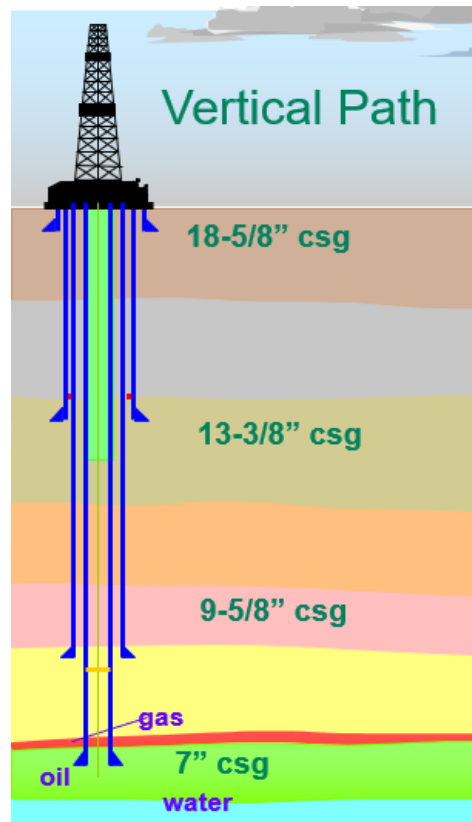


**Fig. 3-4—Casing design sketch.**

Leakage can occur at the well at many locations during drilling or casing operations. In this regard, it is critical to monitor wellbores that have been drilled but not cased, given that these have a direct channel to the surface. In Alberta, of 316,000 wells surveyed 4.6% were shown to have leaked (Watson et al. 2007). In Norway, 13–19% of the wells drilled in the North Sea showed leakage in

production wells, with the percentage increasing to 37–41% in injection wells (Randhol 2008). Common problems seen in offshore Malaysia, for example, are integrity problems, equipment discrepancy, and equipment failure (Costeno et al. 2014).

After the casing has taken place, cement is ordinarily applied in a two-stage lead-and-tail process. The tail, given its position between the freshly drilled formation and the casing, is crucial to the integrity of the well. Usually, the tail is well designed with more cement weight across the reservoir or the critical zone than elsewhere in the well.

Different practices have been developed to cement the hole or the casing safely, including running the casing centralizers, rotating the casing, and even using pumping and mixing methods. In addition, number of additives are usually used to modify the properties of the cement to ensure that it will be suitable for the well conditions. The API's cement classifications are presented in Table 3-2.

**Table 3-2—Cement types and their usage (API 10 A).**

<b>API Class</b>	<b>Composition</b>	<b>Mixing Water %</b>	<b>Description</b>
Class A (ASTM C465) (Type I)	Hydraulic calcium silicate and one or more CaSO <sub>4</sub>	46	Application for a depth of 0–6,000 ft
Class B (ASTM C465) (Type II)		46	Sulfate resistance Application for a depth of 0–6,000 ft
Class C (ASTM C465) (Type III)		56	High to moderate sulfate resistance Sulfate resistance High early strength Application for a depth of 6,000–10,000 ft
Class G		44	High to moderate sulfate resistance Application for a depth of 10,000–14,000 ft
Class H		38	High to moderate sulfate resistance for a depth of 0–8,000 ft

To design any cement operation job, it is necessary to establish the necessary game plan to identify the required tools and volume such as (Fig. 3-5):

- Operation requirements
- Cement quantity
- Casing size
- Volume requirement
- Pressure rating for the casing
- Pore pressure and formation pressure
- Formation temperature
- Fracture gradient
- Rig capacity

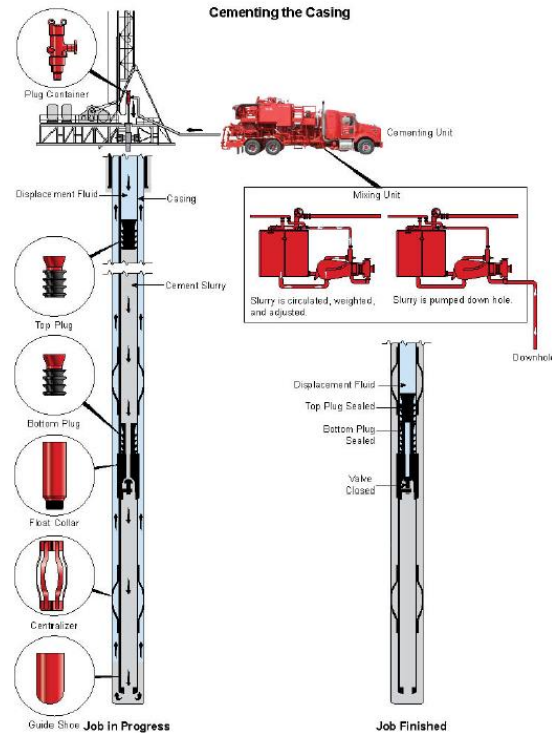


**Fig. 3-5—Cement pumping unit with well sketch (IADC 2015).**

Safety and job details are a priority, as cement pumping requires numerous personnel and a high pump rate through the pipes. Once the decision has been taken to plug and abandon a well, it should be rendered safe for the environment by taking steps to prevent the leakage of fluid (oil and gas) from the wellbore to any reservoir and the surface.

The main factors that can undermine the integrity of the cement casing are corrosion, temperature, stress change, poor cement practice, quality casing centralization, and improper mud removal (Evans and Carter 1962)

### 3.3.1 Cement Plug



Fig. 3-6—Sketch of a cement plug.

A cement plug is defined as the cement pumped into the hole at a certain depth to secure the open zone, treat loss circulation, and prevent leakage (Fig. 3-6). Its purposes can be categorized as:

- Zone isolation: The plug seals a zone in the reservoir or aquifer so that flow from another zone in the reservoir cannot enter.
- Pressure zone isolation: The plug isolates an unwanted high-pressure reservoir from the targeted production zone.
- Lost circulation control: The plug is usually placed in an uncontrollable severe loss zone to continue drilling operations.
- Kick-off points for the directional hole: The plug is placed after the hole has been drilled to sidetrack the well for directional drilling.
- Zone testing: The plug is placed for the leak-off test if two zones have been penetrated to cure the losses zone.

Cement plug placement can be performed with or without a packer, while the BOP is open or closed, or through hesitation (Herndon and Smith 1976). There are three plugging methods: balanced cement plug, dump bailer, and two plugs.

### ***3.3.1.1 Balanced Cement Plug***

In the balanced cement plug method, the cement is pumped from a drill pipe at a certain depth and balance with heavy mud or high-viscous fluid. The volume required is calculated and pumped after the mud or high-viscous fluid, and the pipe is pulled out of the hole after reverse circulation above the plug.

### ***3.3.1.2 Dump Bailer***

In the dump bailer method, a wireline is used to place a calculated volume of cement in a bailer and then dumped above a plug at a given depth (Herndon and Smith 1976).

### ***3.3.1.3 Two-plug Method***

The two-plug method saves time and costs by running several bailers with cement at different points on the same wireline.

## **3.3.2 Cement Plug Usage**

Cement is usually pumped into and placed across the following areas:

- Production zone
- Reservoir
- Opening across the casing
- Loss circulation zone
- Casing sub
- Linear overlap
- Freshwater zone
- Within 500 ft of the surface depth

The standard procedure for pumping cement for conventional plugs is as follows:

- Determine the depth and the required cement volume inside the casing
- Decide on the composition, including the additives following the expected pressure and temperature of the well and the required wait on cement (WOC)
- Calculate the amount of mud and space needed to place the plug and for circulation

- Consider any potential contamination
- Batch mix the cement, pump it, and determine the WOC
- RIH (Run In Hole) and tag the cement to check the depth
- Test and pressure the cement plug by using mechanical force to check the cement strength

Cement plug bonding—including the strength of the bond—is affected by the well conditions and how thoroughly the mud has been removed from the surface of the casing. Further, the texture of the cement has an effect on the bond: i.e., compared with a relatively smooth cement, a relatively rough cement might produce a stronger bond (Albawi et al. 2014).

The cement bond stress and strength are discussed in Appendix B.

## Chapter 4: Background on Cement Experimental Research

### 4.1 Need for Further Experimental Work

Numerous laboratory experiments and research studies have been conducted to estimate the size of the microannulus between the cement and the casing. Increasing levels of stress, including temperature changes, on the sheath due to operations has motivated researchers to determine the effects of environmental changes on the cement sheath. The gas flow path might go through the permeable cement, the cement–casing contact, the cement–formation contact, and the permeable formation (Fig. 4-1). In this chapter, important studies on the cement sheath, microannulus, and system permeability measures are highlighted.

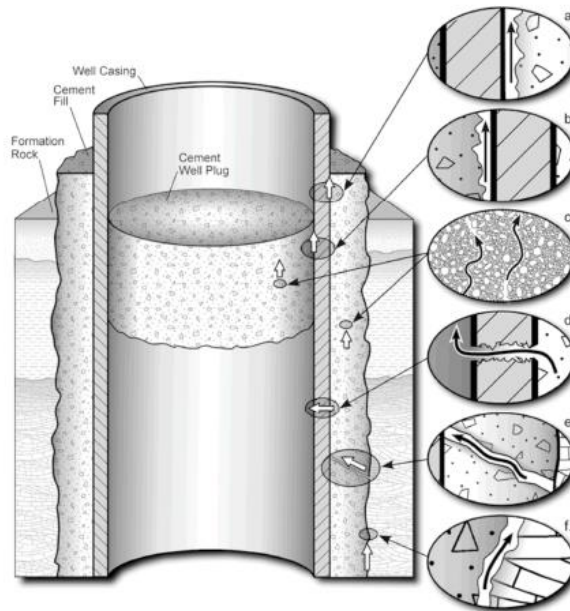


Fig. 4-1—Wellbore system leak pathways (Gasda et al. 2004).

## 4.2 Experimental Literature Review

In this section, some of the most significant research studies on cement sheath are summarized.

Seidel and Greene (1985) measured gas flow in an abandoned well in Alberta and found that the rate ranged from 0 m<sup>3</sup>/day to 2000 m<sup>3</sup>/day with 1 m<sup>3</sup>/day. Plee et al. (1990) found that the permeability of bentonite-based cement ranged from 50 to 100 md.

Plee et al. (1990) found the permeability of bentonite base cement range between 50-100 md.

Jackson and Murphey (1993) examined class G cement over six days' cement age at a pressure of up to 10,000 psi and a temperature of 120 °F. A leak was found at the low pressure of a 1–100 psi load after a drop-in pressure from 4,000 to 100 psi. However, pressurizing the casing to 8,000 psi closed that gap such that no flow occurred in these conditions.

Al-Wad (1996) experimented with the shear bond on class A of both cement-casing and cement-formation contact. He found that casing surface roughness, casing surface cleanness, and casing centralization improve the bonding with the cement. In contrast, Mud Cake will decrease and diminish the cement strength.

Appleby and Wilson (1996) found that cement permeability decrease with an increase in temperature, the cement permeability decrease to 1 md.

Backe et al. (1999) experimented with cement gel permeability and found that at 200 lb/100 ft<sup>2</sup> and 500 lb/100ft<sup>2</sup>, gel strength was five md of permeability.

Boukhelifa et al. (2004) concluded that the cement and rock elastic properties are important for the cement sheath, In an experimental and numerical study of the cement sheath.

Boukhelifa et al. (2005) examined cement with rock on a large scale aged over three days and found the minimum permeability to be 0.01 md (Fig. 4-2), with the gap closed and opened with the different cycles of pressure.

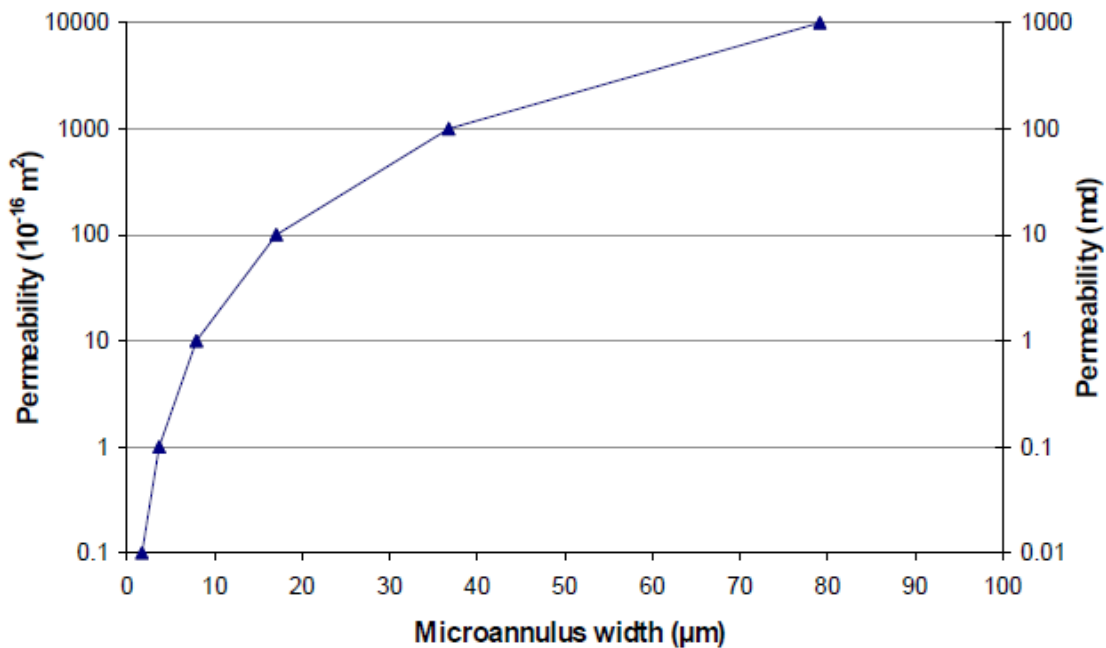


Fig. 4-2—Microannulus width equivalent to permeability (Boukhelifa et al. 2005).

Bachu and Bennion (2008) evaluated the effect of CO<sub>2</sub> on cement class G and measured its permeability. The researchers found permeability in the order of 1 nD calculated without an annular gap, although when a gap of 0.01–0.3 mm was detected, permeability increased to 0.1–1 md.

Teodoriu et al. (2010) found in researching cement class G for gas well storage that the cement bond lost its sealability after 40 MPa under low-load conditions yet maintained a good bond. Also, higher pressure internally was found to indicate a faster loss of the bond's capability.

Nagelhout et al. (2010) experimented with latex cement at a pressure of 15 MPa for one-week cement age. The researchers found that for cement with expandable particles, gas leakage occurred at 0.1 Mpa and that for cement with expandable particles leakage occurred at 1.25 MPa.

Deshmukh (2012) found that permeability calculation increased if the gas molecules collided while flowing (slip flow).

Albawi et al. (2014) studied the thermal cycle for annular class G cement at 66 °C for five days. A copper pipe was used; the change in cement was measured in millimeters by an acoustic emission sensor, and a CT scan was used after the post-experiment measurement (Fig. 4-3). The researchers concluded that stress placed on cement gives rise to radial cracks.

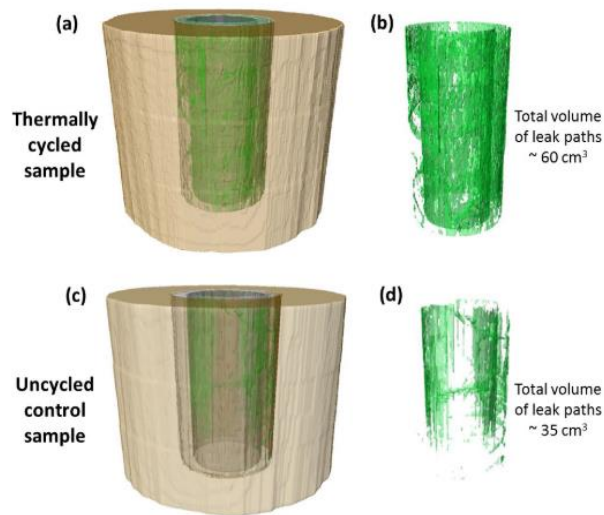


Fig. 4-3— Scan of the void before and after the thermal cycle (Albawi et al. 2014).

Kosinowski and Teodoriu (2012) found in an examination of cement class G with steel that the cement cracked as a result of the load as the cement ages.

Teodoriu et al. (2013) experimented with class G cement at 65 °C and 100 °C and found that the temperature increment caused an increase in the cement at a cement age of one month's compressibility.

De Andrade et al. (2015, 2016) experimented with the leak path on class G cement in a formation of sandstone and shale using a CT scan in an environment with a temperature of 200 to 250 °C. The curing time was five days at a temperature of 16 °C. A crack was observed in the cement body as the temperature increased, and the cement with shale was found to be more resistant than the cement with sandstone during the thermal cycle. The difference between the two cement mixtures in this regard was attributed to the high Young's modulus of the sandstone.

Schreppers (2015) found that cement failed to seal after certain operations based on a numerical investigation into the loading process during well operations in relation to the lifecycle of wells.

Kjøller et al. (2016) examined the fluid flow in cement class G at 60 °C through the cement and caprock contact numerically and experimentally with a CT scan. The researchers found that after 48 hr, permeability was between 10nD and 0.1md.

Eijden et al. (2017) and Opedal et al. 2018 experimented with cement class G at five days' cement age, 10 bar, and 66 °C. The result showed 1.5 ml/min gas leakage for 40 cm unhydrated cement and 60 ml/min gas leakage for 26 cm hydrated cement.

Stormont et al. (2018) studied class G cement cured over seven days with confined pressure of 35 MPa and 20MPa and found permeability of less than  $10^{-18} \text{ m}^2$  with a gap calculated of less than 0.6 micrometers.

Liu et al. (2018) conducted an experimental investigation into casing expansion and hydraulic fractures with the cement sheath in a system consisting of two layers of cement and casing. The study result showed a failure in the tensile strength of the inner casing, and the researchers concluded that an increase in thickness would help stabilize the cement sheath by decreasing tensile strength failure. Further, the researchers recommended applying backpressure as a possible way to reduce the tensile strength of cement.

Liu et al. (2018) studied the stress-strain state through Mohr-Coulomb yield criteria. At the early stage of cement, elastic deformation occurred between the cement and the formation. When the casing pressure increased critically, the cement expanded, and a deformation (a crack) occurred. At the pressure release, another deformation appeared in the cement, which caused a microannulus arising from a reduction in pressure such that leakage occurred in the cement sheath. Based on a CT scan, the deformation was found to be of the magnitude of  $16.23 \text{ mm}^3$  in a sheath volume of  $372,654.32 \text{ mm}^3$ .

Zeng et al. (2019) studied the cyclic effect on cement class G cured for 72 hr with pressure in the range of 50 MPa–110 MPa at  $80^\circ \text{ C}$  with airflow through the casing. Cracks were found on the cement sheath because of plastic deformation, and the researchers concluded that the high-pressure conditions were the cause. The explanation focused on the strain of the cement after the pressure was relieved and the deformation in the cement. As the cyclic pressure increased and the residual

stress increased, an increase in tensile strength resulted. When tensile strength exceeds bonding strength, microcracks may occur.

Asala and Gupta (2019) simulated the cement casing bonding with stresses. They found that microannulus created with the cycle of stress load.

Al Ramadan et al. (2019) experimented with class H and class G cement for 12 hr, 24 hr, and 27 days. The study results showed permeability in the range of 0.01–0.5 md. In addition, leakage time was related to overlap length: As the length increased, the leakage time increased.

Liu and Jia (2020) performed an experiment with cement in a chloride environment with CO<sub>2</sub> for 7–35 days and found that the cement penetration started with 25 mm and increased to 45 mm.

Welch et al. (2020) experimented with cement- casing for one week, one month, and two years to measure the mechanical properties. Then he simulated the cement with 50 psi and found that 6 micrometers have existed for permeability of  $10^{-16}$  m<sup>2</sup>.

Li J et al. (2021) experimented with the development of microannulus in cement class G using a triaxial load cycle. He found that the cement developed microcrack with different loads, and the bonding did not change because of the compressive stress applied on the casing.

#### **4.3 Limitations of Research on the Microannulus**

The research to date on the microannulus and gap estimation focuses on changes in the environment in relation to pressure and/or temperature (Goodwin and Crook 1992; De Andrade et al. 2016; Teodoriu et al. 2019). A significant number of studies center on cyclic pressure and temperature due to operations in the oil and gas field (Bachu and Bennion 2008; Kosinowski and

Teodoriu 2012; Albawi et al. 2014; Zeng et al. 2019). The literature also includes studies in which the microannulus is considered in relation to the cement–casing contact through the radial crack or cement properties. It is also the case that the chemical degradation of cement has been explored in some studies, in the CO<sub>2</sub> environment, in particular (Nygaard et al. 2011; Zhang et al. 2011; Liu and Jia 2020). In terms of determining the extent of permeability, Darcy’s equations are generally used to estimate this property in the literature. The methods used to estimate the gap focus on the CT scan or the acoustic log and provide a volumetric estimation but may overestimate the gap because of the cement’s porosity and permeability. It should also be noted that these methods are used to estimate the average measurement of the whole gap and cannot be used to estimate the extent to which the gap is connected across a sample. The plug and abandonment situation is when the cycle of pressure might be lowest, i.e., during the pressure test of the plug. Also, the temperature change during plug and abandonment is minimal. It is also important to realize that the assumption of a zero-gap is found in almost all the studies before any test begins and that the cement-wetting condition is largely ignored. The time range across the literature is within the range of days of cement age (1 to 27 days) (Stormont et al. 2018, Zeng et al. 2019, and Al Ramadan et al. 2019).

## **Chapter 5: Experimental Procedure and Methodology**

### **5.1 Introduction**

This chapter will discuss the experimental methodology developed to measure the cement hydraulic permeability (system permeability) and the microannulus. The experiment procedures initially started by preparing carbon steel seamless threaded pipes of 4 inches, 6 inches, and 9 inches and a diameter of 1-inch for the tests. The number of specimens tested was 60 in total to have consistent average measurements. Neat class H cement then mixed with distilled water according to API procedure. The pipes are plugged from one side and then filled with mixed cement. A space of 1 inch or less is intentionally not filled with cement to wet the cement surface at all times with distilled water. After aging the cement for 1,2,3 up to 9 months inside, the specimens were then tested.

During testing the specimen, a pressurized air ranges from 0-50 psig is gradually applied from the upstream of the setup. The pressure decay through the specimen to the atmospheric pressure where all the experimental data acquisition started.

The pressure data decay is recorded every second then it is transferred to the computer for data processing. The pressure decay is plotted with time for every pipe and compared across the specimen tested before to check for the data accuracy and repetition. The data then refined and filtered for a pressure decline rate every minute to reduce the pressure recording errors.

The specimens were cut mechanically to 1” long sections. The sections were then polished and cleaned for the microannulus gap measurement. The gap was measured by using a high-resolution microscope.

The system permeability is then determined from the pressure decline curve. The gap is then related to the system permeability. The results are then compared for all the experiments, and the research theory is developed.

A summary flowchart that shows the methodology is presented in Fig. 5-1.

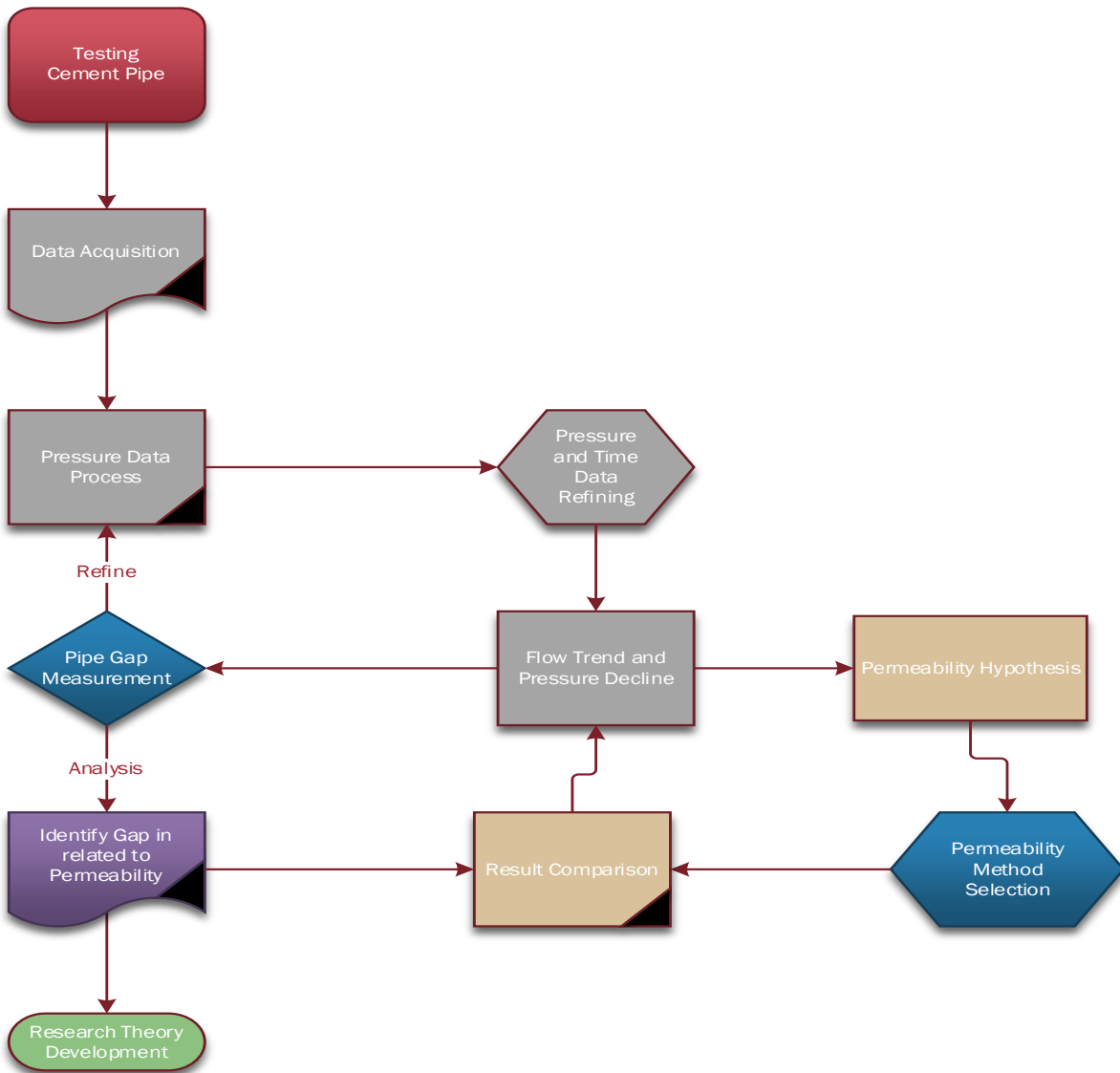


**Fig. 5-1—Flow chart representing the research methodology.**

## 5.2 Experimental Setup and Procedures

Class H Portland cement is the cement type selected for all the experiments in the present research. Class H is one of the most widely used cement in the oil and gas industry (second only to Class G), especially in deepwater formation or high pressure/high temperature (HPHT) wells characterized by more than 10,000 psi and/or 300–350 °F as the industry standard. The cement used herein was from a local company in Oklahoma (Central Plain Cement Company).

### 5.2.1 Cement properties

In this study, class H cement with the following oxide composition was selected for the experimental investigation (Table 5-1).

**Table 5-1—Class H cement composition (Central Plain Cement Company).**

Class H Neat Cement	Chemical Analysis	%
	C <sub>3</sub> S	61
	CaO	63.3
	SiO <sub>2</sub>	20.5
	Fe <sub>2</sub> O <sub>3</sub>	5.5
	Al <sub>2</sub> O <sub>3</sub>	3.2
	SO <sub>3</sub>	3.1
	MgO	2.4

### 5.2.2 Steel Properties

Table 5-2 shows the mechanical properties of the steel pipe used in the experiments. Thick-wall seamless steel pipes with an outside diameter (OD) of 1 inch were used.

**Table 5-2—Steel properties used in the experiments**

Pipe Properties	Psi
Min, Tensile Strength	60,000
Min, Yield Strength	35,000

### 5.2.3 Cement Mixing and Curing Procedures

The following procedures followed in the experiments to collect the data and obtained the measurements:

- i. The cement slurry was prepared according to API standards with water-cement ratio of 38%. The neat cement was mixed with distilled water at room temperature (20–21 °C) (Fig. 5-2).



**Fig. 5-2—Measuring cup for cement and water.**

- ii. The cement slurry mixing was performed following API recommendations, at 4,000 RPM (revolutions per minute) for 15 seconds when the mixture of cement is added to the water, and then at 12,000 RPM for 35 seconds (Fig. 5-3).

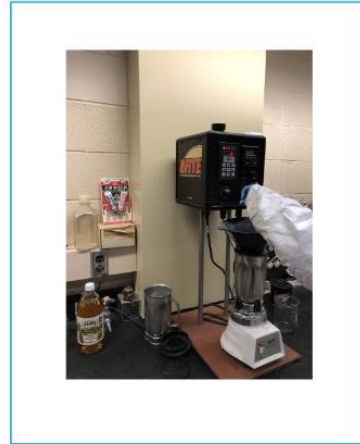


**Fig. 5-3—Cement mixer.**

- iii. The slurry was poured into a cubical mold of  $2 \times 2$  inches to be cured and tested. The cube was tested before any specimen test to verify the consistency of measurements (Fig. 5-4).



**Fig. 5-4—Cement molds with cement.**

- iv. The cement slurry was simultaneously poured into the pipe and cured under wet conditions (with water on the top) until the end of the predetermined curing time. Also, some pipes are cured without water (dry condition) until the test day.
- v. The test was carried out in two stages after the cement density is established for strength measurements.

#### 5.2.4 Cement Strength Measurements

- Ultrasonic (Non-destructive test)

The strength of hardened cement was measured by running ultrasonic waves at a frequency of 250 kHz across the cubes (Fig. 5-5), and the velocity was recorded with an accuracy of  $\pm 0.05$ mm. The test was conducted according to API 10 B-2 standard.



Fig. 5-5—Ultrasonic measurement at the center of the cement cube.

- UCS (destructive test)
- The unconfined mechanical strength test consists of a mechanical force applied to a hardened cement sample in which the average strength of the cement was recorded before

the cement cracks (exhibiting plastic deformation). The test has an accuracy of  $\pm 0.5\%$ . Compressive strength is calculated by the measured force and surface area of the cubical sample (Fig. 5-6 and Fig. 5-7).



**Fig. 5-6—Cement cube crushing.**

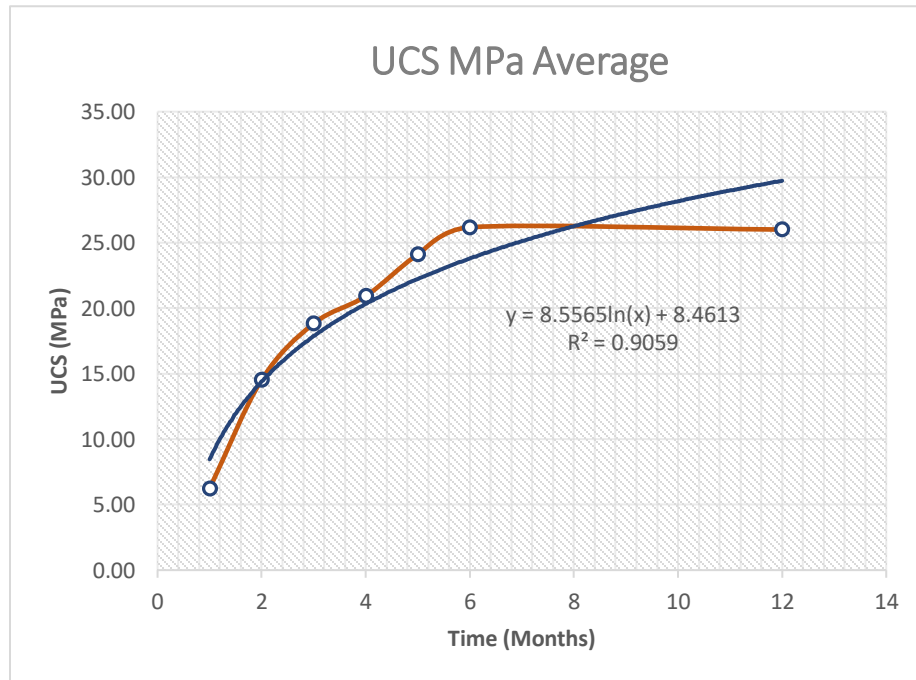


**Fig. 5-7—UCS data trend for class H cement tested.**

### 5.2.5 Pressure Decline Measurement

The specimens (specimens) used in the experiments were cured in a wet condition (Fig. 5-8)



**Fig. 5-8—Specimen before testing.**

Notes:

- In all the tests, the cement slurries placed in the pipe and cup were shaken to remove any bubbles from the solution before they began to thicken.
- The drying of cement was prevented by continuously adding distilled water to the top.
- Several tests were performed without adding water to the top to measure the difference.
- The curing temperature was always room temperature (in the lab conditions where the temperature might change at night).
- The cement was poured while the pipe was maintained in a vertical orientation.
- The cement was placed into some of the pipes by squeeze injection.

- The destructive test and the non-destructive test were performed before any of the specimen were tested.
- To measure the flow rate through the specimen, an experimental setup comprising a downstream part and an upstream (Fig. 5-9) part was developed.

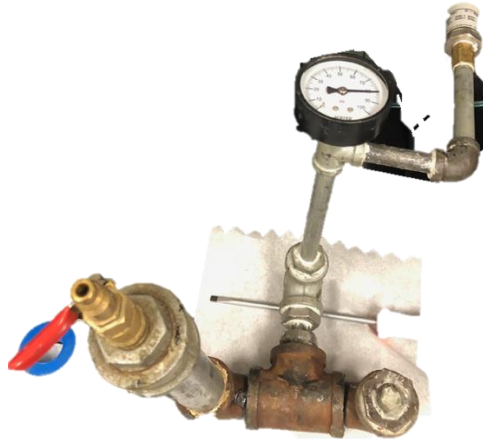


**Fig. 5-9—Upstream setup for the experiment.**

- i. The downstream part has two pressure sensors: analog and digital sensors with an error of  $\pm 0.05$  psi. The digital sensor was connected to the computer to record the pressure every second. The upstream volume ( $V_1$ ) was measured as 290 cc ( $\text{cm}^3$ ). The downstream of the specimen was opened to the atmosphere. Specimens were 4, 6, and 9 inches long at an approximate volume of 50–115 cc. Figures 5-10 and 5-11 depict the schematic of the test setup, showing the upstream, and downstream parts of the experimental setup.

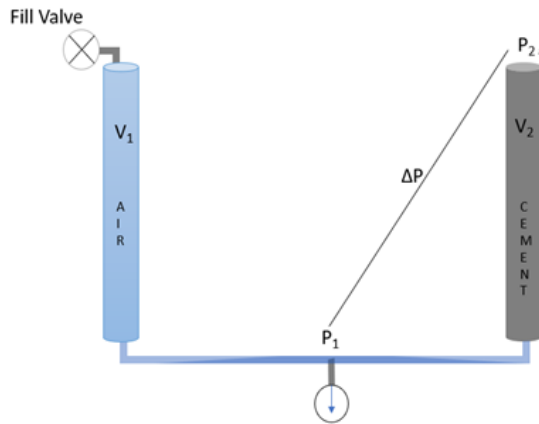


**Fig. 5-11—Upstream and downstream experiment sketch.**

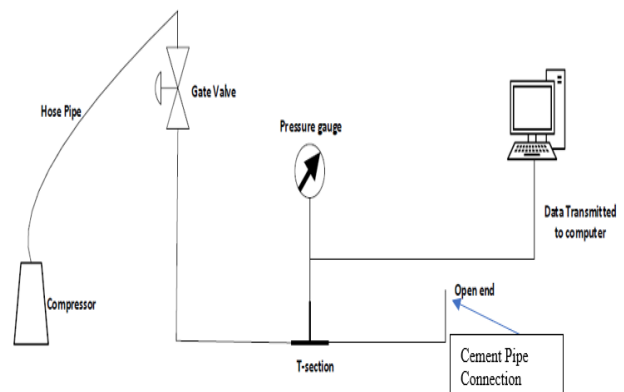


**Fig. 5-10—Hydraulic (pneumatic) cement casing permeability setup.**

- ii. The downstream side was air-tested for any leakage at 30, 50, and 70 psi for a week to check the integrity of the setup. The specimen was then connected to the downstream side, and the setup was put in a water bath to maintain a constant temperature of 20°C during the testing period (Fig. 5-12).

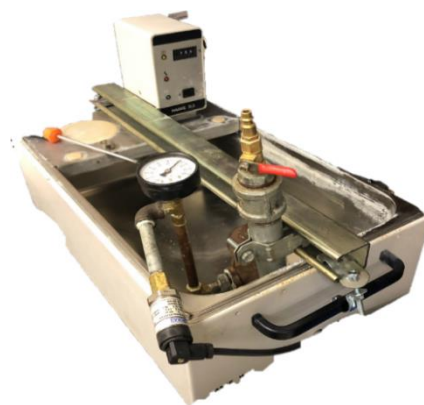


**Fig. 5-12—Control temperature bath for the experiment.**

- iii. The upstream side was gradually pressurized to 50 psi using compressed air. Then, the air supply was cut and the sensor started measuring the pressure drawdown and sending the data to the computer. The data was collected with DASYS Lab software and recorded on the computer on a second-by-second basis
- iv. After the pressure-drawn-down test was completed, the specimen was disconnected from the setup and prepared to be mechanically cut into 1-inch long pieces (Fig. 5-13 and Fig. 5-14).



**Fig. 5-14—Specimen prepared for mechanical cutting.**



**Fig. 5-13—Specimen cut into 1-inch section**

- v. The magnification of the microscope used to measure the specimen's gap ranges from 20x–50x. The ImageJ program was used to measure the surface cement–casing phase after segmenting the surface in eight angles (Fig. 5-15 and Fig. 5-16).



**Fig. 5-15—Specimen 1-inch × 1-inch after polishing.**

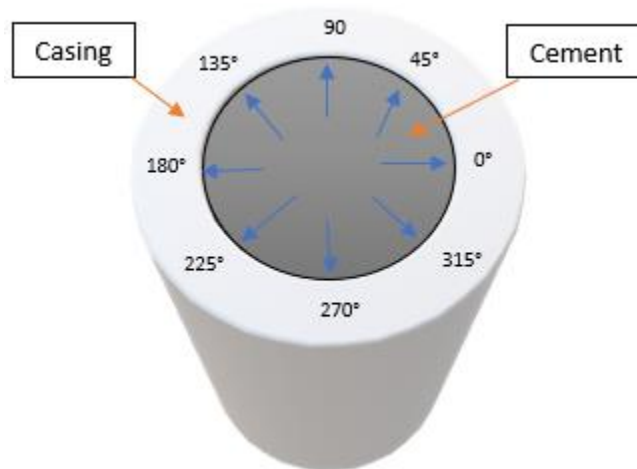


**Fig. 5-16—Angular positions for the microscopic measurement.**

- i. Every cut section was sandblasted with an 8-inch mesh to measure the annular gaps using the microscope. A high-resolution optical microscope was used for the first batch of the experiments and then the results were compared with those from a standard microscope. The results were similar; therefore, the standard microscope connected to a high-resolution digital camera was used for the rest of the experiments (Fig. 5-17, Fig. 5-18, and Fig. 5-19).

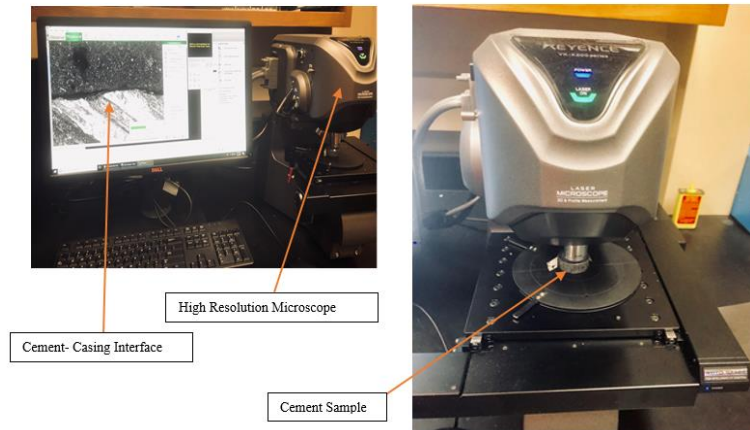


**Fig. 5-17—High-resolution optical microscope.**



**Fig. 5-18—Microscope attached to a high-resolution camera.**

- vi. The gap was measured by the average of 60 points across each angle (Fig. 5-19).

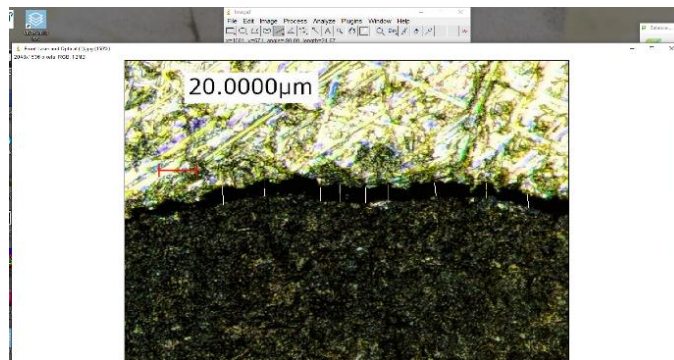


**Fig. 5-19—Microscopic sample gap measure (20 micron-scale).**

- vii. The specimen was left to dry out for one month – one year, and then the gap is measured again.
- viii. The experiments were repeated to confirm the results.

### 5.3 Data Process for Lab Experiments

Fig. 5-20 summarizes the data journey (processing setup) started by removing the data's noise then validating the data and trend across all the samples. The data collection began by moving all the data acquired by DASyLab to an Excel sheet and removing the noise across them. Then, the pressure-drop behavior with time was studied and the flow rate calculated. Next, the data trend was analyzed and the system permeability estimated. After the gap measured using ImageJ, the gap analysis starts. The data is then plotted to identify and investigate any relationship between the measurements and test parameters.

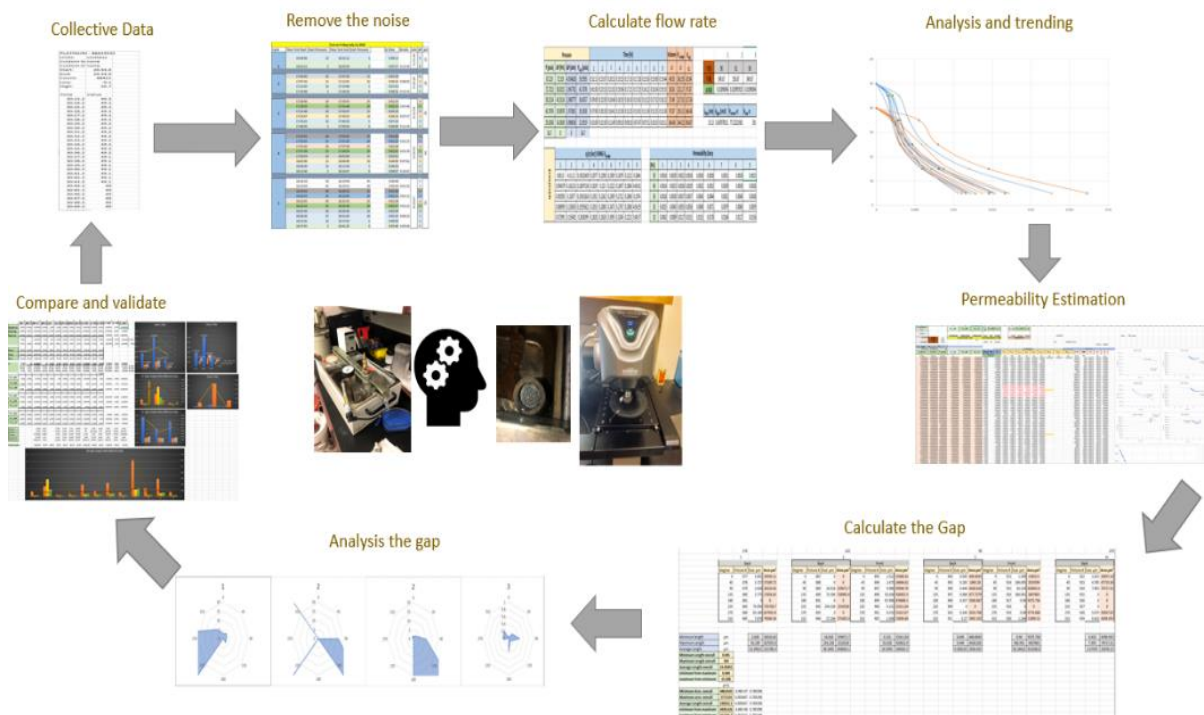


**Fig. 5-20—Summarizes the data journey across research steps.**

## Chapter 6: Results and Analysis

### 6.1 Introduction

In this chapter, the overall trends and the statistical analysis of the experimental data are discussed. Data acquired during the experiments and subsequently analyzed include the change of pressure with time, the gap space, and the cement age. System permeability is analytically calculated using various equations.

A study of the gas decline behavior with various specimen length, system permeability, and gap measurement trends is reviewed. One of the most dominant trends is a strong correlation between system permeability and the gap measured, indicating a clear connection between the two. The aging process of the specimen surface continuously wetted in water was shown to decrease both the gap and the system permeability. Some deeper investigations of one-year cement drying-out properties were also included as well as early exposure of the cement sample to pressure.

The pressure at the specimen inlet was pressurized up to 50 psig and left to decay naturally to the atmospheric pressure. This was done for three specimens (4 inches, 6 inches, and 9 inches). From that data, the system permeability was calculated using various analytical solutions as described in the system permeability section 6.3.

This chapter references a gap in several instances. The measured gap is the space between the pipe (steel) and the first layer of the cement perpendicular to it. This distance was taken at multiple angular degrees of the circular cross-section of the samples. The 4 inches, 6 inches, and 9 inches of steel pipe with solidified cement were cut into one-inch specimen samples, each of which was measured for the gap in the front and back. The opening between the steel and the cement is the

measured gap from a high-quality sample image. Table 6-1 shows a summary of the initial experimental conditions.

**Table 6-1—Experimental data initial conditions**

	Experiment	Unit
Initial Pressure	50	psig
Final Pressure	0	psig
Temperature	68	F
Pipe Length	4, 6, 9	inch
Pipe Diameter	1	inch
Loop Volume ( $V_1$ )	291	cm <sup>3</sup>
Cement Volume ( $V_2$ )	50.9, 76.7, 115.3	cm <sup>3</sup>
Air Viscosity	0.018397	cp

## 6.2 Data and Analysis

The relation and behavior of the data with the change in length and cement age are investigated.

### 6.2.1 Pressure Decline Analysis for Various Lengths

As stated earlier, the lab experiments were conducted on three length sizes. The long-term analysis was performed on the 6-inch specimen. The pressure on the 6-inch specimen was performed at a cement age of one, two, three, and nine months. Throughout the aging time, the samples were hydrated (wet hydration).

The plots in Fig. 6-1 and Fig. 6-2 show the trend line for pressure decay at multiple cement ages for the 6-inch specimen. The chart has 5% errors due to the electronic gauge usage and data sensitivity recorded. Fig. 6-2 clearly shows the pressure with a less steep decline as the cement aged (hydrated). As the cement aged, it took longer to diffuse the same amount of pressure, indicating a higher level of sealability between the cement and the casing.

The 9-inch specimens show a slightly different pattern for aging at one and two months (Fig. 6-1). Aging at one month showed a steady decrease to 40 psi and then a steeper reduction in pressure after that. However, for the one-month aged cement, the decline was more obvious, indicating a larger flow area.

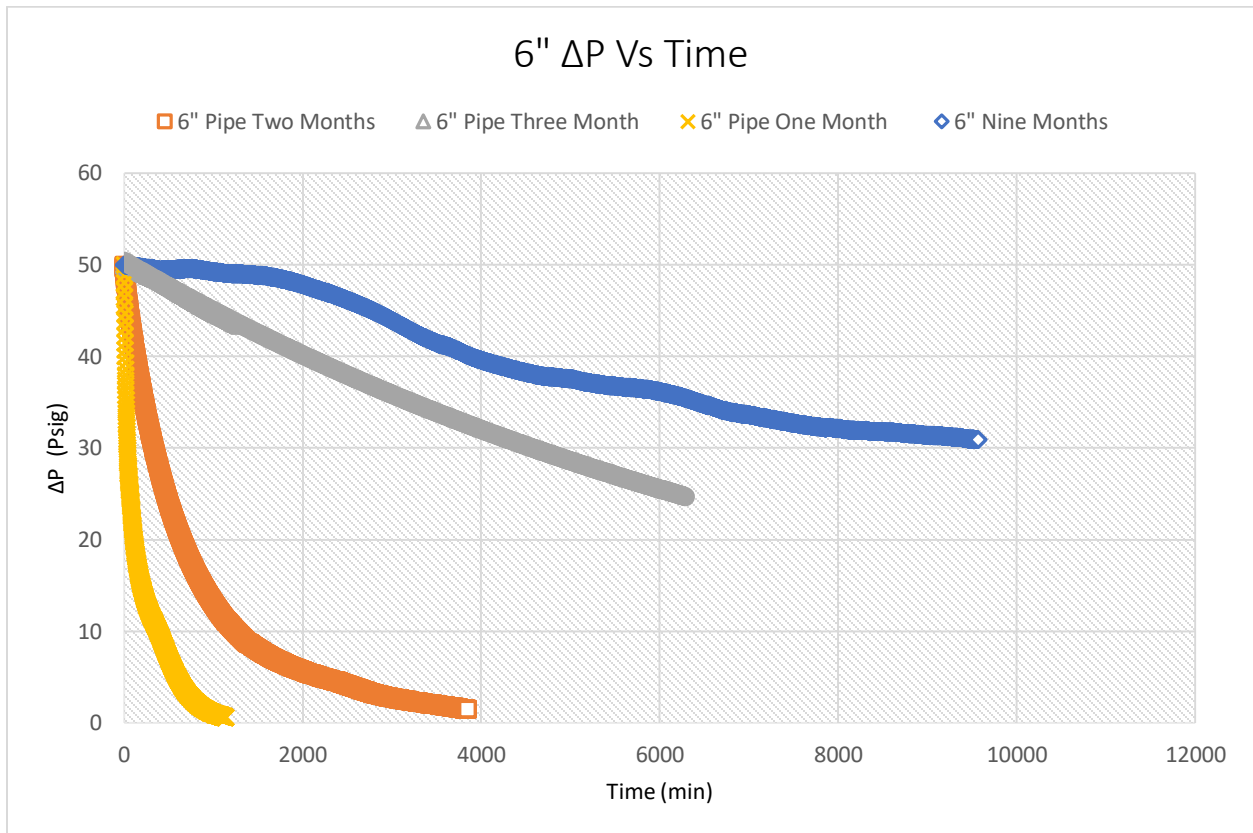


**Fig. 6-1—Pressure behavior decline vs time for 6-inch specimen at (1, 2, 3, and 9 months) cement age (5% error).**

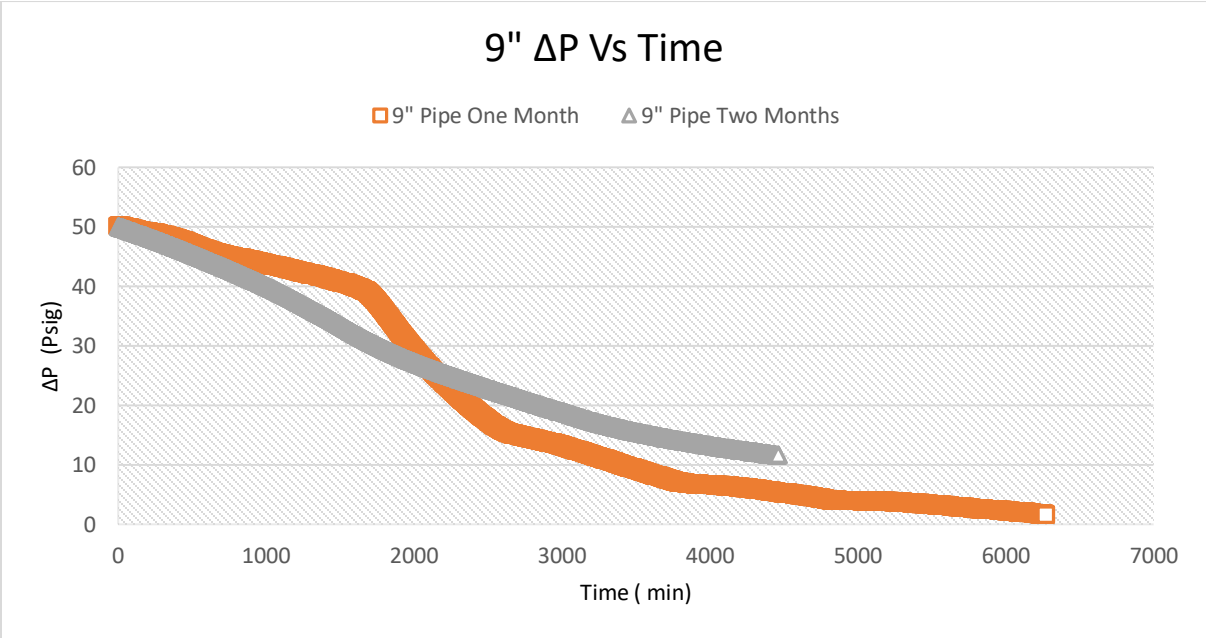


**Fig. 6-2—Pressure behavior decline with time for 9-inch pipe at 1- and 2-month cement age (5% error).**

The 4-inch and 6-inch specimen results agreed in a higher rate of decline with shorter hydration time. The one-month curve for the 4-inch specimen is almost identical in shape to the curve for the 6-inch specimen (Fig. 6-3).

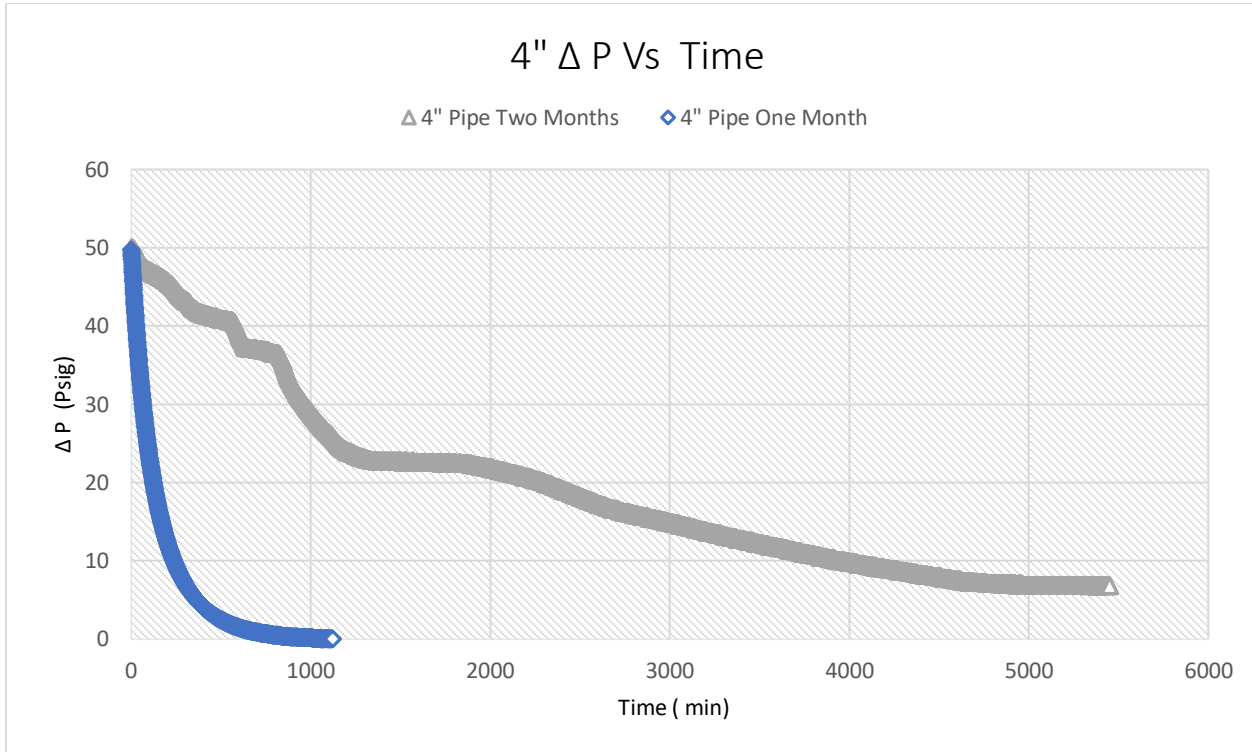


**Fig. 6-3—Pressure behavior decline with time for 4-inch specimen at 1- and 2-month cement age (5% error).**

The three specimen lengths result at a one-month cement age time showed that as the length increases, the rate of decline mostly decreases (Fig. 6-4). the decrease could indicate that the flow area across the annulus is smaller and might be disconnected in a longer sample. This consideration will be discussed further in this chapter. Fig. 6-5 follows the same trend for the cement age of two months, showing a much flatter pattern than for cement age of one month due to the smaller gap at the two-month mark. The flatter graph shows the tight flow path for the air to escape into the atmosphere (0 psig).

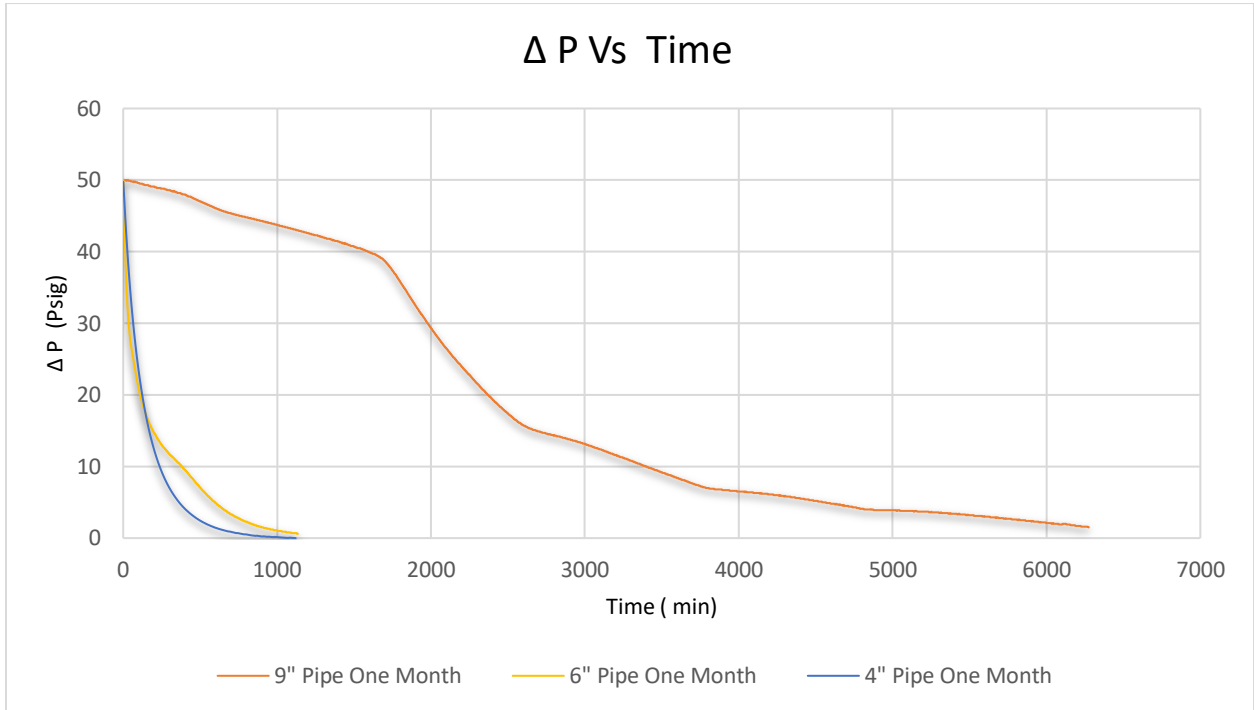


**Fig. 6-4—Pressure behavior decline with time for 4-, 6-, and 9-inch-length specimens at 1-month age.**

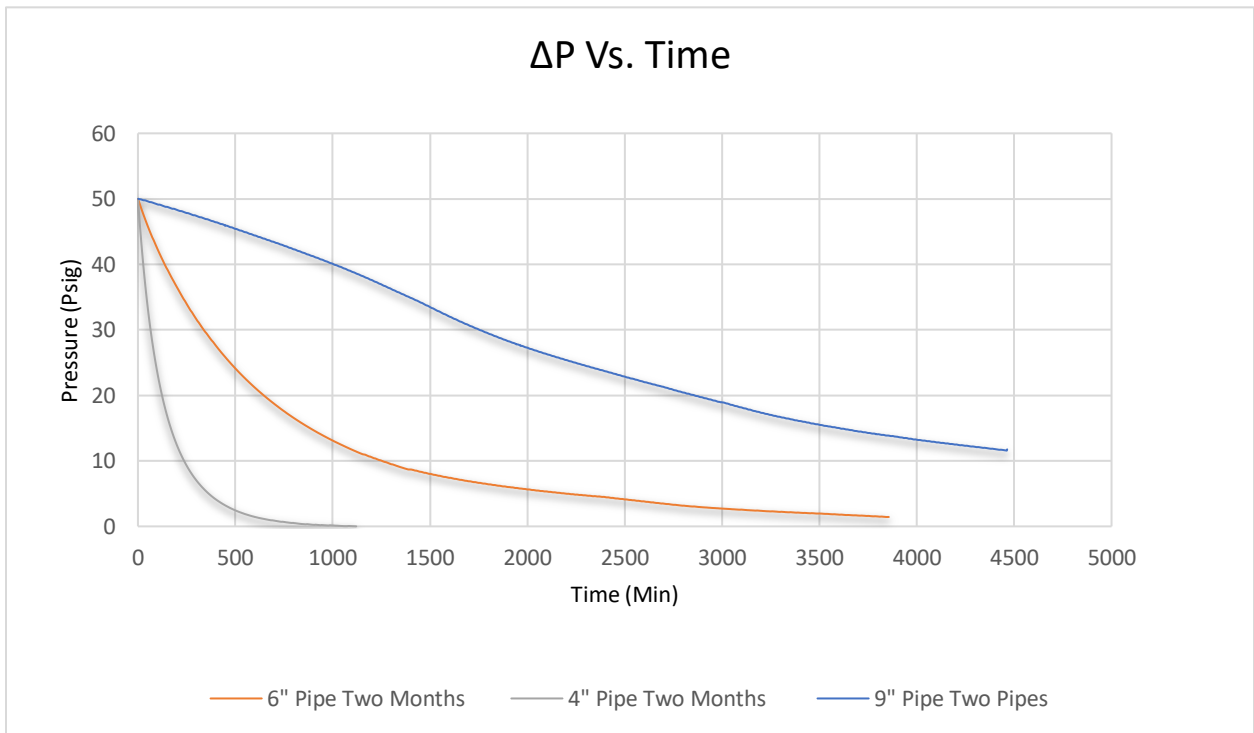


**Fig. 6-5—Pressure behavior decline with time for 4-, 6-, and 9-inch-length specimens at 2-month age.**

### 6.3 System Permeability Calculation

Darcy's law is the main method used to estimate permeability in the oil and gas field. In this section, Darcy's equation and other methods are examined and applied to the data obtained from the experiments. System permeability is defined as the ease with which the fluid can flow through a passage. Darcy performed his experiment by flowing water through sand and measuring the pressure difference with the flow rate (Glover 2006).

#### 6.3.1 Darcy's Law

Darcy's law is the simplest version of the Navier-Stokes equation. The basic assumption of Darcy's law is applied for a laminar flow. To calculate the Reynold number for the experiment,

Eq. 6-1 is used:

$$Re = \frac{\rho q D}{\mu A} \dots\dots\dots(6-1)$$

$\rho$  Air Density (kg/m<sup>3</sup>)

$q$  Air Flow Rate Across the Gap (m<sup>3</sup>/sec)

$D$  Hydraulic Gap Diameter (m)

$\mu$  Air Viscosity in (Pa.s)

$A$  Gap Cross-Section Area (m<sup>2</sup>)

The Reynold number calculated was of the magnitude <<1500; therefore, the flow in the experiment was assumed to be laminar. It is also relevant here that Darcy's law flow should be laminar with single-phase fluid, steady-state flow, and isothermal to be accurate.

Four main correlations were used to calculate system permeability:

- Gas flow escape (Darcy's equation)
- Modified gas flow (mass flow rate)
- Gas flow at an average pressure
- Gas flow at an average density

**6.3.1.1 Gas Flow Escape (Darcy's Equation)**

The flow rate of gas in Darcy's equation is calculated by:

$$K = 2000 \mu \frac{L}{A} q \frac{P_{atm}}{P_o^2 - P_i^2} \dots\dots\dots(6-2)$$

q Flow Rate (cm<sup>3</sup>/s)

L Sample Length (cm)

K Permeability (md)

P<sub>o</sub> Outlet Pressure (atm)

P<sub>i</sub> Inlet Pressure (atm)

A Sample Area (cm<sup>2</sup>)

μ Viscosity (cp)

The viscosity is estimated using Sutherland's correlation (Eq. 6-3):

$$\mu = \mu_0 * \frac{0.555 T_0 + C}{0.555 T + C} * \left(\frac{T}{T_0}\right)^{\frac{3}{2}} \text{ (Sutherland's)} = 0.018397 \text{ cp} \dots\dots\dots(6-3)$$

**6.3.1.2 Modified Gas Flow**

Darcy's equation has errors in permeability estimation because incompressible fluid is assumed. However, the calculation of system permeability was adjusted to account for gas compressibility

by introducing the gas ideal law and volumetric flow rate to the equation. Darcy's modified equation was derived by treating the inside of the specimen as a closed system after being subjected to pressure. The mass inside the sample is conserved unless the pressure constraints to which it is subject to change. Once changed, the volume is recalculated for each time step based on the same principle. Moreover, the volume of air inside the sample pore space or microannulus at a certain point in time is governed by the ideal gas law, which directs the air density inside at all points in time. The analytical equation derivation based on introducing the volume of gas escape with time instead of flow rate (Eq. 6-4):

$$K=2000 \mu \frac{L}{A} \frac{\text{Volume of gas escape}}{\text{Time}} \frac{P_{\text{atm}}}{P_0^2-P_1^2} \dots\dots\dots(6-4)$$

$$K=2000 \mu \frac{L}{A} \frac{\frac{\Delta m}{\rho_{\text{at } P}}}{\text{Time}} \frac{P_{\text{atm}}}{P_0^2-P_1^2} = 2000 \mu \frac{L}{A} \frac{\frac{m_2}{\rho_{\text{at } P_2}} - \frac{m_1}{\rho_{\text{at } P_1}}}{\Delta t}} \frac{P_{\text{atm}}}{P_0^2-P_1^2}$$

Since gas density from the ideal gas law at pressure (P)  $\rho = \frac{PM}{RT}$  then

$$\frac{\Delta m}{\rho_{\text{at } P}} = \frac{m_2}{\rho_{\text{at } P_2}} - \frac{m_1}{\rho_{\text{at } P_1}} = \frac{m_2}{\frac{P_2 M}{RT}} - \frac{m_1}{\frac{P_1 M}{RT}}$$

For the experiment at an ambient temperature of 68 °F (293.15 °K) with air flow of molecular weight of 0.02897 kg/mole with constant gas of 82.05745 cm<sup>3</sup>.atm. mol<sup>-1</sup> K<sup>-1</sup>, the volume flow rate can be rewritten as:

$$\frac{\Delta m}{\Delta \rho} = \frac{m_2}{\frac{P_2 M}{RT}} - \frac{m_1}{\frac{P_1 M}{RT}} = \frac{m_2}{P_2} - \frac{m_1}{P_1} = \frac{\Delta m}{1.2043E-6 \Delta P}$$

Given that P<sub>atm</sub> = 1 atm, substitute in Eq. 6-4:

$$K=1660.693E6 \mu \frac{L}{A} \frac{\frac{\Delta m}{\Delta P}}{\Delta t} \frac{1}{P_0^2-P_1^2}$$

The modified Darcy's equation can be rewritten as (Eq. 6-5):

$$K = 1660.693E6 \mu \frac{L}{A} \frac{\Delta m}{\Delta t} \frac{1}{(P_o^2 - P_i^2)(P_o - P_i)} \dots\dots\dots(6-5)$$

$m_1$  Mass Flow at  $P_1$  (kg)

$m_2$  Mass Flow at  $P_2$  (kg)

$\Delta t$  Time (second)

$L$  Sample Length (cm)

$K$  Permeability (md)

$P_o$  Outlet Pressure (atm)

$P_i$  Inlet Pressure (atm)

$A$  Sample Area (cm<sup>2</sup>)

$\mu$  Viscosity (cp)

**6.3.1.3 Gas Flow at Average Pressure**

One of the main objectives of the experiments is to find the system permeability for an application that fits the sizes of the samples at hand. In this context, the flow rate is among the variables that require further investigation. The averaged pressure method is introduced to account for the pressure regime across the cement. The governing assumption is based on the pressure inside the specimen (closed system) is the average pressure between the inlet and the outlet at each point of time. The flow rate is found through the following steps.

The first step is to find the volume of the average pressure using the ideal gas law in standard laboratory conditions. Then, secondly, the flow rate is calculated at any given time:

$$q = \frac{\text{Volume of gas escape at } P_{avg}}{\text{Time}} \text{ using average pressure across the specimen}$$

Next, the flow rate is applied in Darcy's law.

#### **6.3.1.4 Gas Flow at Average Density**

Gas flow at average density was achieved by treating the inside of the specimen as a closed system. The mass inside the sample is conserved unless the pressure constraints change. Once changed, the volume is recalculated for each time step based on the same principle:

$$q = \frac{\text{Volume of gas escape using mass flow rate}}{\text{Time}} = \frac{\Delta m}{\rho_{\text{avg}}} \text{ using the average density of the air between the inlet and}$$

the outlet. The mass is found using the ideal gas law, and system permeability is calculated using Darcy's law.

#### **6.3.1.5 Darcy's Law Correction**

Two corrections were tested to account for the experimental environment of the airflow rate in specimen, i.e., the Klingleberg effect and Forchheimer's correction (Ebrahimi et al. 2017, Takhanov D. 2011).

##### **6.3.1.5.1 Klingleberg Effect**

The effect of gas slippage plays a role in the experiment, as the air flow across the cement is slow because of the low pressure and small microannulus. Following the standard process to correct the gas factor, the calculated system permeability of the air was plotted versus the inverse of the average pressure ( $1/P_{\text{avg}}$ ). The results (for 6-inch specimen in Fig. 6-6) showed no indication of any straight line to correct for the system permeability at infinite pressure (Y-Intercept). This trend

was observed in the unconventional reservoir because of the low permeability in a reservoir with nano- to micro-Darcy (Ebrahimi et al. 2017).

Klinkenberg's correction was not applicable for the experiment since no plot fitting was obtained.

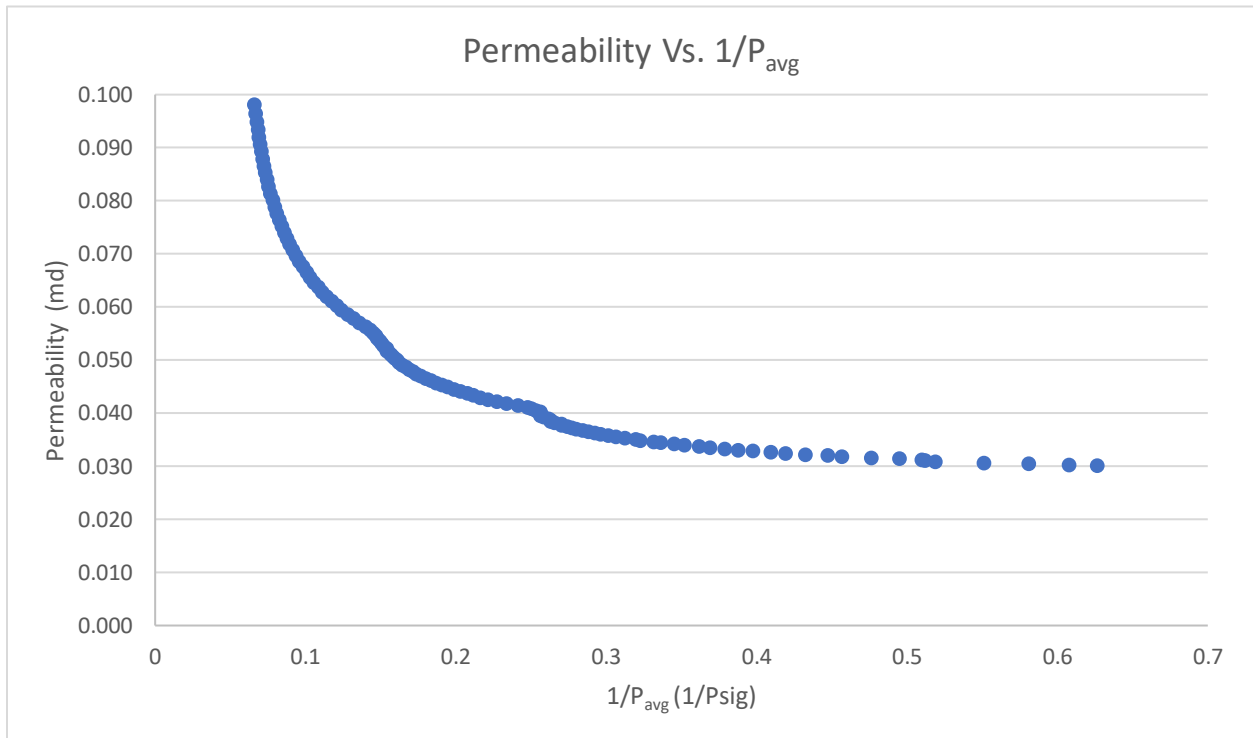


**Fig. 6-6—Darcy’s permeability correction (Klingenberg).**

### 6.3.1.5.2 Forchheimer’s Correction

Forchheimer’s correction is used to correct for Darcy’s permeability for steady-state, turbulent, and low-permeability environments using Eq. 6-6:

$$\frac{MA(P_1^2 - P_2^2)}{2ZRT\mu L\rho q} = \frac{1}{k} + \frac{\rho q}{MA} B \dots\dots\dots(6-6)$$

Plotting the left side  $\frac{MA(P_1^2 - P_2^2)}{2ZRT\mu L\rho q}$  (Y) vs the right side  $\frac{\rho q}{MA}$  (X) should have a straight line; then, the y-intercept represents the corrected inverse of the permeability.

*M* Gas Molecular Weight (g/mol)

*A* Pipe Area (m<sup>2</sup>)

*P*1 Inlet Pressure (Pa)

*P*2 Outlet Pressure (Pa)

*Z* Gas Compressibility (Pa<sup>-1</sup>)

*R* Gas Constant (8.314 J/molK)

*T* Temperature (K)

$\frac{1}{k}$  Permeability (m<sup>2</sup>)

*L* Length (m)

*q* Flow Rate (m<sup>3</sup>/sec)

*B* Forchheimer Coefficient (m<sup>-1</sup>)

Forchheimer's correction was applied to the dataset for various sample sizes. However, the equation is relevant to steady-state turbulent flow and does not apply to the experiment conditions (Fig. 6-7).

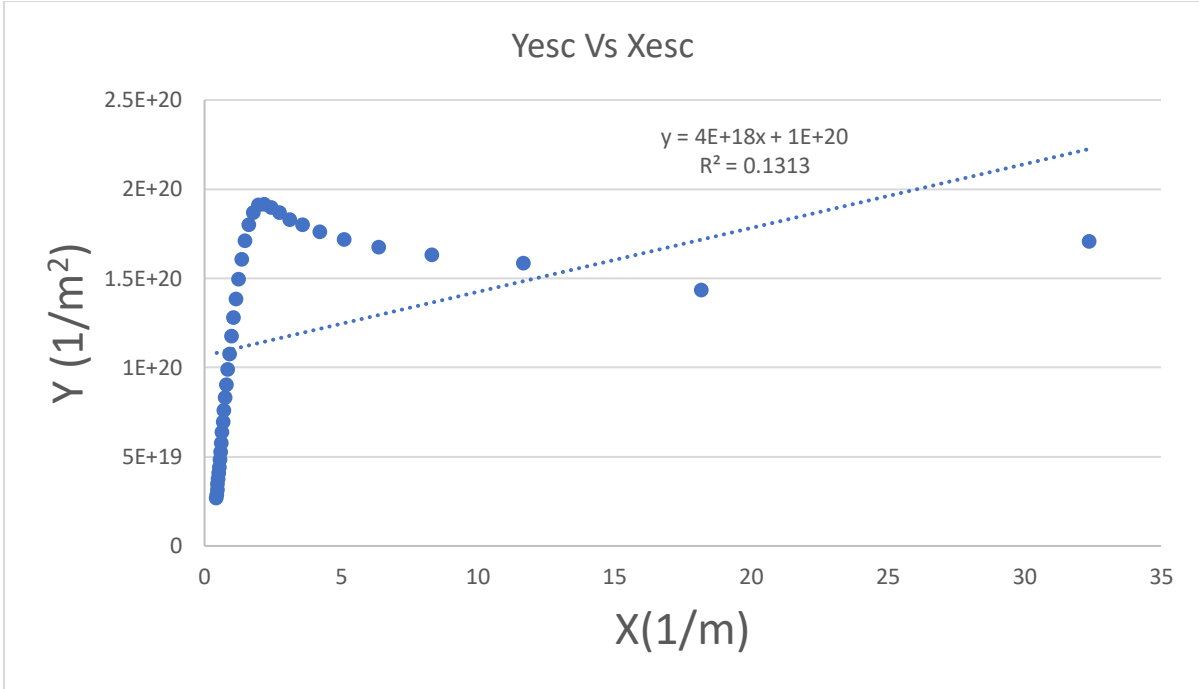


**Fig. 6-7—Darcy’s permeability correction (Forchheimer’s) (m²).**

Even if the steady-state portion of the plot was taken, the estimated system permeability is too low at a magnitude of less than a fraction of nano-Darcy’s correction (Fig. 6-8).

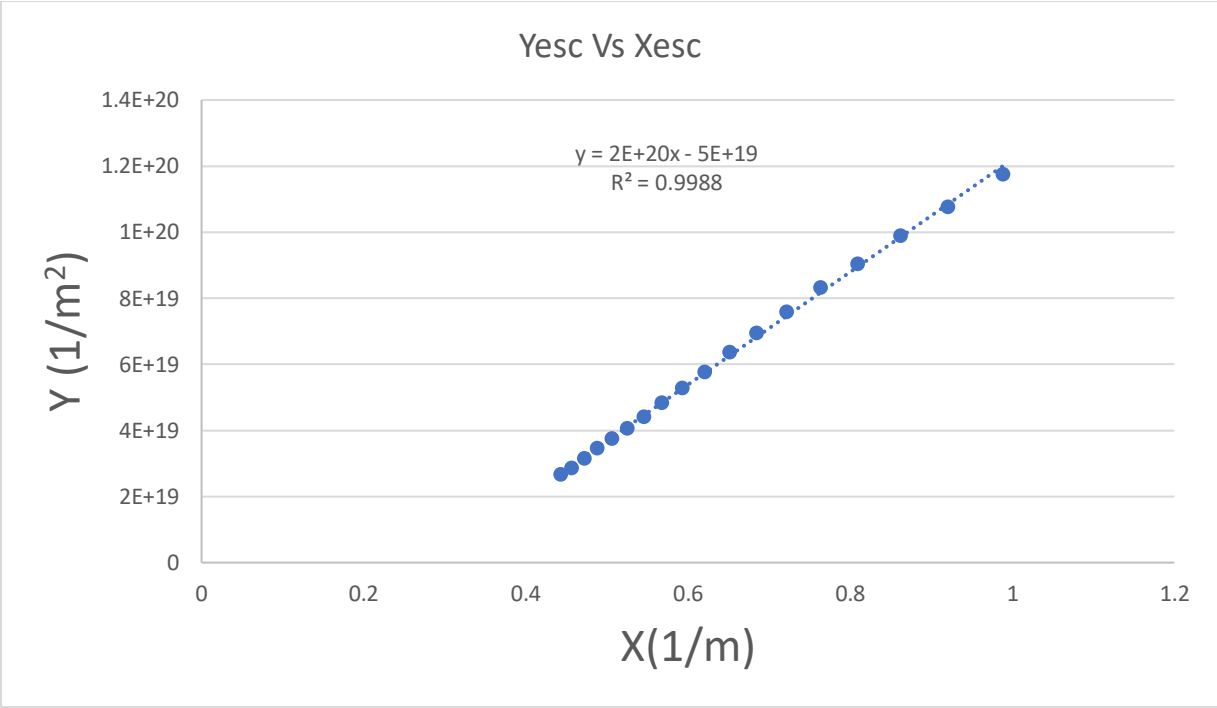


**Fig. 6-8—Darcy’s permeability correction (Forchheimer’s) steady state (m<sup>2</sup>).**

**6.3.2 Brace Method (Pulse Decay)**

The Brace method (pulse decay) is the primary base method for system permeability estimation in the experiments. This method has been utilized in the industry for fractured reservoirs with fixed reservoir pressure and low permeability (0.1 md to 0.01μd) (Brace et al. 1968). The pulse decay method has an advantage over Darcy’s law in as much as the equation depends mainly on the pressure decay with time, which represents the experiment setup by removing the flow rate varies with time. Initially, the method is utilized to measure the permeability of granite under high-pressure conditions (Eq. 6-7):

$$\Delta P = \Delta P_0 \frac{V_2}{V_1 + V_2} e^{-\alpha t} \dots\dots\dots (6-7)$$

$$\alpha = \frac{K.A}{\mu \text{ cg L}} * \left( \frac{V_1 + V_2}{V_1 * V_2} \right)$$

$\Delta P$  Pressure Step Difference (Pa)

$T$  Time (sec)

$K$  Permeability ( $m^2$ )

$L$  Length (m)

$V1$  Volume Upstream ( $m^3$ )

$V2$  Volume Downstream ( $m^3$ )

$A$  Pipe Area ( $m^2$ )

$\mu$  Viscosity (Pa.s)

$C_g$  Gas Compressibility (1/Pa)

The pulse decay method involves plotting pressure versus time and fitting that to a curve on a logarithmic scale. The fitting equation is then extracted, and the system permeability is calculated from that curve. Fig. 6-9 shows an example of the 6-inch sample plot and how the value was found.

These calculations were performed in detail for every sample tested in the experiments.

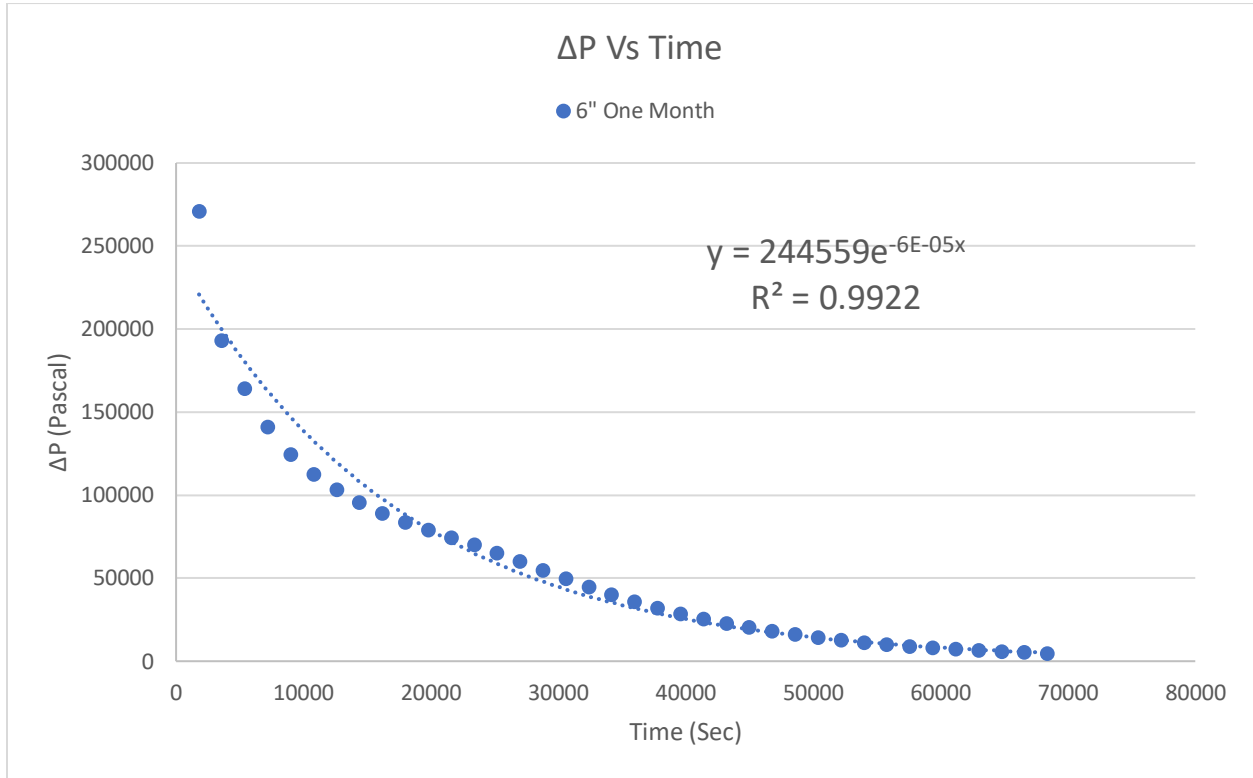


**Fig. 6-9—Pulse decay (Brace method) pressure with time.**

#### **6.4 Selected System Permeability Method**

As stated earlier, several estimations of system permeability were used for this research. All the results were considered together to select the most relevant and most applicable estimations for the experiments' data and conditions (Table 6-2 and Fig. 6-11). All the estimations were computed for all of these samples. However, for illustration, only the average results of a few of the selected pipes tested are summarized below. At least three pipes of each length were tested to yield similar results, given that cement behavior is unpredictable.

**Table 6-2—Summary of system permeability calculations by different methods for the specimens.**

	<b>Permeability (md)</b>				
	<b>Average Density</b>	<b>Average Pressure</b>	<b>Gas Escape (Darcy)</b>	<b>Modified Gas Escape</b>	<b>Pulse Decay</b>
<b>Sample</b>	<b>K (avg density)</b>	<b>K (avg)</b>	<b>K (esc)</b>	<b>K (modify)</b>	<b>K (pulse)</b>
<b>4" One Month</b>	3.36E-02	7.776E-03	9.396E-03	1.223E-02	1.081E-02
<b>4" Two Months</b>	4.66E-02	1.622E-02	1.976E-02	3.764E-03	1.081E-03
<b>6" One Month</b>	6.98E-02	2.481E-03	2.809E-03	2.563E-02	4.557E-02
<b>6" Two Months</b>	7.61E-03	4.842E-03	5.842E-03	7.610E-03	7.595E-03
<b>9" One Month</b>	1.93E-02	4.474E-03	5.393E-03	7.027E-03	1.554E-02
<b>9" Two Months</b>	3.45E-02	7.532E-03	8.031E-03	1.112E-02	9.323E-03

The system permeability for the experiments is based on the Brace (pulse decay) method, as it depends to a great extent on the behavior of the pressure with time as the main factor. The use of Brace method eliminated many errors in the gas flow rate calculation across the samples. Table 6-3 shows the results of the pulse decay method as a representation of the system permeability of the specimen of different sizes and aging time.

**Table 6-3—Pulse decay system permeability method (research-based method).**

	<b>Permeability (md)</b>
	<b>Pulse Decay</b>
<b>Sample</b>	<b>K (pulse)</b>
<b>4" One Month</b>	1.081E-02
<b>4" Two Months</b>	1.081E-03
<b>6" One Month</b>	4.557E-02
<b>6" Two Month</b>	7.595E-03
<b>9" One Month</b>	1.554E-02
<b>9" Two Months</b>	9.323E-03

The modified escaped method is the nearest to the pulse decay method. The average error between the pulse decay method and the modified gas escaped method was approximately 30%. Moreover,

system permeability calculated by Darcy's method and the gas escaped modification method was underestimated in comparison with the system permeability calculated using the pulse decay method.

The column graph of various sample sizes and aging periods and the graph of the pulse decay method show that they both follow the same trend between a month to month. The chart illustrated all system permeability calculations taken together for an overview of trends and behavior. Sample sizes are not included, as the purpose of the graph is to present all the system permeability results for the various specimen. The system permeability results show that the average pressure, average density, escaped gas, and modified escaped gas all align with the trend shown by the pulse decay method. However, there is a major difference in the results for the 4-inch specimen, although this is considered an outlier. The overall trend is the same (Fig. 6-10,6-11).

Furthermore, the one-month aging system permeability calculations for all the sample sizes are plotted in a column format showing that the highest estimation of system permeability comes from the average density method. The closest to the modified gas escaped method is the plus decay method. In the rest of this chapters, system permeability should be understood as referring to system permeability measured by the pulse decay method and the calculated outcome results.

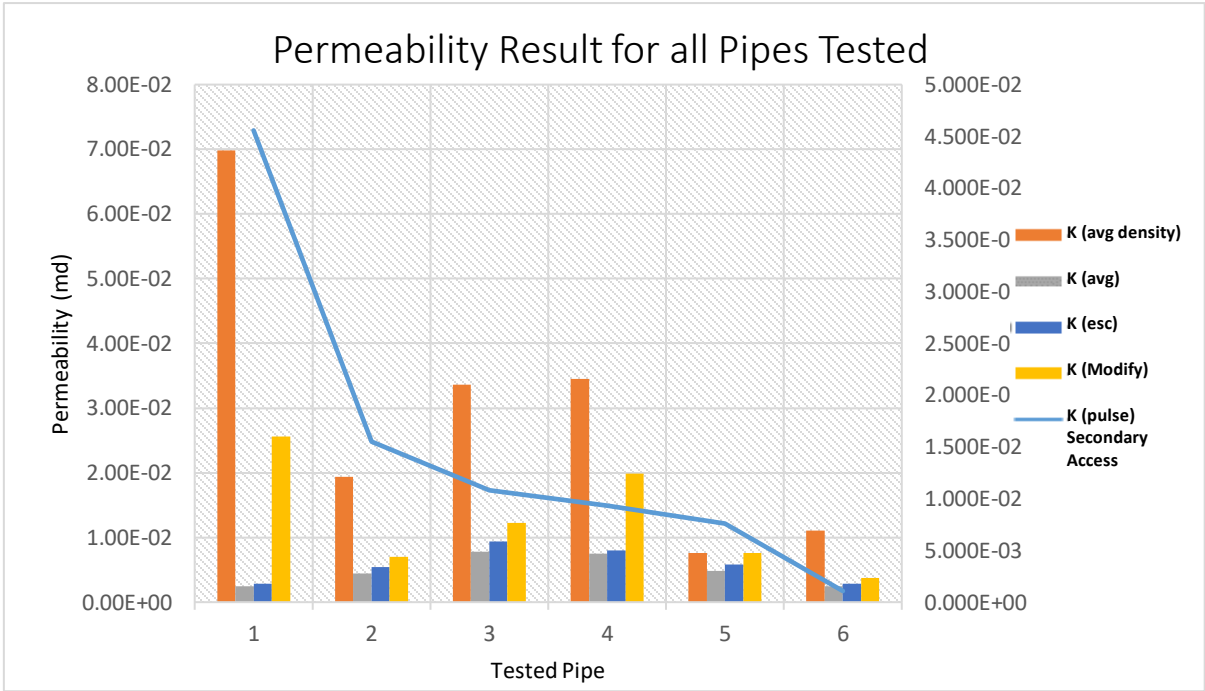


Fig. 6-11—System permeability calculations for 4-, 6-, and 9-inch- specimen at 1- and 2-month cement age.

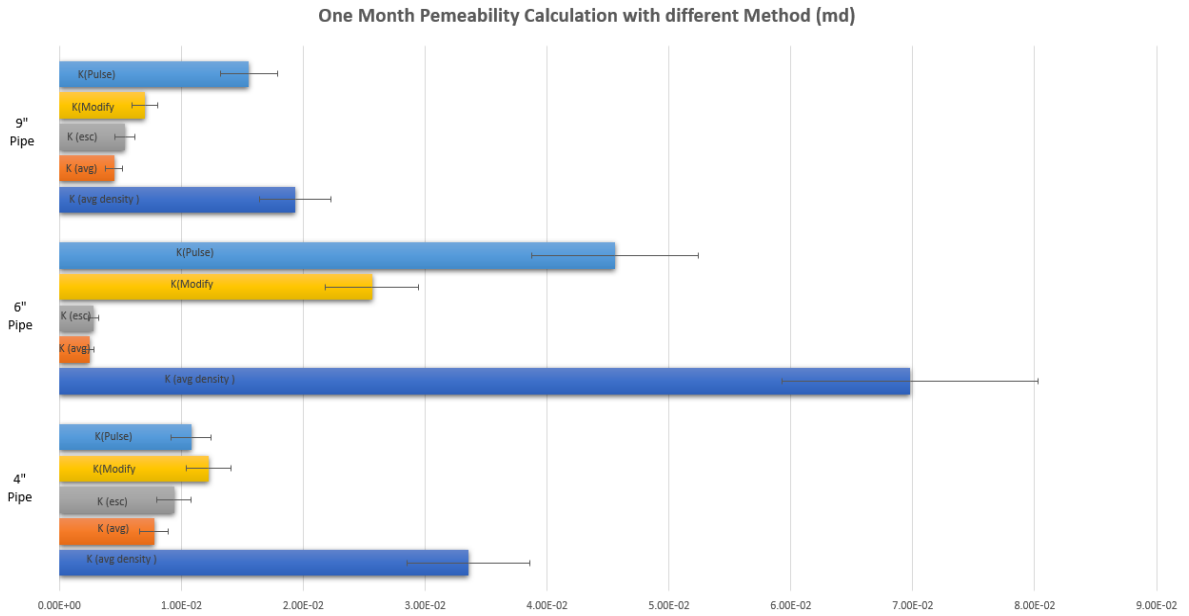


Fig. 6-10—Permeability calculations for 4-, 6-, and 9-inch-length specimen at 1-month cement age.

#### 6.4.1 Sample Length Variation Effect on System Permeability

Within the scope of these experiments, specimens of multiple lengths were tested. These specimens range from 4-, 6-, and 9-inch, aged for at least a month.

Table 6-4 shows the system permeability of the 6- and 9-inch specimen using the pulse decay method. Cement pipes from the 4-inch were not included, as these did not fit the trend line and were scattered. Therefore, the comparison between the 4-inch and 6-inch samples was not easily fitted. However, as an overall trend in terms of the data, most of the experiments had a trend whereby increasing specimen length is associated with a higher probability of decreasing system permeability (Fig. 6-12).

**Table 6-4—Comparison of 6- and 9-inch-specimen at one- and two-months cement age.**

		Permeability (md)		Permeability (md)
<b>6" One Month</b>		4.557E-02	<b>6" Two Months</b>	7.595E-03
<b>9" One Month</b>		1.554E-02	<b>9" Two Months</b>	9.323E-03

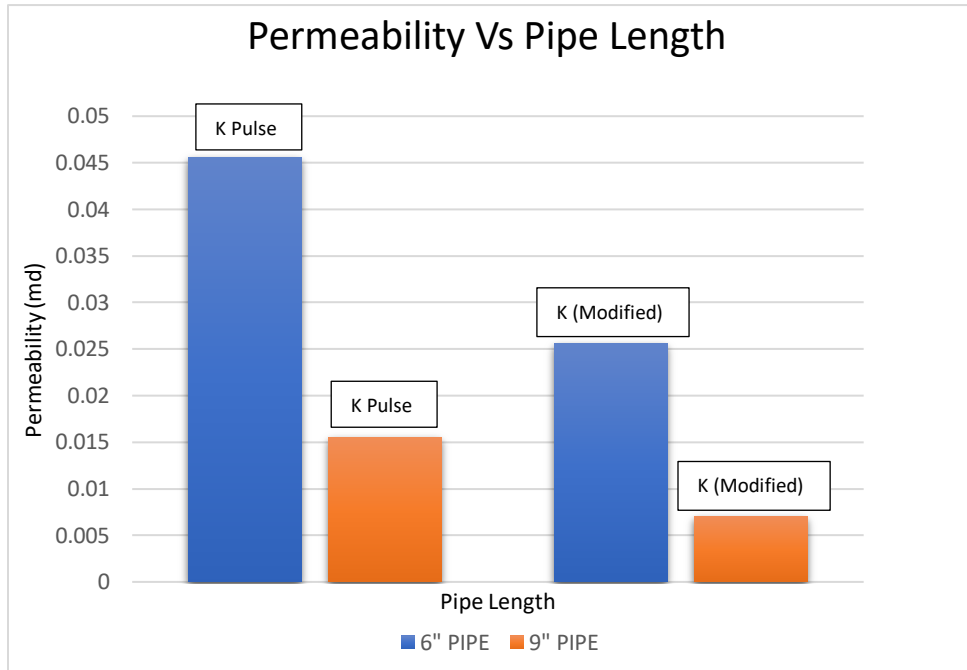


**Fig. 6-12—Comparison of system permeability with two methods for 6- and 9-inch-length pipes.**

#### **6.4.2 Sample Age Variation Effect on Cement System Permeability**

The first factor investigated is the changes in the system permeability calculations in the aging process of the cement. As an example of these changes, the system permeability of the 6-inch specimens sample decreased at least four times with only one month of cement age (Fig. 6-13). Most of the other experiments showed the same trend of an extreme reduction in system permeability during the short period of one month of aging. However, the one exception was the sample with 4-inch specimen, for which the results were inconsistent. It may be that these results indicate that compaction of cement in the smaller cemented pipes is not enough. Also, water segregation from the cemented pipes might be more prominent since the cemented pipes are kept vertically.

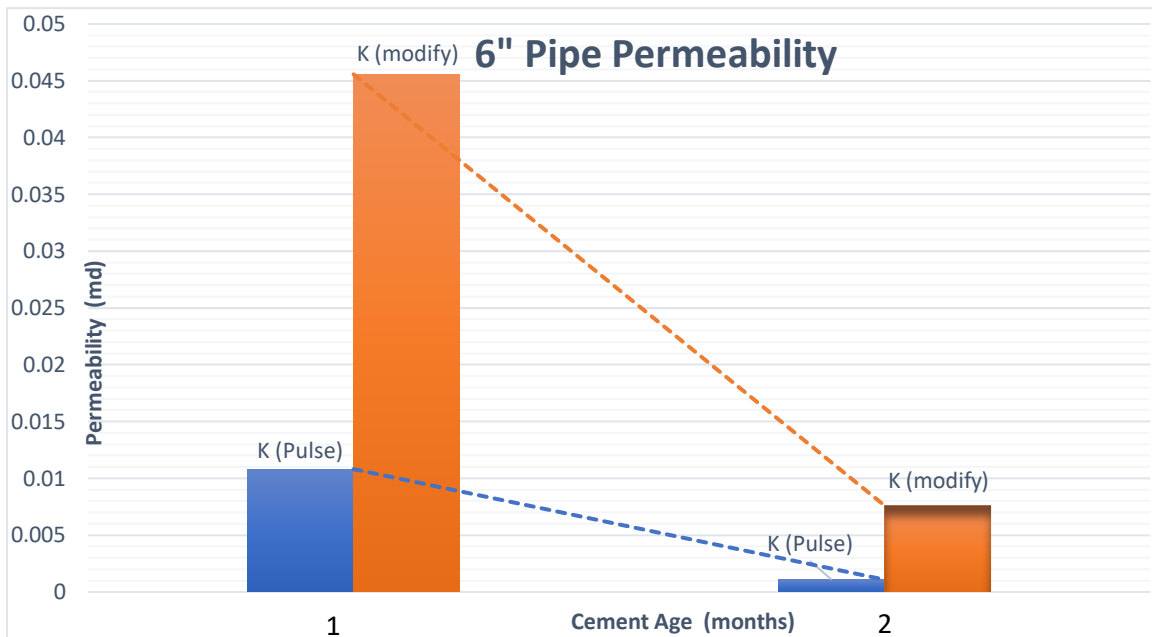


Fig. 6-13—Comparison of system permeability with two methods at 1- and 2-month cement age.

Therefore, the overall conclusion on changes concerning system permeability for the cement hydration is that cement age plays a vital role in determining the extent to which such changes occur. The following plot of specimen shows the calculated system permeability of all the samples over time (Fig. 6-14 and Table 6-5).

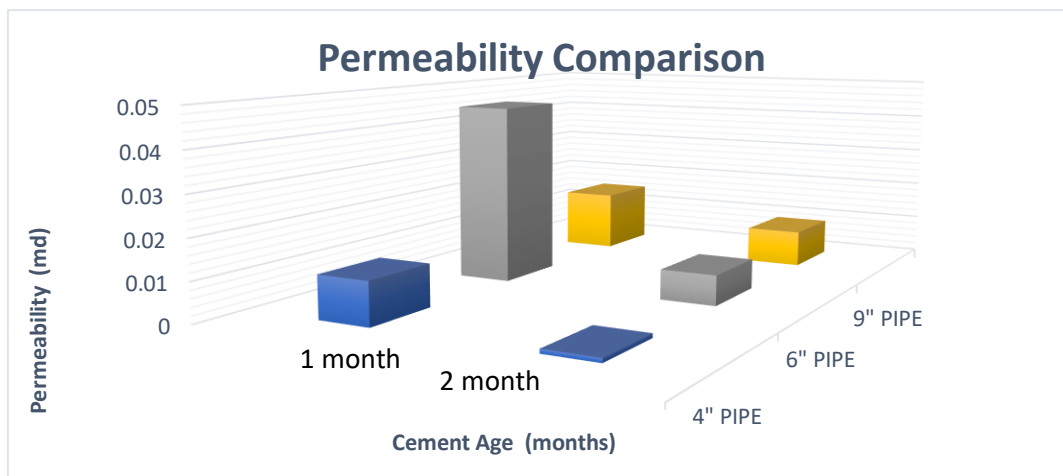
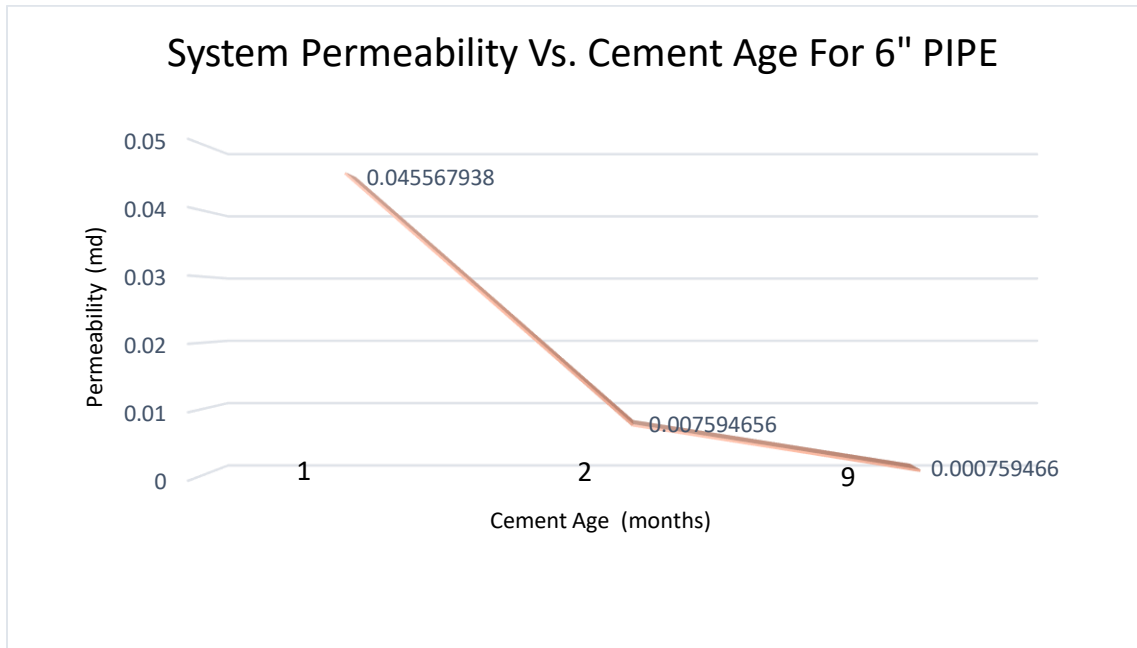


Fig. 6-14—Comparison of system permeability at one- and two-months' age and length of 4, 6, and 9 inches.

**Table 6-5—Comparison of system permeability (md) at one- and two-month cement age.**

	4"	6"	9"
	Cemented Pipe	Cemented Pipe	Cemented Pipe
Permeability (md)			
One Month	0.01081	0.045568	0.015539
Two Months	0.001081	0.007595	0.009323

Further investigations into the aging process and the continuous hydration of the cement properties for the sample at two months' aging showed similar results. At nine months of aging, the results also showed system permeability decrease in the range of 300–1000% (Fig. 6-15).



**Fig. 6-15— Specimen6-inch pipe system permeability calculation at different cement ages (1, 2, and 9 months).**

Both samples were of a magnitude of  $10^{-2}$  md, and when aged and hydrated for an additional month, i.e., month two, the magnitude changed to  $10^{-3}$  md.

### 6.5 Cement Gap and Behavior

One of the major objectives of this research is to determine the long-term behavior of cement in different aspects, including in regard to changes in the microannulus, system permeability, and possible further shrinkage. The long-term conditions were achieved principally by the hydration of the cement during the aging process. This means that the sample was wet-drying in water throughout the entire experimental period, including when the pressure test was performed.

A further equally consequential objective is to quantify the gaps between the steel pipe and the cement. The microannulus path inside the specimens was investigated by cutting the pipe length to one-inch pipe specimens. The specimens were then placed under a microscope described in the measurement setup. For each one-inch specimen, the gap was measured at various degrees around the specimen cross-section surface. Eight measurements at least were taken for each side of the one-inch specimen (front and back). An example is shown in Fig. 6-16.

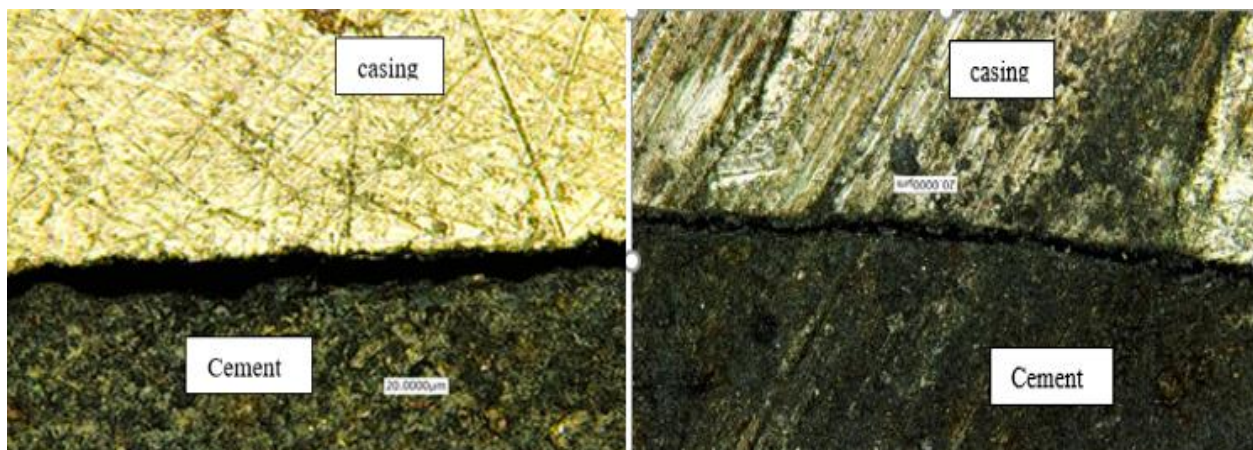
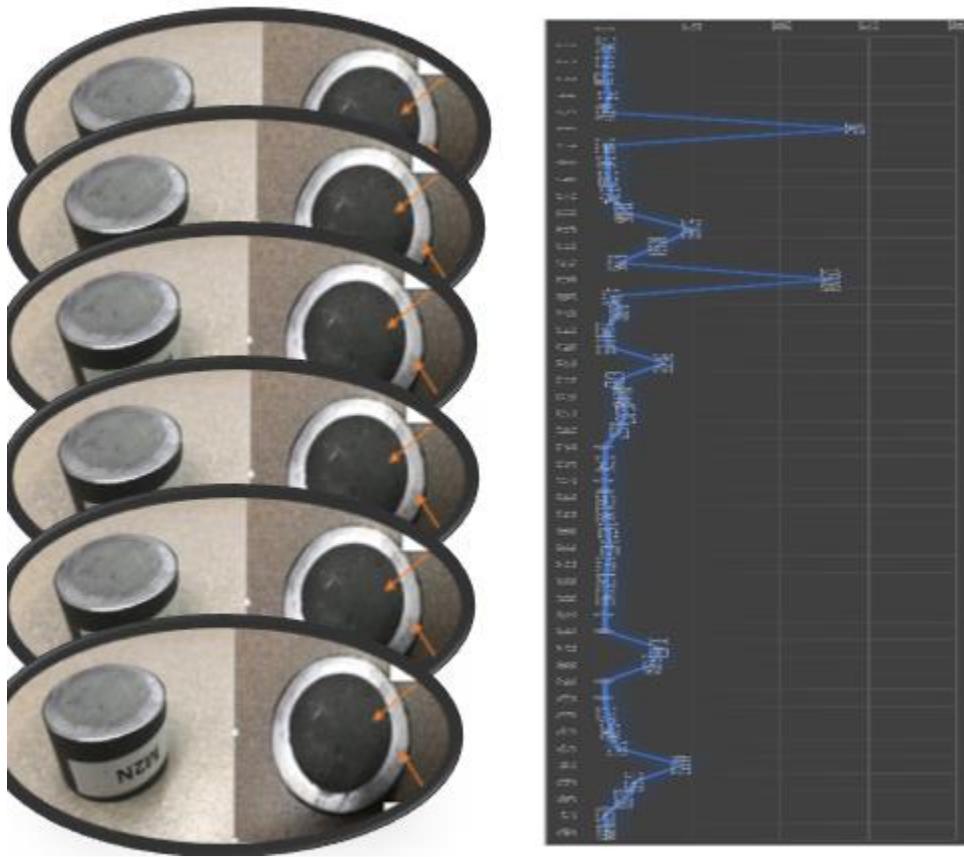


Fig. 6-16—Cement-casing gap (20-micrometer scale) (Al Ramis et al. 2020).

Since specimen gaps measured were not uniform, the results divided into minimum, maximum, and average. Then, the controlled gap measured was considered the minimum gap out of the maximum in each specimen. Fig. 6-17 and Fig. 6-18 show the complexity of the gap behavior across the specimens.



**Fig. 6-17—Gap measurement across the specimen.**

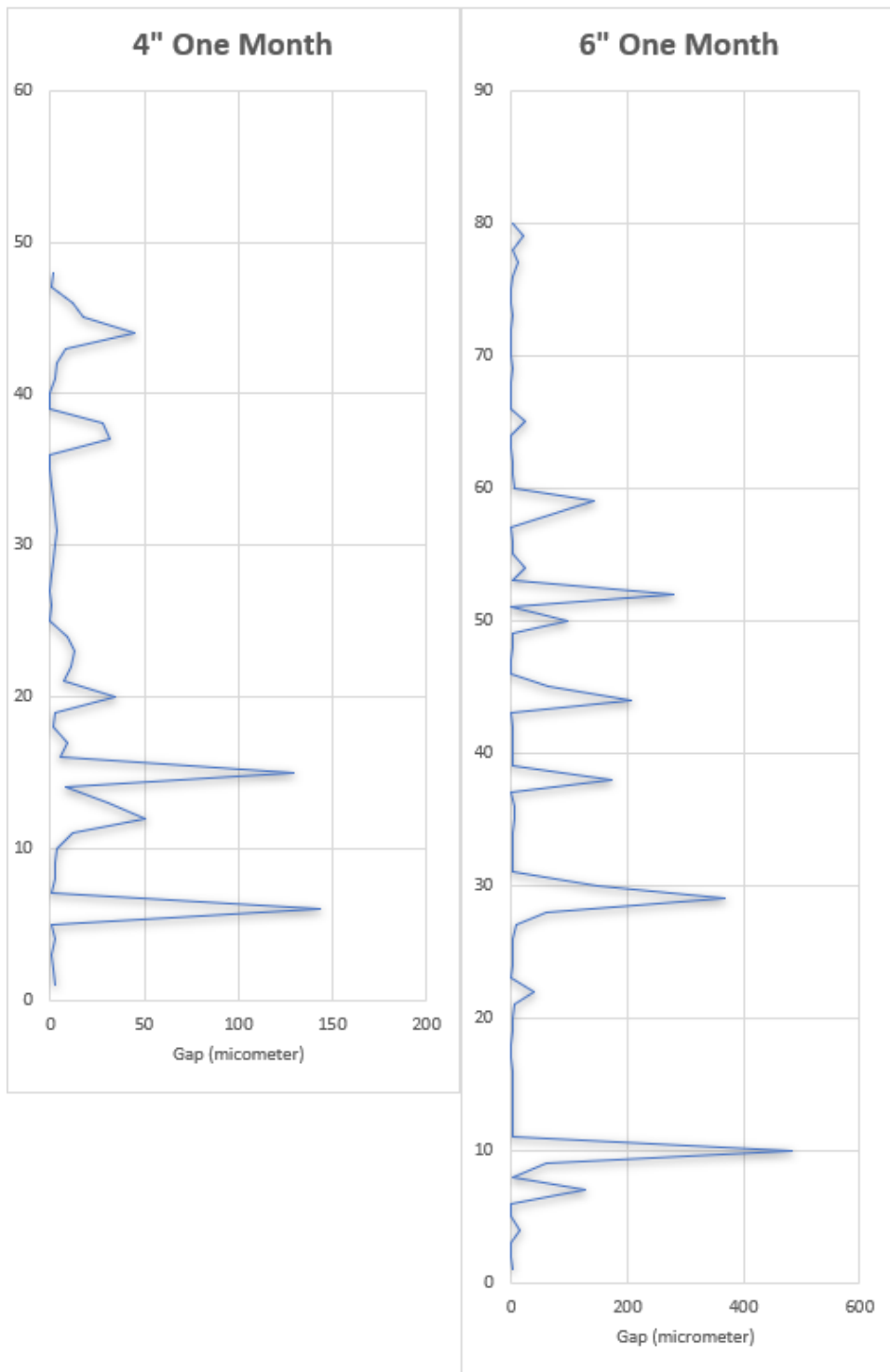


Fig. 6-18—Pipe length of 4-inch and 6-inch gap measurement across the points of measurement.

Table 6-6 summarizes all the calculations for the gap across the specimen: the minimum, maximum, average, and minimum gap from the maximum in each cut and the maximum from the minimum.

**Table 6-6—Summary of the gap measure across the specimen cut.**

Summary	One Month			Two Months		
	Micrometer					
	4"	6"	9"	4"	6"	9"
<b>Minimum Length Overall</b>	0.4	0.3	0.1	0.5	0.2	0.4
<b>Maximum Length Overall</b>	143.0	484.4	384.0	224.6	201.0	206.7
<b>Average Length Overall</b>	13.4	31.6	20.0	13.6	14.5	3.8
<b>Minimum from Maximum</b>	3.4	21.8	0.4	1.9	0.4	0.8
<b>Maximum from Minimum</b>	2.6	2.2	65.8	1.5	99.4	206.7

Note that the controlling gap was the smallest gap opening, excluding the 0 gaps (no gap) across the 1-inch specimen. As the flow travels across the easiest path in each specimen, the gas will go through the maximum opening across specimens. However, the controller among these specimens is the one that restricts the flow, i.e., the minimum of the maximum.

The gap size measurements were captured at 0°, 45°, 90°, 135°, 180°, 270°, and 315° around the circle (more angle locations in some samples) in each side of the 1-inch specimen (Fig. 6-19).

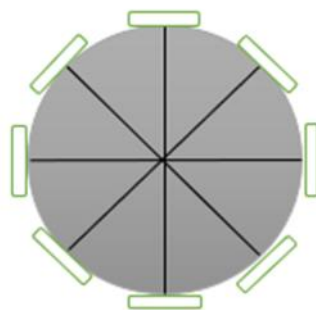


**Fig. 6-19—Sketch of the points of measurement.**

It was apparent that the microannulus (gap) did not maintain a consistent value over the length of the sample. Not only did the size of the gap vary with the angle even in the same cross-section, but a comparison of the gaps for different cuts showed a range of gap distances as well. More importantly, the gaps were not found to be in a straight line: The microannulus location changed throughout the cross-section of the specimen, thereby suggesting that the flow from a gas leak follows a pathway that is evidently tortuous in nature. That is, the connected path across the specimen was not a straight line but one that meandered around the circumference of the specimens.

These results are presented as a star-like graph with the long side of the cylinder shown as cut perpendicular to the circumference and the center of the circle (Fig. 6-20). The specimens were then opened and rotated inward so that the steel pipe is placed in the center of the graph. The representation aims to show how the openings of the microannulus change in location and in size. Whereas the microannulus is connected in some areas, it is disconnected in others. For instance, a small path that begins at  $225^\circ$  becomes a larger path for this particular specimen at the  $270^\circ$  marks. After that, the direction of the microannulus moves to  $225^\circ$  but with a medium-size opening. This pattern and behavior were found across all the specimens. It is clear from the visual representation that the behavior of the microannulus does not reflect a straight-line path.

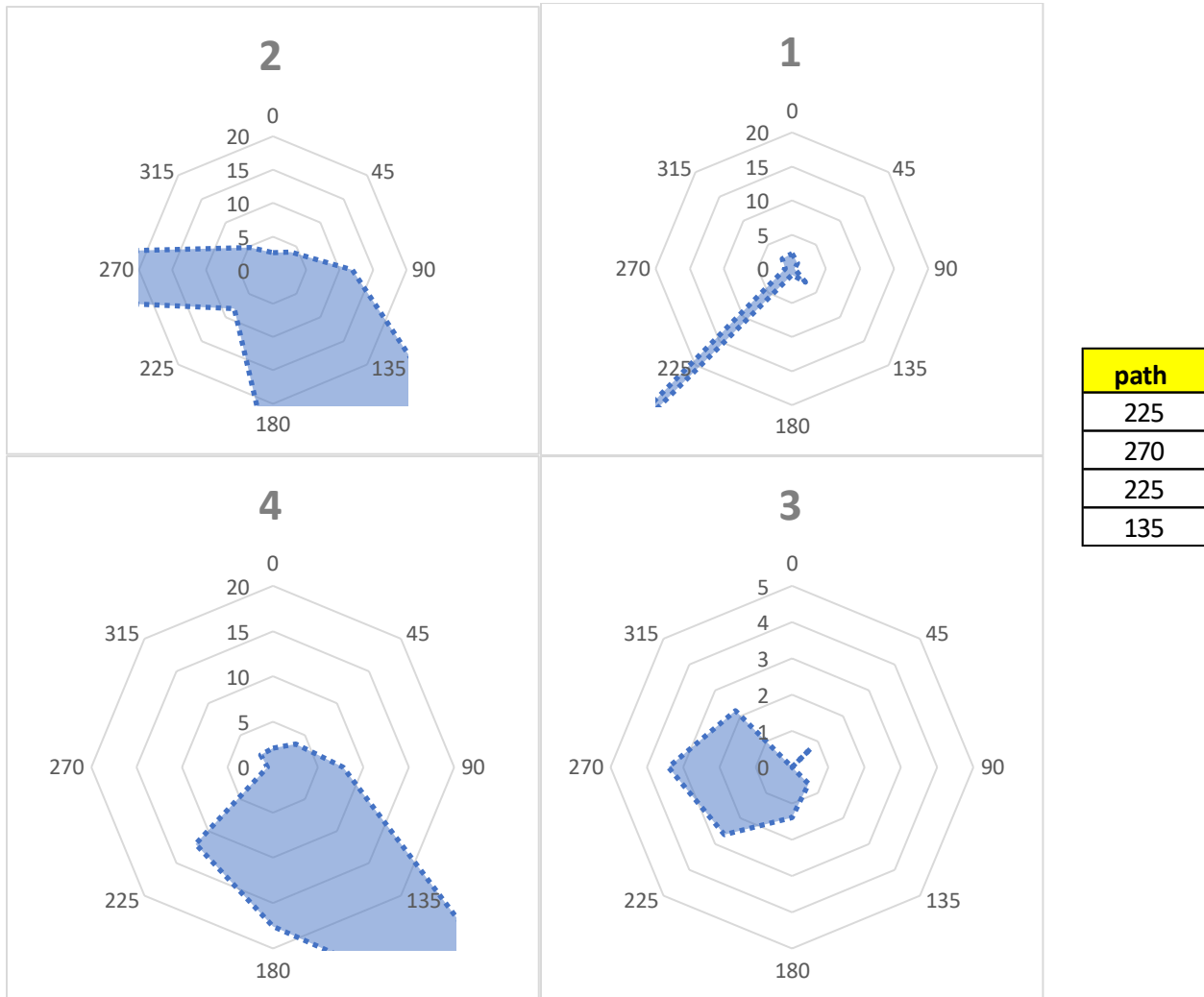


**Fig. 6-20—Gap representation of 0-20 microns.**

### 6.5.1 Sample Length Variation Effect on the Microannulus

Given that the flow path indicated anything but a straight line, a new variable referred to as “effective length” was introduced. The definition of the effective length is the actual diagonal flow path inside the cement. This tortuosity means that the effective length is longer than that of a straight line. The cylinder geometry estimated the effective length.

Specifically, the effective length was calculated by a straight line that goes diagonally from the side of the opening from the front to the side of the opening from the back of the 1-inch specimen. Therefore, the measurement of a triangle was drawn across the two open gap spaces (Fig. 6-21 and Table 6-7).



**Fig. 6-21—Effective length of gas flow across the sample.**

**Table 6-7— Effect length range calculated.**

Length	Effective Length
in	in
4	5.6–6.217
6	8.4–9.28
9	12.7–15.42

The volume was determined using established methods, defined at the beginning of the chapter, for the flow rate inside the cement. The methods used include the volume escaped, the average density, and the average pressure methods.

### 6.5.2 Measured Gap Versus Literature Equation

The gap was estimated by Aas et al. (2016) equation. The equation connects the flow rate of the leakage to the radius of the opening of the microannulus.

To compare the measured result for the opening of the microannulus in the samples, the equation and average density method were used to calculate the leakage through the microannulus as defined by Aas et al. (2016) and as shown in Eq. 6-6:

$$Q = \frac{\pi R_c \Delta P}{6\mu L} R^3 \dots\dots\dots (6-6)$$

Where

$Q$  = Flow Rate ( $m^3/s$ )

$R_c$  Casing Radius (m)

$R$  Microannulus Gap (m)

$\Delta P$  Difference in Pressure (Pa)

$\mu$  Fluid Viscosity (Pa. s)

The results for the gap opening calculation through the different flow rate calculations from the same method of the system permeability estimated are summarized in (Table 6-8).

A visual representation of the data is provided in (Fig. 6-18) to show the results clearly. The gap calculated with the system permeability calculated is plotted as well. It is clear that the gap is directly proportional to the system permeability.

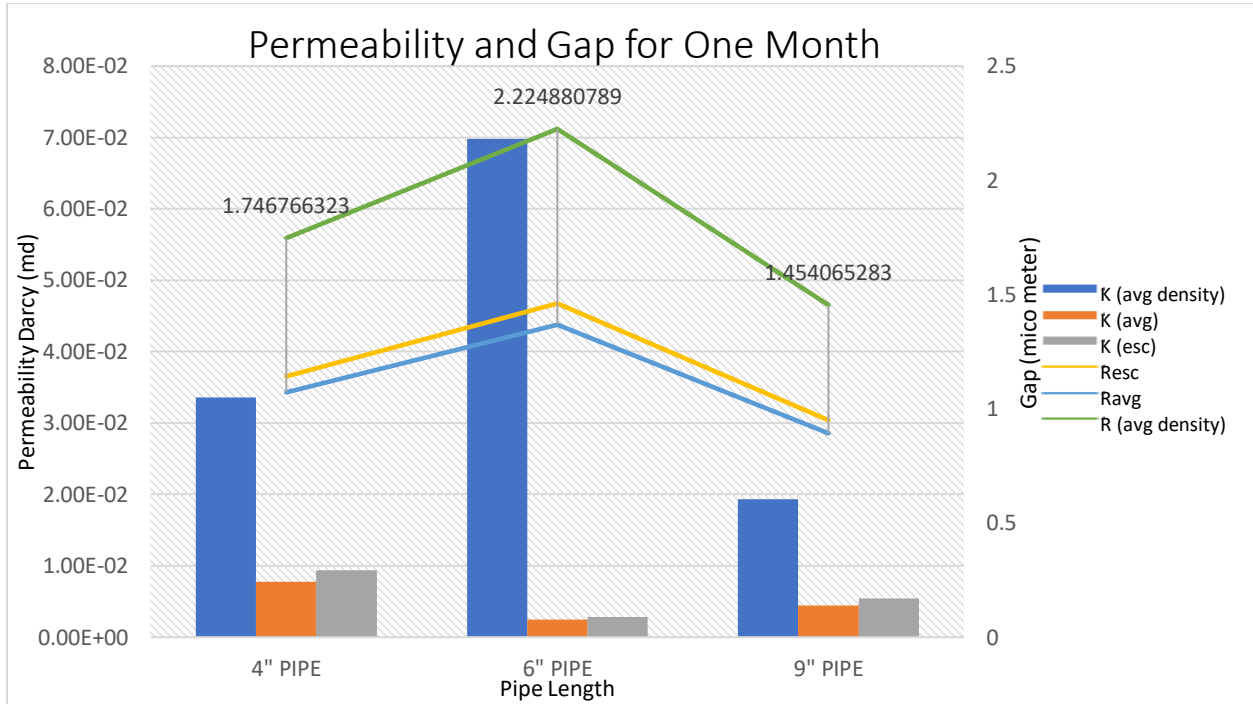
**Table 6-8—Summary of the gap calculated by flow rate (Darcy, ave. pressure, ave. density).**

		One Month			Two Months		
		4" PIPE	6" PIPE	9" PIPE	4" PIPE	6" PIPE	9" PIPE
Leakage microannulus	<b>R<sub>esc</sub> μm</b>	1.14	1.46	0.95	0.77	0.92	1.11
	<b>R<sub>avg</sub> μm</b>	1.07	1.37	0.89	0.74	0.94	1.08
	<b>R<sub>avgdensity</sub> μm</b>	1.75	2.22	1.45	1.22	1.60	1.80

### 6.6 System Permeability Relationship with the Microannulus Measured

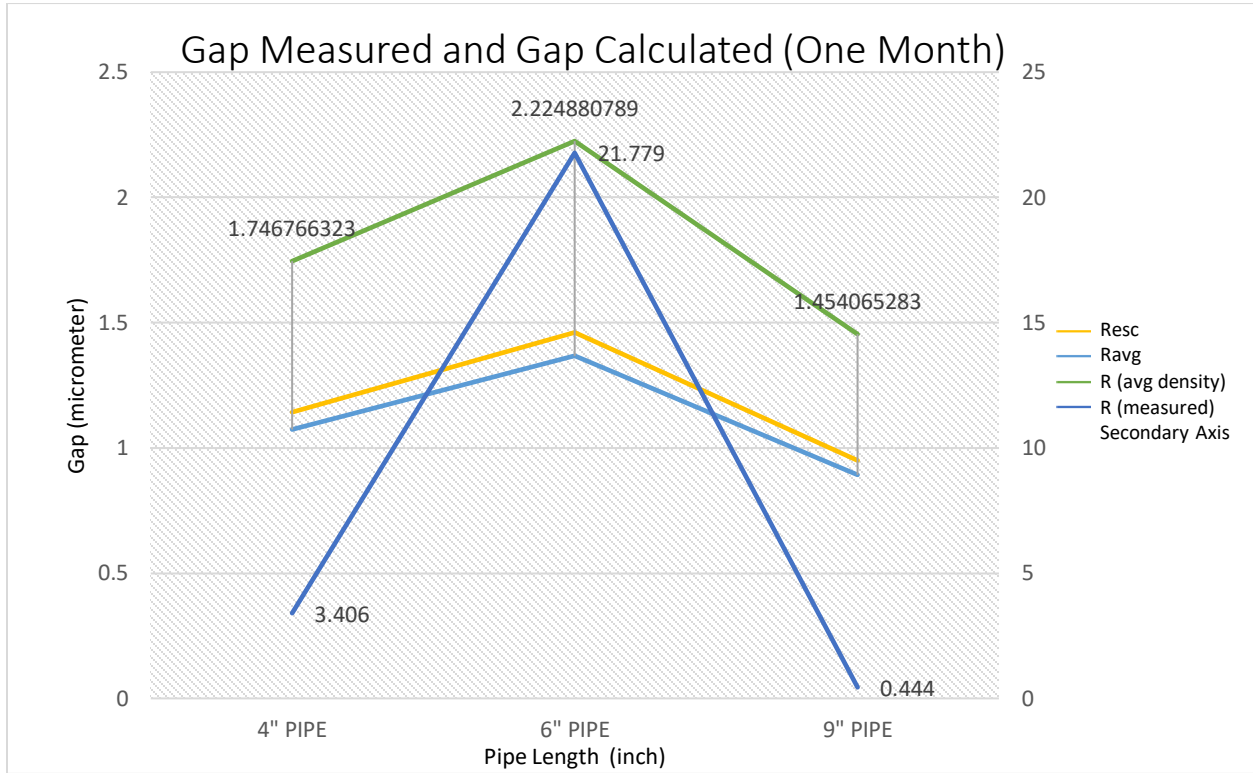
The system permeability and the gap opening follow the same trend (Fig. 6-22): when the gap increases, so does the system permeability. This correlation shows that the cement system permeability is directly dependent on the microannulus and the extent to which it is connected over the length of the sample. This finding is in agreement with the earlier finding according to which the effective length and the microannulus follow a meandering path rather than a straight line.

Combining the finding of a meandering microannulus with the system permeability correlation results supports the theory that leakage occurs from the microannulus. The porosity of the cement itself may have a minimal effect on the flow rate of the gas in the cement at the pressure tested, as the trend arises predominantly from the gap opening—an observation that is explored in more detail in the next section.



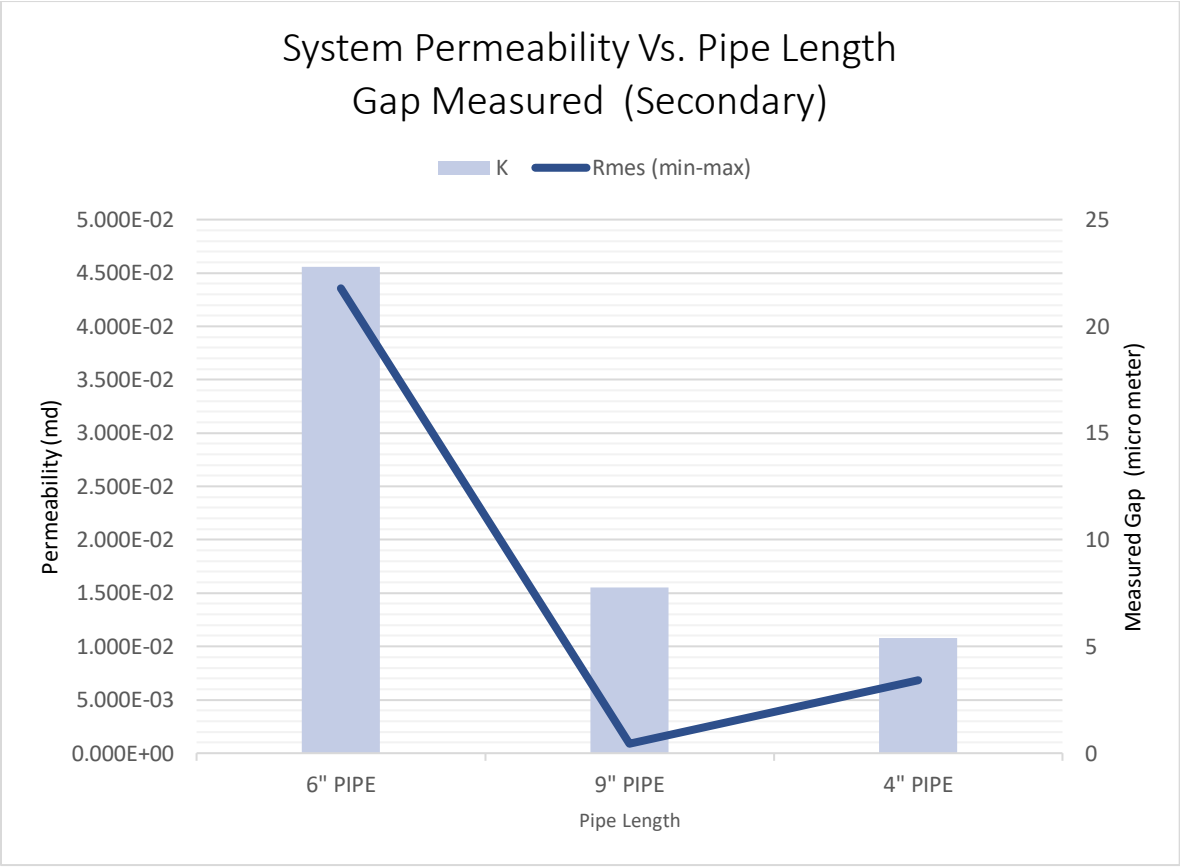
**Fig. 6-22—Comparison of pipe length (4-, 6-, and 9-inches) across system permeability and gap.**

Fig. 6-23 shows the gap measured and the gap calculated from the Aas method plotted together. The gap calculated and the gap measured in all the specimens tested move in the same way and show the same trend, although the gap measured shows a significant underestimation of the gap calculated by Aas et al. (2016). The values of the gap measured were in the range of 0.44 micrometers to 21 micrometers, whereas the gap calculated values were in the lower range of 1.45 to 1.746 micrometers.



**Fig. 6-23—Comparison between the measured gap and the calculated gap for 4-, 6-, and 9-inch-length pipes at 1-month cement age.**

The gap measured was found to be more correlated with the system permeability value obtained by the pulse decay method, thereby indicating that the flow is mainly through the annular gap between the cement and casing (Fig. 6-24).



**Fig. 6-24—System permeability calculated with the gap measured for 4-, 6-, and 9-inch-length pipes.**

**6.7 Effect of Application of Pressure Before Complete Hardening**

One more set of experiments was conducted in the lab. The major objective of the experiments was to compare cement at early setting time with cement after two months of aging. During the two months of curing, the cement was continuously wetted with water. The sample was first put under pressure of 50 psi after only 24 hours, at which point it is still fresh paste.

Next, the same sample was tested at the end of two months. The pressure measurements were recorded, and then the pulse decay method was used to calculate the system permeability value.

Interestingly, the results of the two specimens showed very obvious bubble-like behavior on the cement surface (Fig. 6-25).



**Fig. 6-25—Bubbles appear in the cement surface after cured if tested before hardening.**

The system permeability results of the early test conditions were compared. The summary shows that the system permeability increases for the specimens tested at the early stage of cement age and the gap measured as well.

The system permeability results of the calculation and a representation of the two specimens are presented in Fig. 6-26.

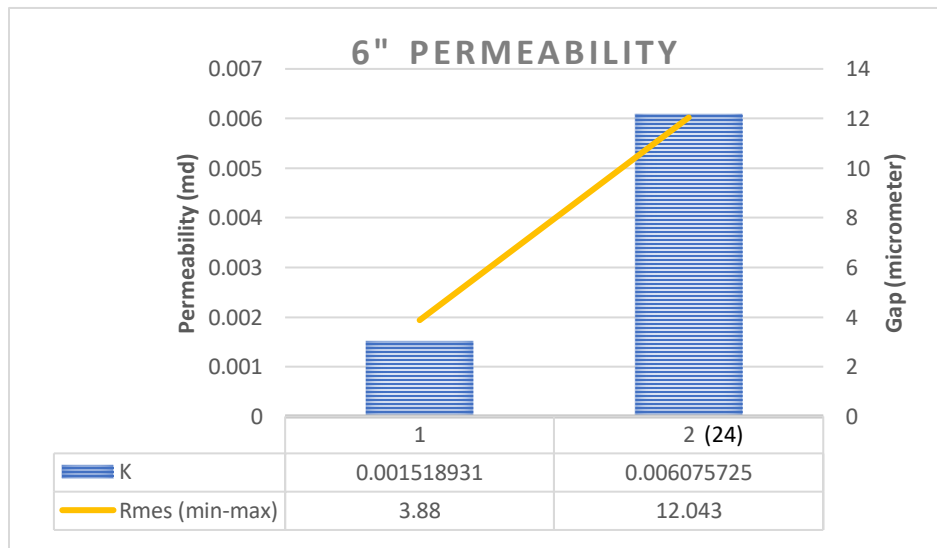


**Fig. 6-26—System permeability increment for cement is tested while curing with gap measurement.**

Fig. 6-27 represents the data for the measured gap increase with the increase in system permeability and shows a clear correlation between them.

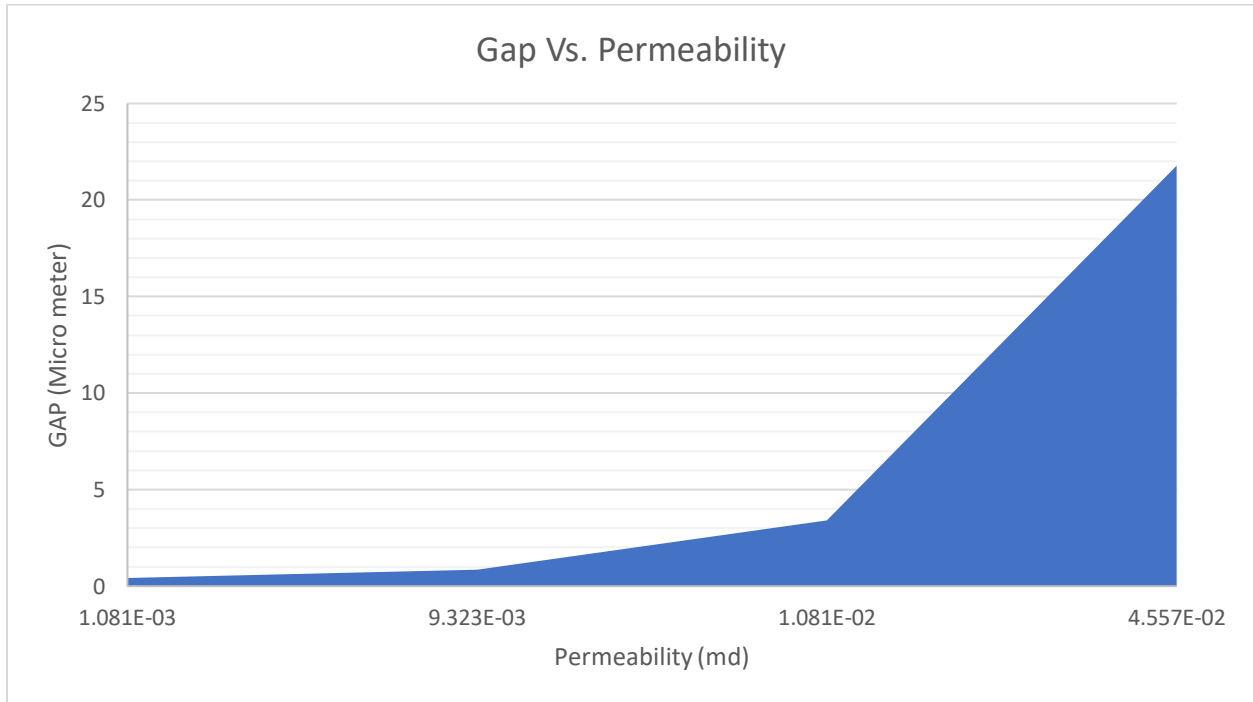


**Fig. 6-27—Gap measured with system permeability values calculated.**

### **6.8 Non-Wetted Cement Effect on Gap (Shrinkage)**

The effect of hydration on the gap measurement was investigated by the 1-inch specimens cut with the cement age. However, this time, the aging process did not involve wetting the samples with water. The samples were left to dry out and exposed to environmental air.

These tests were performed over a long-term period, i.e., an entire year. The gap was measured before and after dehydration using a microscope and high-definition camera. Remarkably, the samples that had zero openings and a non-existing gap showed a microannulus after a year of drying out. The microannulus measurement was between 1.7 micrometers up to 5 micrometers for the samples that had exhibited no gap at the beginning. The gap follows a uniform pattern over the

gap measured before the dry-out. This observation proves that the pressure creates a microannulus radially across the cement–casing contact and that shrinkage contributes to the microannulus as well.

The specimen was tested, then gaps were measured across the specimens. After that, the specimens were left to dry out (out of water). After one year, the gaps were measured again. The result proves that the cement still reacts chemically even after two or three months. Further, the gap was quadrable in some cases (Table 6-9) (Fig. 6-28).

**Table 6-9 Summarize some points of measurement for 6-inch-length pipe two months (wet) and one year (dry)**

6 inch after Two Months (Wet) then after One Year (Dry)											
	2 Month	1 Year		2 Month	1 Year		2 Month	1 Year		2 Month	1 Year
Degree	Size $\mu\text{m}$	Size $\mu\text{m}$		Size $\mu\text{m}$	Size $\mu\text{m}$		Size $\mu\text{m}$	Size $\mu\text{m}$		Size $\mu\text{m}$	Size $\mu\text{m}$
0	0	3.915		0	1.744		0	1.744		0	3.611
45	1.808	6.826		1.893	1.8		1.893	1.129		0	4.201
90	0	4.986		1.417	2.341		1.417	2.341		0	4.412
135	1.8	6.442		0	3.682		0	3.682		15.785	17.81
180	0	4.5		7.782	7.87		7.782	7.87		19.305	23.199
225	0	4.854		0.708	3.91		0.708	3.91		23.757	11.808
270	0	4.987		0.757	5.002		0.757	5.002		0	3.504
315	0	4.74		0	2.357		0	2.357		0	2.167

During the waiting time of the year, six specimens were examined after one and two months for gap formation. The examination showed no clear gaps in the system. Therefore, changes in the gap and gap formation process are possible even after two months. The cement–steel contact continued to develop even after the two-month mark. Therefore, for plug and abandonment

purposes, pressure tests after only one or two months are not indicative of the long-term behavior of gas flow and leakage with gap formation.

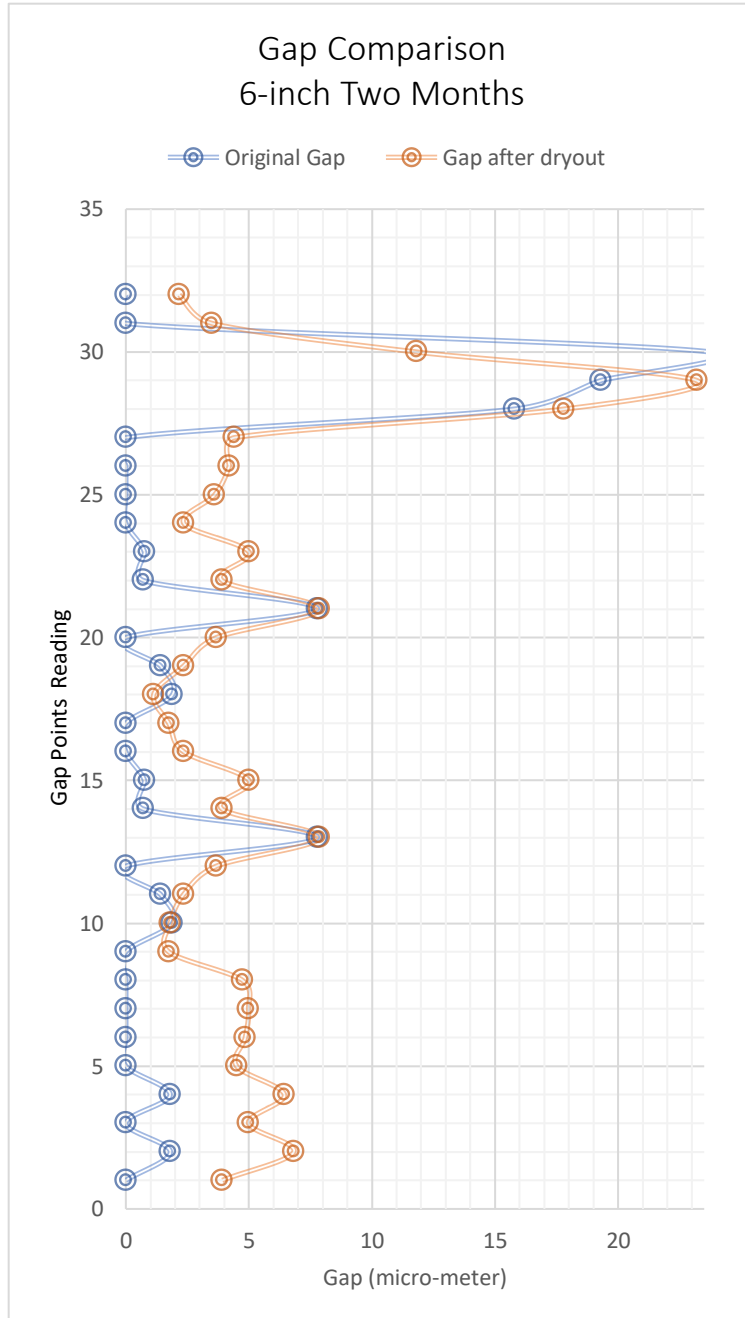


Fig. 6-28—Plot of gap increase after dry-out (2 months-1 year)

Graphically representing the data reveals additional insights. For example, the points that showed zero gaps are now slightly open (Fig. 6-28). Gaps magnitude increase were in the same range for all zero-starting gaps. However, the points that originally showed high gaps (microannulus) stayed the same. The shrinkage factor of the cement could explain this change in the original zero points. The gap increased 4-fold with 15% errors for most of the measurement points.

## **6.9 Statistical Analysis**

In this section, an overview of the statistical consideration of various data points is presented. The SAS and Python programs were used to evaluate the data, with a particular emphasis on the gaps measurement in the micrometer space between the steel and the cement. The gap data point consisted of over 736 points collectively for all the specimen performed rigorously using a microscope and high-definition pictures.

The objective of this statistical analysis is to understand the spread of values and the applicability of each finding. Length and age were considered for the effect of changes in the microannulus.

### **6.9.1 General Data Statistics**

Most of the specimen were aged for 1 to 3 months. The mean value of the gaps across all the recorded data points was 15.2 micrometers. The spread of the data is quite large, as the standard deviation shows 46 micrometers. Many of the gap measurements were of a zero value, as, shown in the mode (Fig. 6-29 and Table 6-10).

**Table 6-10—Summary of the statistical gap results.**

Gap Basic Statistical Measures $\mu\text{m}$			
Location		Variability	
Mean	15.23	Std Deviation	46.65
Median	0.42	Variance	2176
Mode	0	Range	484.4
Skewness	5.1	Interquartile Range	4.41

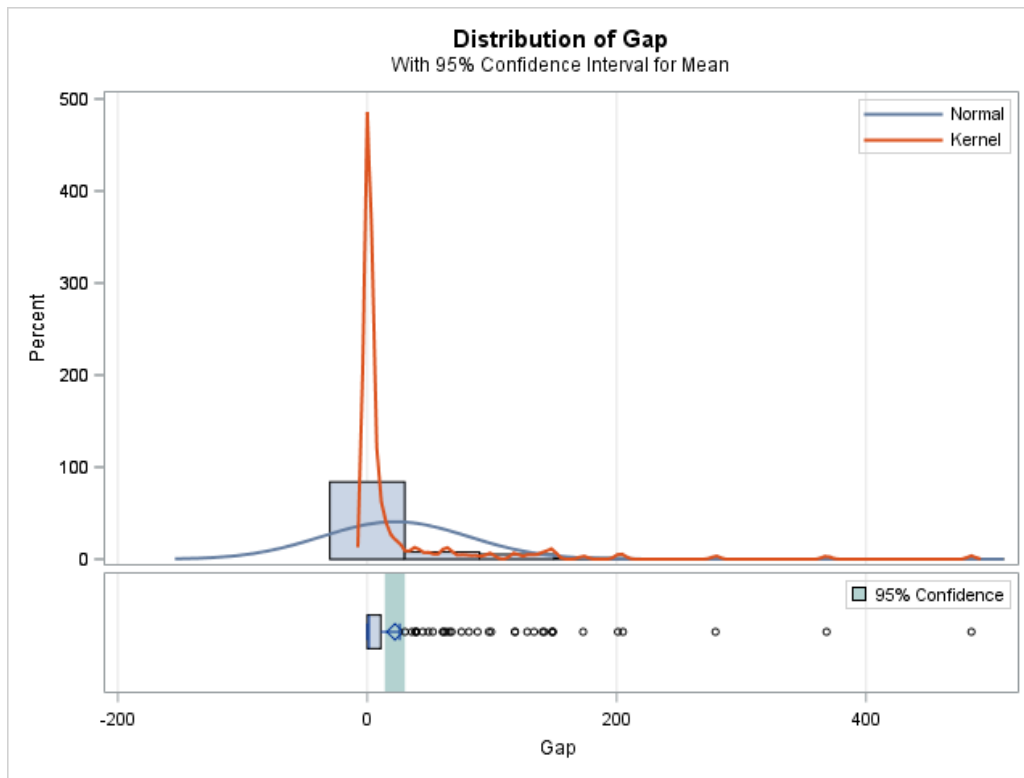


**Fig. 6-29—Gap distribution for all samples tested.**

The lower 50% quartile consisted of zero-gap values. Therefore, the curve skewed to the left with a skewness of 5.09. The interquartile range was 4.4 micrometers, which measured the bulk value across all the samples (Table 6-11).

**Table 6-11—Confidence intervals of all gaps.**

Mean	95% CL Mean		Std Dev	95% CL Std Dev	
15.23	11.86	18.61	46.65	44.39	49.17

Some points were deemed outliers: i.e., those found in only one of the cemented sample size pipes and those with a very high value of more than 300 micrometers with a maximum of 484 micrometers.

The plot shows the gap measurement count across all the samples with the time indicated for 30 micrometers and below (Fig. 6-30).

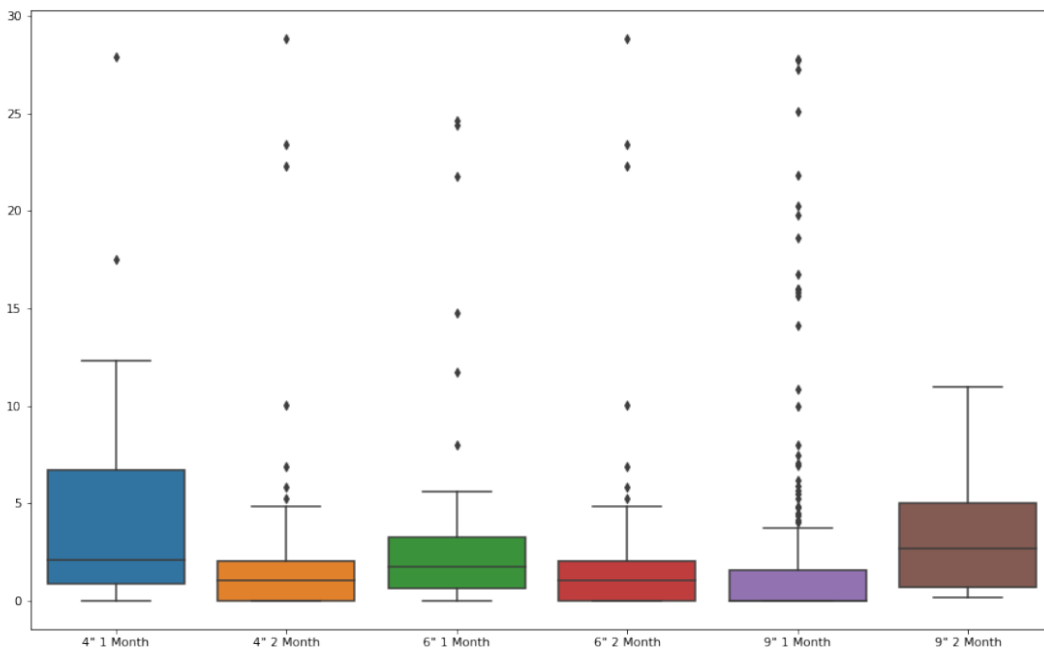


**Fig. 6-30—Gap count (less than 30 micrometers) for all the pipes with age and length.**

The Pearson correlation for the entire dataset shows straight-line correlations ignoring all other factors between the variable (Table 6-12). However, correlations, especially for age, can be correlated indirectly with a non-linear representation.

**Table 6-12—Pearson correlation for all gaps measured.**

<b>Pearson Correlation Coefficients, N = 736</b>			
<b>Prob &gt;  r  under H0: Rho=0</b>			
	Gap	Age	Length
Gap	1	0.0289	0.2018
Age	0.0289	1	.0002
Length	0.2018	0.0002	1

The upper value of the confidence interval for the 4-inch specimen showed a value of 20 micrometers for both times (1,2 months), which suggests no major change in the gap after two months. However, the 6-inch and 9-inch specimen each showed different values between the one-month and the two-month marks. For example, in the first month for the 6-inch specimen , 95% confidence of the upper interval was 49  $\mu\text{m}$  but, for two months it was 26  $\mu\text{m}$ , which confirms the conclusion of the results from the method used for the gap measurement. The lower and upper confidence intervals for all the specimen are shown in Table 6-13.

**Table 6-13—Mean confidence interval for all pipes tested (4-, 6-inch, and 9-inch length).**

<b>Variable</b>	<b>N</b>	<b>Mean</b>	<b>Std Error</b>	<b>Lower 95%</b>	<b>Upper 95%</b>
				<b>CL for Mean</b>	<b>CL for Mean</b>
4" One Month	48	13.39	4.12	5.11	21.67
4" Two Months	48	13.57	6.11	1.28	25.86
6" One Month	80	31.63	9.14	13.43	49.83
6" Two Months	104	18.37	3.99	10.45	26.29
9" One Month	224	20.00	3.61	12.89	27.11
9" Two Months	192	3.85	1.38	1.13	6.57

### **6.9.2 Statistical Prediction of the Gap for the 6-inch Pipe**

The increase in the length (in) was estimated (excluding the data for the 4-inch-pipe) to decrease the gap by 0.66 micrometers. For the 6-inch specimen, therefore, the estimated gap will decrease

by 0.66 micrometers if the length increases by 1 unit of 1 inch. This result is not significant, as the P-value is greater than 0.05, and the data pool is only for 6-inch cement pipe (Table 6-14).

**Table 6-14—Effect of pipe length on the cement gap for the 6-inch-length pipe.**

Parameter	Estimate	Standard	T Value	Pr >  t
		Error		
Intercept	10.05682	10.69952418	0.94	0.4166
Length	-0.66792	1.45602082	-0.46	0.6776

For the gap measured with the cement age, if the cement age increases by 1 month the gap will decrease by 3.13  $\mu\text{m}$ . This result is significant, as the P-value is less than 0.05 (Table 6-15).

**Table 6-15—Effect of pipe length on the cement gap for the 6-inch-length pipe.**

Parameter	Estimate	Standard	T Value	Pr >  t
		Error		
Intercept	20.47716	2.94585411	6.95	<.0001
Age	-3.131562	1.43077995	-2.19	0.0289

### 6.9.3 Statistical Prediction of the Gap for All specimens

In summary, pipe length, cement age, and system permeability are significant factors in the gap measured between the cement and the specimen. The regression linear model and the R-square for all the experiments show 73.16% dependency on these factors. Table 6-16 shows all the variables tested with their P-value and estimated parameters.

**Table 6-16—Dependency of length, cement age, and system permeability on the gap.**

Parameter Estimates						
Variable	Label	DF	Parameter	Standard	T Value	Pr >  t
			Estimate	Error		
Intercept	Intercept	1	18.96	0.50347	37.66	<.0001
Length	Length	1	-2.2027	0.05746	-38.34	<.0001
Aging	Aging	1	0.01875	0.00099	18.96	<.0001
KgPulse	KgPulse	1	277.869	9.19071	30.23	<.0001

A comparison of the average gap calculated for the selected specimen with the confidence interval shows that the average measurement is within the predicted value by SAS (Table 6-17).

**Table 6-17—Predicted mean value of gap across all pipes with the selected pipe.**

	Gap (micrometer)		
	<b>95% CL Mean</b>		<b>Average Selected for the Experiment</b>
6" One Month	13.4312	49.8279	31.6
	<b>95% CL Mean</b>		
6" Two Months	14.1007	30.2544	14.5
	<b>95% CL Mean</b>		
9" One Month	12.8858	27.1141	20.0
	<b>95% CL Mean</b>		
9" Two Months	1.2252	6.4231	3.8
	<b>95% CL Mean</b>		

## Chapter 7: Numerical Validation

### 7.1 Decline Curve Analysis Basics

The fundamental principles of well testing were applied to the samples of various sizes to evaluate system permeability. This methodology was selected based on the first few figures (Fig. 6-1,6-2,6-3,6-4,6-5) of this chapter showing a change in the rate of decline of pressure diffusivity, which directs the theory to the diffusivity equations. Although wellbore pressure in the field decay is larger than in lab experiments for the present study, the underlying assumptions and theories are the same. The diffusivity equations are derived from the mass conservation theorem, which should also be applicable to the lab experiments. For example, to eliminate the effect of wellbore storage at an early stage, the percentage of the upstream  $V_1$  should be more than three times lower than the percentage of the downstream  $V_2$ . The critical cement volume is 97 cc, after which it is necessary to include the wellbore storage. The 9-inch specimen has a larger volume than the critical volume. Therefore, the wellbore storage should be accounted for in this case.

The lab experiments performed on the cemented samples from the various specimen sizes could be described using a pressure-transient fall-off test in a reservoir under uncertainty. They are demonstrated as fluid injection followed by shut-in for pressure fall-off. The pressure decline occurs because of the airflow through the porous media between the casing and the cement, whereas the cement represents a low-permeability rock in the reservoir. The pressure fall-off test was modeled in Kappa software (Saphir) by matching the drawdown pressure with time using the fundamental diffusivity equation.

### 7.1.1 Model Equations

The diffusivity equation for compressible fluid (Equation 7-1) is as follows:

$$\frac{1}{r} \frac{\partial y}{\partial r} \left( r \frac{P}{\mu z} \frac{\partial P}{\partial r} \right) = \frac{\mu \Phi C_t}{0.0002637 K} \frac{P}{\mu z} \frac{\partial P}{\partial t} \dots\dots\dots (7-1)$$

By integrated the equation with time and flow radius  $\int_0^t \frac{\partial P}{\partial t}$  and  $\int_0^r \frac{\partial y}{\partial r}$  for compressible unsteady-state flow homogenous for pressure less than 2000 psi, the result is as follows (Eq. 7-2):

$$\Delta P = \frac{162.6 q_g B_g \mu_g}{Kh} \left[ \log \left( \frac{Kt}{\Phi \mu_g C_t r_w^2} \right) - 3.23 \right] \dots\dots\dots (7-2)$$

where

$\Delta P$  Pressure Different in (Psi)

$q_g$  Gas Flow Rate (ft<sup>3</sup>/day)

$B_g$  Formation Volume Factor (sft<sup>3</sup>/ft<sup>3</sup>)

$\mu_g$  Gas Viscosity (cp)

$K$  Permeability (md)

$h$  Pay Zone (ft)

$t$  Time (days)

$C_t$  Total Compressibility (1/psi)

$r_w^2$  Well Radius (ft)

$\Phi$  Porosity

The diffusivity equation explains how the pressure behaves with time in the porous media across certain intervals. Conservation of mass, Darcy's law, and compressible fluid are the conditions in which the diffusivity equation is derived:

- Mass conservation law (Eq. 7-3):

$$(\text{Mass flow})_{\text{in}} - (\text{Mass flow})_{\text{out}} = (\rho\Phi\partial x)_{t+\Delta t} - (\rho\Phi\partial x)_t \dots\dots\dots (7-3)$$

- Darcy (Equation 7-4):

$$-0.23394 \frac{\partial}{\partial x} \left( -\frac{K_x A \rho}{887.2 \mu} \frac{\partial p}{\partial x} \right) = A \frac{\partial(\rho\Phi)}{\partial t} = \frac{\partial(\rho\Phi)}{\partial t} = 0.0002637 K_x \frac{\partial y}{\partial x} \left( -\frac{\rho}{\mu} \frac{\partial P}{\partial x} \right) \dots\dots\dots (7-4)$$

- Compressible fluid (Equation 7-5):

$$0.0002637 \frac{K_x}{\rho\Phi} \frac{\partial}{\partial x} \left( \frac{\rho \partial P}{\mu \partial x} \right) \dots\dots\dots (7-5)$$

For modeling, pure dry N<sub>2</sub> was selected and its properties calculated by the following equations (7-6, 7-7, 7-8, 7-9, and 7-10):

- Gas Specific Density  $\gamma_g = \frac{\rho_g}{\rho_{air}} \dots\dots\dots (7-6)$

- Z factor calculated from  $PV=ZnRT \dots\dots\dots (7-7)$

- Formation Volume Factor  $B_g = \frac{ZP_{sc}T}{PT_{sc}} \dots\dots\dots (7-8)$

- Gas Compressibility  $C_g = \frac{1}{p} - \frac{1}{Z} \left( \frac{dZ}{dp} \right) \dots\dots\dots (7-9)$

- $\rho_g = (\rho_{air})_{sc} V_{sc} \frac{P \gamma_g}{ZRT} \dots\dots\dots (7-10)$

The experiments show that the gas flowed path was through the cement–casing bonding. It is, therefore, assumed that the flow rate is linear and a linear flow diffusivity equation is utilized (Eq. 7-11):

$$\frac{\partial p}{\partial t} = 0.0002637 \frac{K}{\mu \phi C_t} \frac{\partial^2 P}{\partial x^2} \dots\dots\dots (7-11)$$

The setup of the experiments was an open end-of-pipe to air. Therefore, it is modeled as an infinite acting reservoir and the well model selection as a vertical well with a high level of microannulus penetration. Eq. 7-12 and Eq. 7-13 describe the conditions stated:

$$\Delta P = \frac{162.6 q \mu}{K h} \left[ \log(t) + \log\left(\frac{K}{\phi \mu C_t r_w^2}\right) - 3.228 \right] \dots\dots\dots (7-12)$$

$$\Delta P = 141.2 \frac{q \mu}{K h} s \dots\dots\dots (7-13)$$

The specimen is assumed to be the vertical reservoir. For the vertical well with full microannulus across the cement body, Eq. 7-14 is used:

$$\left[ r \frac{\partial p}{\partial r} \right] = 141.2 \frac{q B \mu}{K h} \dots\dots\dots (7-14)$$

The most important results for the 6-inch specimen at two months and for the 9-inch specimen at two months will be discussed in 7.1.3.

### 7.1.2 Modeling Construction

The pressure-transient simulation process via Saphir started with uploading the pressure profile and injection rate with time followed by an analysis of the pressure decline. Matching the experimental data was performed by creating an analytical solution then fitting the models. Assigning the system permeability and altering skin factor and wellbore storage is the way to reach a practical match.

The model assumes an infinite acting reservoir and a vertical well for the 6-inch specimen at one-month age, the pressure decay starts at around 50 psig to 0 psig and a reservoir temperature of 20–21 °C (68 °F). The specimen radius was equivalent to 0.5-inch, and porosity was estimated at 11%. Total compressibility was found to be 0.0154753 psi<sup>-1</sup>. The cement properties were estimated for class G cement from the literature (Ichim, 2017).

The simulation started by injecting gas to 50 psig as the experimenting pressure followed by the pressure fall-off. The flow regime was observed by pressure-derivative stabilization. System permeability, well-bore storage, and the skin factor were used as matching parameters to mimic the pressure-decline trend. A practical pressure match was achieved with 0.0455 md and -2 of permeability and skin factor, respectively, for the 6-inch specimen at one month.

A similar approach was applied to the 6-inch specimen at two months and nine months of aging. The same parameters were used for the 6-inch specimen at one-month age except for system permeability. The 6-inch specimen in the two-month flow regime was observed at a system permeability of 0.007 md. For the 6-inch specimen at nine months, a system permeability reduction to 0.00075 md was not enough to mimic the pressure decline; a positive skin of 5.5 is required. A decrease in system permeability is expected as the cement ages. The simulation showed that as the aging time increased, the well-bore storage dominated and it was necessary to introduce the positive skin factor to match the pressure decline.

For the 9-inch specimen at one month, the experimental pressure decline was not smooth due to the heterogeneity of the gap measured. A pressure match of the stabilized pressure at the end of the test was achieved with 0.0155 md and 1<sup>-4</sup> bbl/psi of system permeability and wellbore storage, respectively. The simulation shows that it is possible to match the 9-inch specimen one-month

pressure decline with a lower system permeability than that of the 6-inch specimen at one month, as the experiment showed. For the 9-inch specimen at two months, a permeability reduction to 0.0093 md was not enough to mimic the pressure decline; a positive skin is required. This behavior is repeated as the system permeability decreased significantly from either shorter aging or a shorter specimen.

Each specimen was simulated with almost 100 attempts to match the pressure, and then the skin was introduced as the cement aged to match the drawdown style. It should also be noted that the model assumes a fully saturated gap with a single-phase flow (gas).

It is evident from the lab experiments and the well-test analyses that the flow capacity decreases with aging and with a longer specimen. The impact of time is understandable because of the chemical reaction that leads to the water hydration and the creation of the bond. However, the system permeability decrease in the longer specimen needs further study and more information if it is to be fully understood. Tortuosity, which is commonly used to describe diffusion and fluid flow in porous media, could be one of the reasons impacting the flow capacity.

KAPPA Saphir v5.30.02 was used to establish the model as shown in Fig. 7-1,7-2.

**Analysis information**

Info Comments

Name:  ■

Type:  Standard  Interference  Minifrac

Reference well:

Multi-layer 

---

**Test parameters**

Well radius:  in

Pay zone:  in

Rock compressibility:  psi<sup>-1</sup>

Porosity:

Top reservoir depth:  in

Active model is numerical

keep model parameters

OK Cancel

**Fig. 7-1—Initial conditions for Saphir software.**

Man

Fluid system

Gas properties

**Dry Gas (Pure N2)**

Fluid type

Oil / Gas

Dry gas

Wet gas

Dead oil

Saturated oil (bubble point fluid)

Volatile oil (bubble point fluid)

Condensate (dew point fluid)

Define from lab report

Equation of State

Water

Reference parameters

Pressure:  psig

Temperature:  °C

Variable ranges

	Minimum	Maximum	Increment	
Pressure:	<input type="text" value="0.00000"/>	<input type="text" value="50.0000"/>	<input type="text" value="50.0000"/>	psig
Temperature:	<input type="text" value="20.0000"/>	<input type="text" value="21.0000"/>	<input type="text" value="0.9999"/>	°C

Increment:  # points:   Value

OK Cancel

**Fig. 7-2 —Properties for the initial conditions in Saphir software.**

As the reservoir thickness was assumed to be very small, the change in pressure was noticed immediately at the start of the drawdown. Compressibility has a limited effect, as the reservoir pressure is low (50 psi). Therefore, the default value of  $3E-6 \text{ psi}^{-1}$  is acceptable. The assumed gas to flow is  $N_2$  (pure dry gas), and the gas properties, such as viscosity and the Z-factor, are calculated from the PVT. The pressure was below 2000 psi such that the change was minimal for the term  $\mu Z$  (viscosity with Z-factor).

The skin factor replaced the damage in the cement column (gap measurement). The behavior analysis of the pressure drawdown was studied using a semi-log plot and a log-log plot.

### **7.1.3 Modeling Results**

From the semi-log graph for the 6-inch specimen at two months, the negative skin effect is obvious in increasing the drawdown behavior. This could be explained by the contribution of the microannulus to pressure decay. Also, the behavior showed a two-slope value at the early stage and late stage, which indicates the unsymmetrical quality of the microannulus with the air flow between the gap's pores (Fig. 7-3).

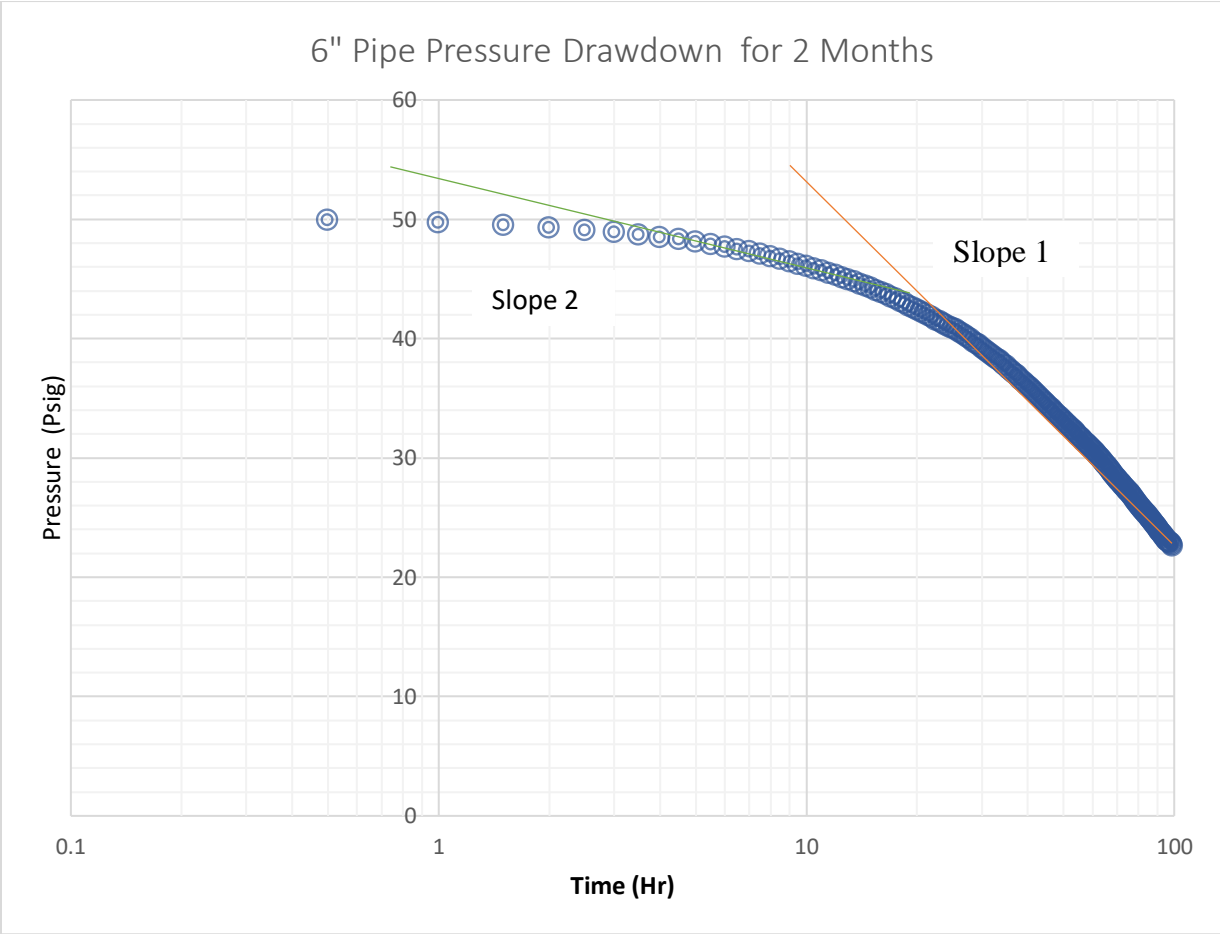


**Fig. 7-3—Drawdown pressure for the 6-inch-length pipe at 2-month (wet) cement age.**

For the log-log chart, the pressure derivate is higher than the pressure curve. The main reason for this behavior, which is observed in most pressure-transient analyses, is the very short injection time compared to the pressure decline duration. This is acceptable because this standard test is similar to the slug test, which can be analyzed regardless of the injection stage. The pressure derivative showed an early time representing wellbore storage and skin, followed by an unstable

mid-time region. The unstable region is an indication of changing system permeability along the specimen, as observed in the gap measurements after the specimen were cut.

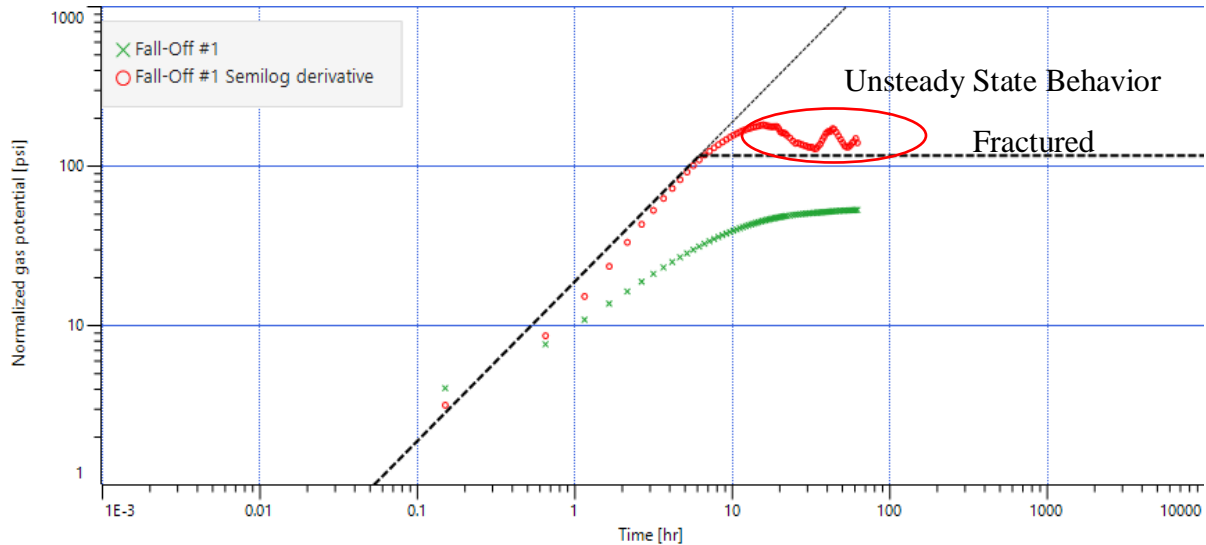


**Fig. 7-4—Pressure derivative of the 6-inch-length pipe at 2-month cement age.**

The unsteady-state behavior of pressure decline is clear from the pressure derivative plot (Fig. 7-4). In the early stage of the test, the wellbore storage is seen if there is any. This wellbore storage will affect the start of the real pressure drawdown. The pressure drawdown calculation should start after the wellbore storage. In the case of low-permeability rock, the wellbore storage will mask the mid- and late-time regions. Therefore, the test must be performed over a longer time to reach these regions.

The system permeability value was used to fit the data as the first stage in the history match. The higher the permeability is, the larger the drop at an early stage. Also, once the pressure is stabilized, the slope could be calculated to obtain the system permeability from the inverse of the slope. The trial changing of system permeability is shown in the derivative (log-log chart). Fig. 7-5 shows the effect of the system permeability change in the pressure decay and its derivative.

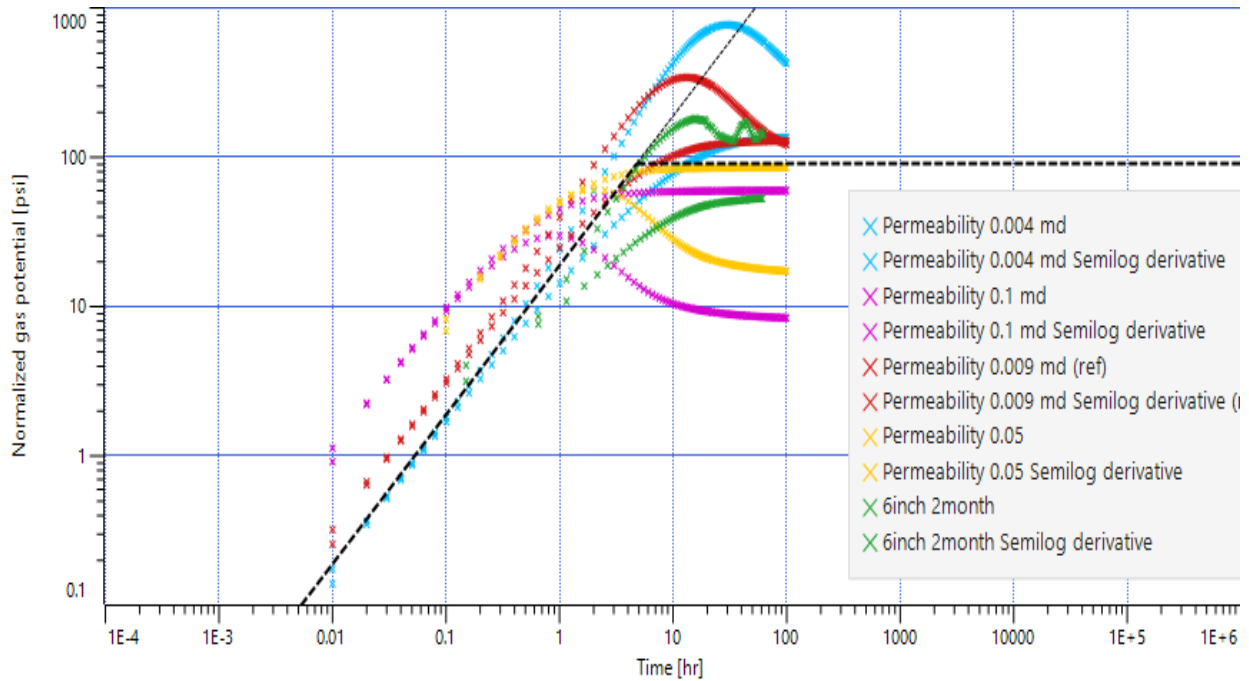


**Fig. 7-5—Derivative match for the 6-inch-length pipe at 2-month cement age.**

It is also evident that skin does not change the early-time slope but does affect the magnitude of the hump. As the skin increases, the hump becomes larger. The trials resulted from changing the skin in the experiment in both the derivative and drawdown pressure regime are shown in Fig. 7-6. The best fit for the skin was found to be -2. A negative skin value is an indication of stimulated rock. In such cases, part of the stimulated area could be represented by the observed microannulus. Aging and longer specimens make the microannulus narrower and show system permeability closer to that of the cement. Here, no flow capacity contrast could be detected in the well testing.

Fig. 7-7 shows the pressure decline with time. Changing the skin directly influences the pressure trend. The higher the positive skin, the lower the gas leak into the wellbore, which makes the pressure change with time smaller.

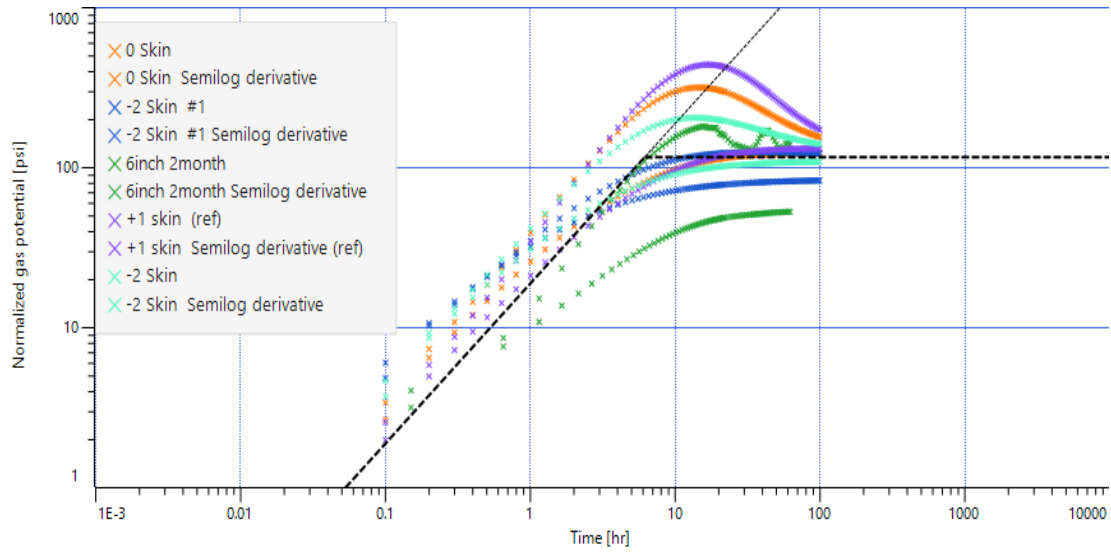


Fig. 7-6—Derivative match for the 6-inch-length pipe at 2-month cement age with different skin factors.

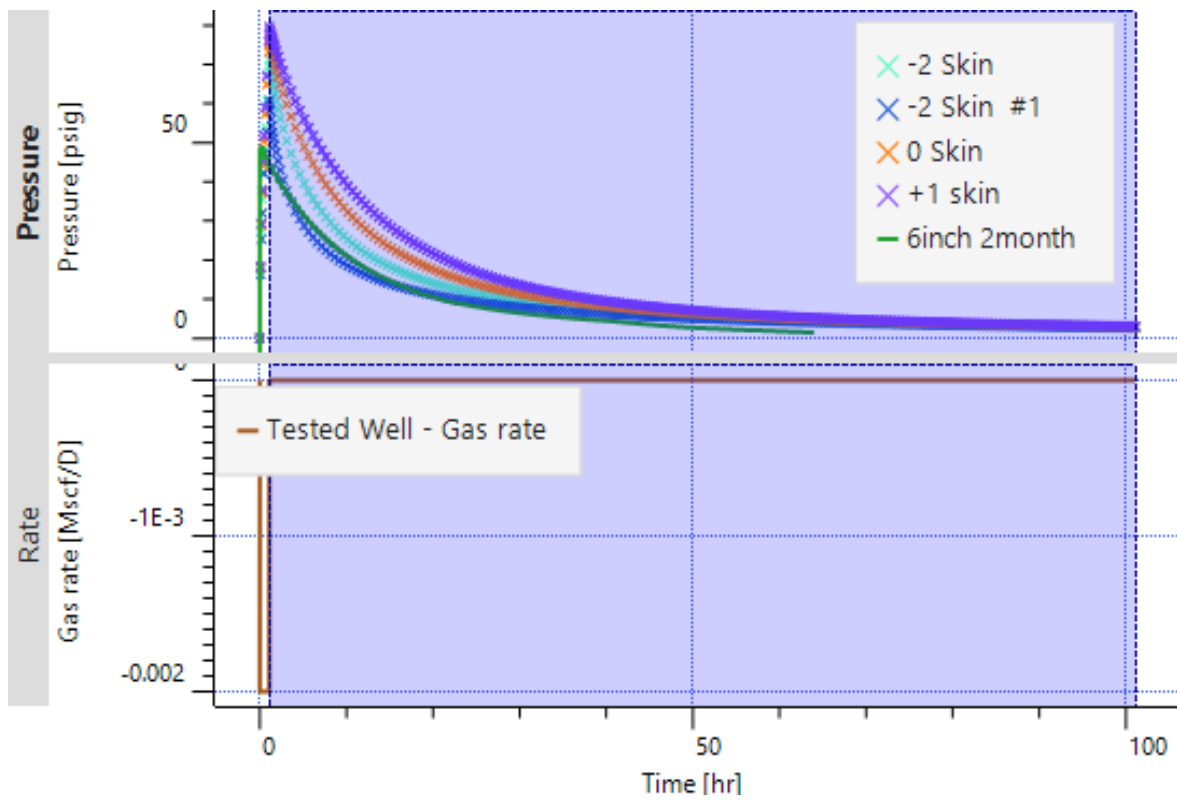


Fig. 7-7—Permeability match for the 6-inch-length pipe at 2-month cement age.

Fig. 7-8 shows the fitting of the system permeability for a 6-inch specimen (two months) at 0.009 md and -2 skin. The fitting plot has an error of 5–15% from the original experimental data.

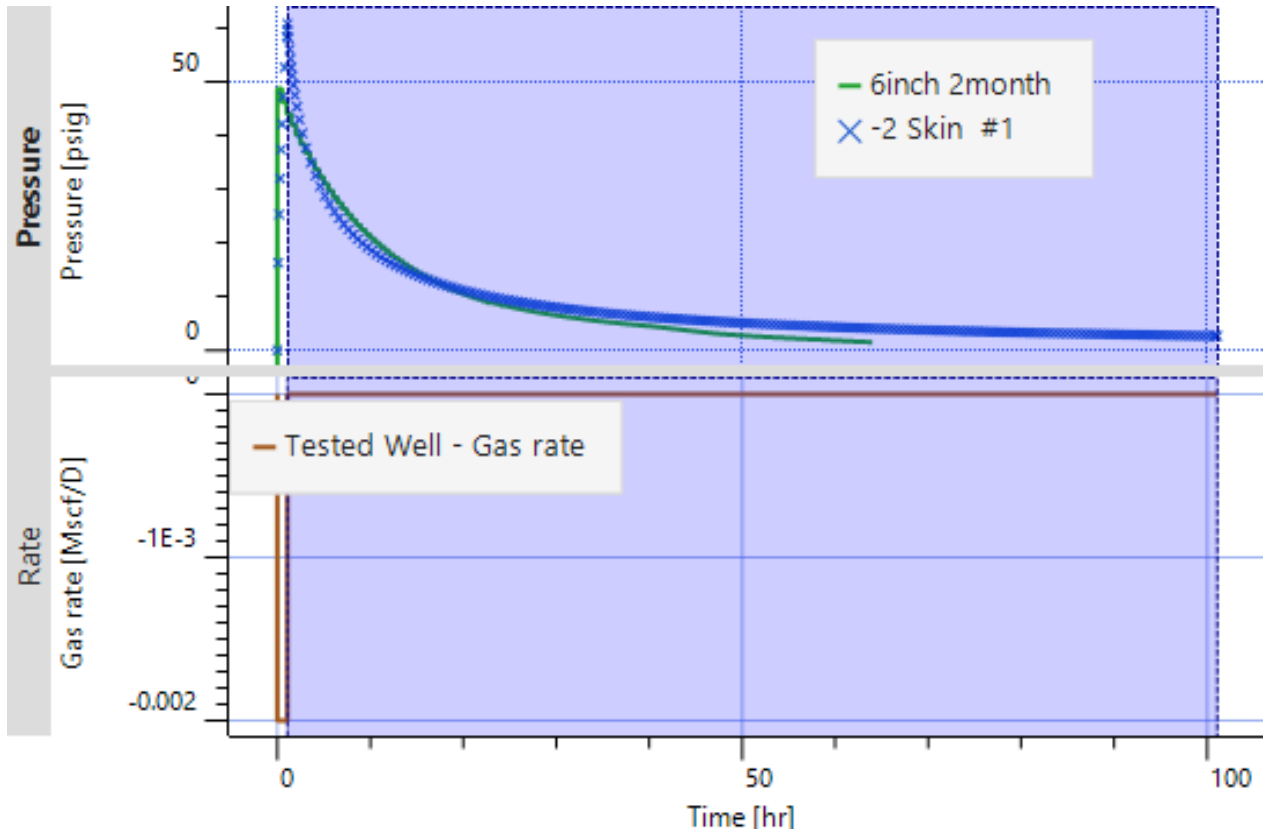
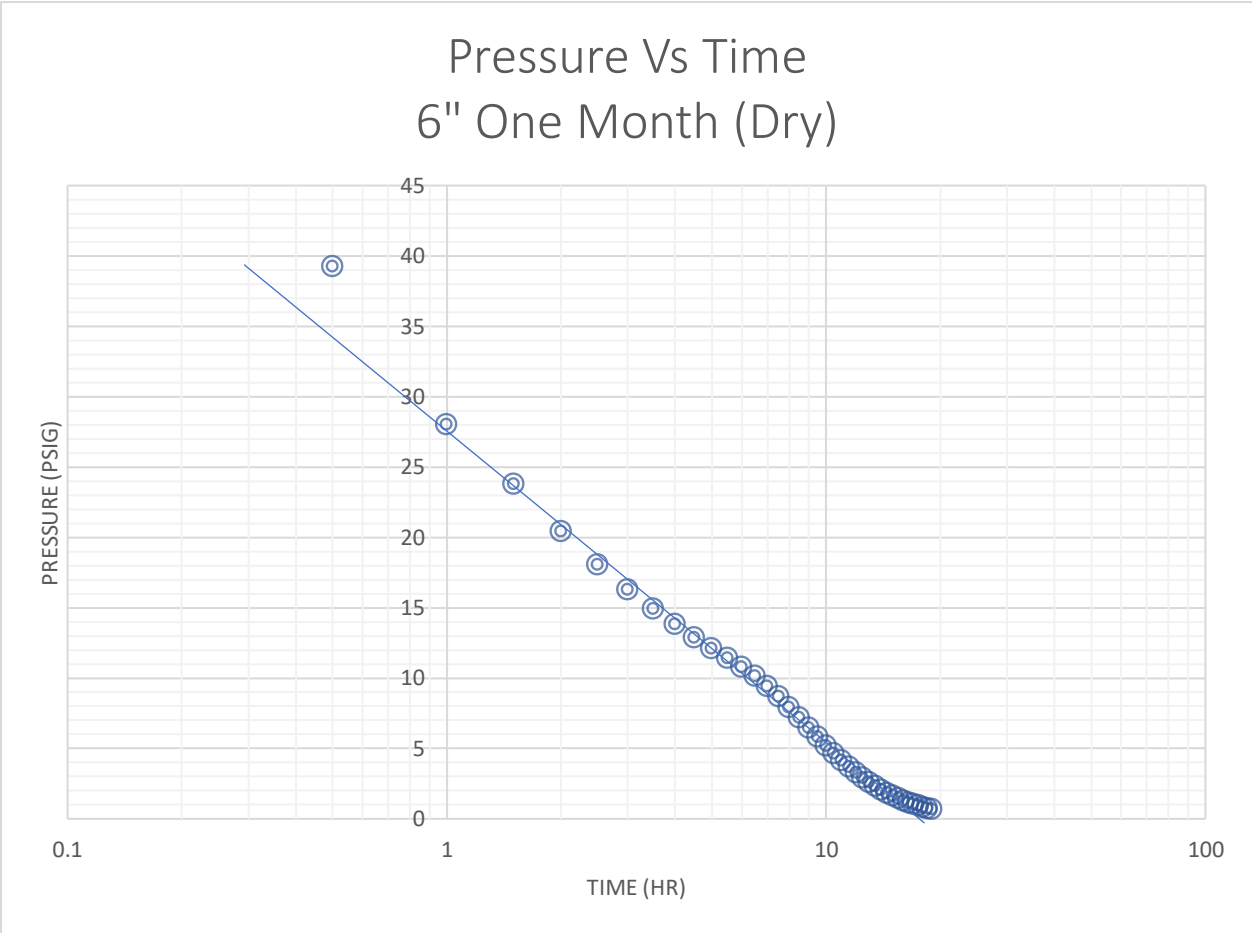


Fig. 7-8—Permeability fitted for the 6-inch-length pipe at 2-month cement age.

The plot in the semi-log for the specimen hydrated in dry conditions (no water added) had one slope, indicating a uniform skin around the wellbore (Fig. 7-9). The microannulus is large in this case and the shrinkage is uniform around the circumference in the 6-inch specimen left to dry out after one month.



**Fig. 7-9—Drawdown pressure for 6-inch-length pipe at 1-month (dry) cement age.**

For the wellbore storage, the simplest model was used, i.e., constant wellbore storage, assuming that this remains constant with time. This model was applied to the 9-inch specimen. Fig. 7-10 shows the system permeability and derivative of the 9-inch specimen.

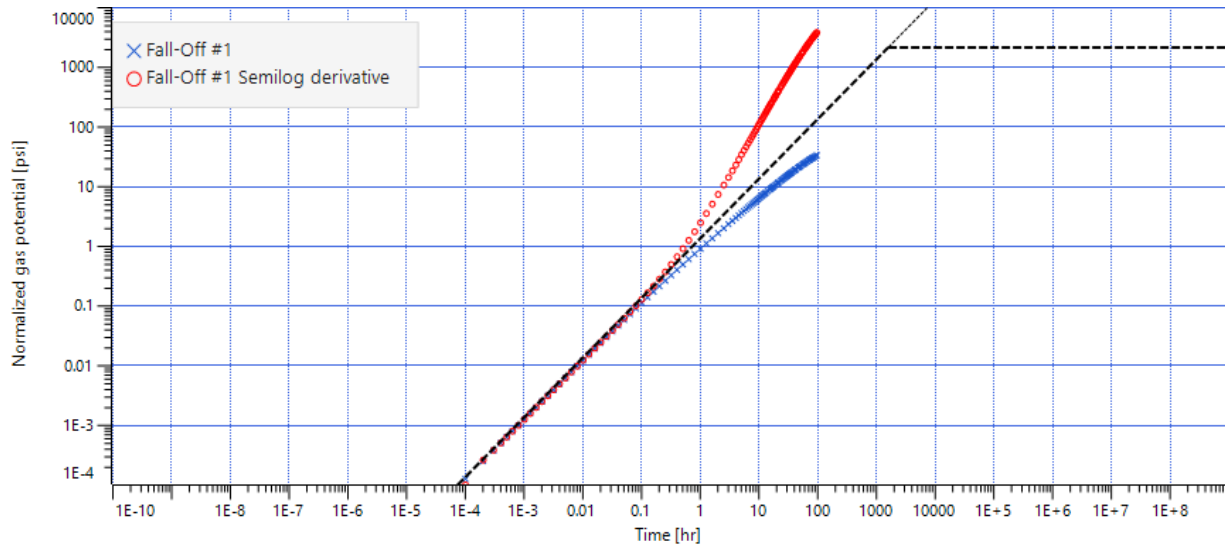


**Fig. 7-10—Derivative pressure of the 9-inch-length pipe at 2-month cement age.**

A different iteration was performed to obtain the nearest wellbore storage to fit the experiment. The 9-inch specimen with a value of 0.0001 at two months with a skin factor of 8 was the nearest fit (Fig. 7-11 and Fig. 7-12).

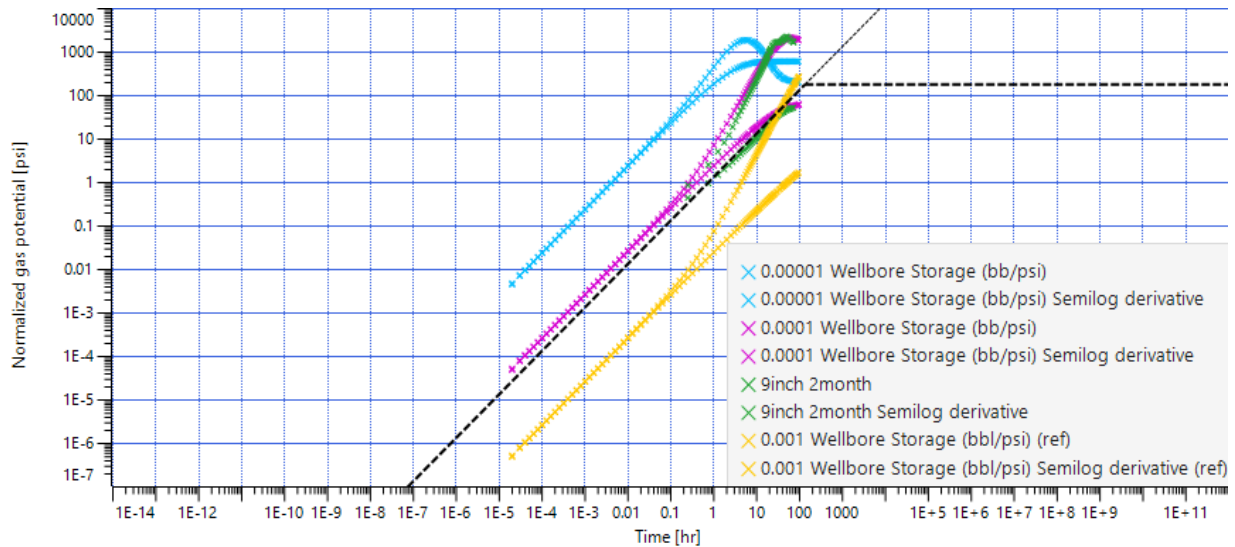


**Fig. 7-11—Derivative match wellbore storage fitting of the 9-inch-length pipe at 2-month cement age.**

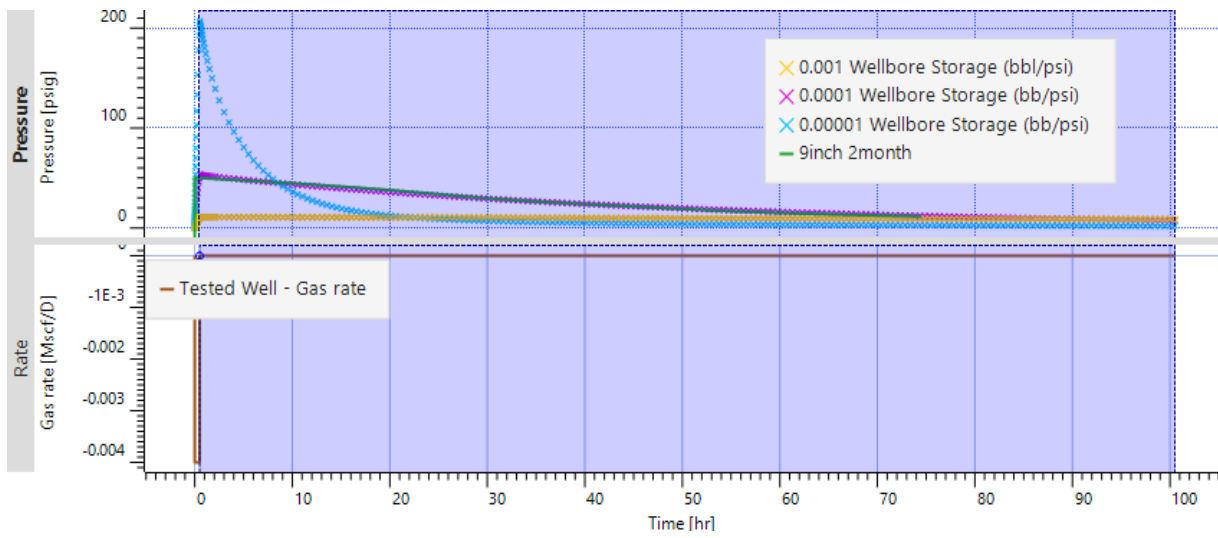


**Fig. 7-12—Permeability fitted for the 9-inch-length pipe at 2-month cement age with wellbore storage.**

Future numerical simulation study for the deboning between the cement and the casing is discussed in Appendix C.

## **Chapter 8: Summary and Conclusions**

### **8.1 Summary**

The barriers in oil and gas wells are designed to isolate two zones and prevent flow between them. Standards have been developed to recommend standards and best practices worldwide by bodies such as NORSOK, API, ISO.

The present research study was designed around plugging and abandonment integrity, focusing on the leaking phenomenon when cement is the plugging material. The main purpose was to identify the flow path by studying the hydraulic permeability (system permeability) and gap geometry between the cement and the casing.

Cement failure occurs due to many stresses to which the cement is subjected: tensile strength overexertion can cause cracks that may allow fluid to flow through its body. Shrinkage, temperature and pressure cycling, and hydraulic failure might cause the cement to fail.

Researchers have performed extensive experiments related to cement behavior under different conditions, which have been comprehensively reviewed in the present study. However, more investigations focused on the gap trajectory and system permeability are needed, which constituted the principal motivation for the present study.

In this study, a methodology was developed to study the flow regime of gas across cement in P&A applications. The experimental setup pressurizes 4-, 6-, and 9-inch-length pipes filled with cement. These pressure tests were performed after the cemented samples had been hydrated for one, two months, and up to 9 months. The pressure decline was then studied and correlated to the

permeability equations. The experimental work continued with a new method focused on visualizing the gap between the cement-pipe contact. In the experiments, the specimens were cut into 1-inch specimens that were measured using an optical microscope to find the gap between the specimens and the cement.

The lab experiments showed a relationship between the cement age and specimens' length in the air flow across the sample. The longer the cement was aged and hydrated, the more the gap measured decreased. Also, as the cement sample length increased, the greater possibility is that the gap opening decreased. The gap was found to increase when the cement cured in dry conditions, i.e., for cement not wetted with water during the waiting period.

The statistical analysis showed a more significant relationship between the gap opening and the cement hydration age compared to pipe length. As the cement age increased, the gap measurement of the cement decreased.

A numerical simulation was developed to validate the experimental data. The experiment included consideration of the trend of a pressure fall-off test with an injection period and a shut-off period. The experiment's pressure decay was simulated using Saphir software. The data obtained showed that the sample behaved similarly to a fractured formation, indicating a microannulus gap. The fracture was modeled in relation to an increase in the skin factor.

## 8.2 Recommendations

Based on the experimental results and the overall data trend, these points should be considered in relation to any cement applications in oil and gas cementing operations.

- Most of the leakage occurred in the microannulus in the cement–casing contact. Industrial specifications to seal this should be included in both international standardization and operators’ best practices.
- The long-term integrity of the cement plug must be ensured, which is achieved by wetting the cement with water. The author recommends adding water and spacer to sit on top of cement even after cement solidified. Shrinkage will be reduced in a wet environment; therefore, the possibility and amount of leakage will decrease.
- A polymer or resin that has sealing capabilities of an average size of 0.5–20 micrometers is a possible solution for the microannulus formation.
- A small cap of gas pressure could cause failure in the cement bond around the cement–casing contact. Therefore, any exposure to a pressure regime should be tracked in operations.

### 8.3 Conclusions

Based on the observations and results presented, the following major conclusions were reached:

- The pulse decay method is a reliable representation of the system permeability of cement.
- The system permeability of the samples was found in the range of 0.01 millidarcy to 9 micro-Darcy.
- Darcy's law estimation of system permeability underestimated system permeability by 13–93% across all the experiments compared with the results of the pulse decay method.
- The new approach of measuring the gap between the cement and the casing estimated the controller gap as between 0.4 and 20 micrometers. However, the average gap was 3–30 micrometers.
- Cement system permeability decreased with cement aging (hydration) by 60–1000%.
- The gap is directly proportional to the reduction in the system permeability with a 50–80% reduction in the average gap because of cement age.
- The gap was not uniform and does not follow a straight path across the casing–cement contact. The trajectory of the gap meandered across the sample, including changing direction around the specimen's circumference and gap size.
- The effective length of the gas flow across the sample was calculated as 40–70% higher than the length of the specimens.
- The measured gap increased four-fold on average for cement cured in dry-out conditions after one year.

- Statistical analysis showed that cement aging contributes more than 70% to control the cement gap.
- The pressure-transient analysis model demonstrated that the pressure decay trend had more than one slope, which indicates the tortuosity of the gap across the sample.

## 8.4 Future Work

The following research directions would advance the work presented in this study:

- Lab experiments to study the annulus cement-casing contact with two layers of cement and to measure the gap to mimic cement squeeze operations
- Tests to determine the effect of adding unfiltered water samples with different salinity levels and mud as hydration before testing the cement to mimic the conditions of the field
- Chemical studies of the additive of polymer between the size of 0.5 and 20 micrometers and its effect on the gap with time
- Lab work with confined pressure across the sample effect on the cement gap
- Experiments on the basic additive and weight change, especially with anti-shrinkage additive and defoamer
- Studies of the gap behavior with the volume of the cement and the length of the cement considered

## Nomenclature

$A$	Pipe Cross-Sectional Area ( $m^2$ )
API	American Petroleum Institute
ASME	American Society of Mechanical Engineers
ATSME	American Society of Testing and Materials
$B$	Forchheimer Coefficient ( $m^{-1}$ )
$B_g$	Formation Volume Factor ( $sft^3/ft^3$ )
BHST	Bottom Hole Static Temperature
BSEE	Bureau of Safety and Environmental Enforcement
CCA	Casing-Casing Annulus Pressure
$C_g$	Gas Compressibility ( $1/Pa$ )
$C_t$	Total Compressibility ( $1/psi$ )
CT	Computed Tomography
$D$	Hydraulic Pipe Diameter (m)
ID	Inner Diameter
EIA	Energy Information Administration
EOR	Enhanced Oil Recovery

GoM	Gulf of Mexico
H.	Cement Sheath Height
h	Pay Zone (ft)
IEA	International Energy Agency
ISO	International Organization for Standardization
K	Permeability ( $m^2$ , md)
L	Length (m or cm)
M	Mass Flow (Kg)
NORSOK	Norwegian Standard
OGUK	Oil and Gas United Kingdom
P&A	Plug and Abandonment
$P_i$	Inlet Pressure (atm, pa, or psi, dynes/cm <sup>2</sup> )
$P_o$	Outlet Pressure (atm, pa, or psi, dynes/cm <sup>2</sup> )
Q	Air Flow Rate Across the Pipe ( $m^3/sec$ or $cm^3/s$ )
$q_g$	Gas Flow Rate ( $ft^3/day$ )
R	Microannulus Gap (m or micrometer) or Gas Constant (8.314 j/molK)
r	Radius of the Pipe (cm)
rw	Well Radius (ft)

$R_c$	Casing Radius (m)
SCP	Sustain in Casing Pressure
$T$	Temperature in (K)
$t$	Time (days, sec)
$V_1$	Volume Upstream (m <sup>3</sup> )
$V_2$	Volume Downstream (m <sup>3</sup> )
$Z$	Gas Compressibility (Pa <sup>-1</sup> )
$\tau_y$	Cement Yield Stress
$\mu$	Viscosity (c.P, Pa.s, Poise)
$\mu_g$	Gas Viscosity (cp)
$\rho$	Air Density in (kg/m <sup>3</sup> )
$\Phi$	Porosity
md	Milli Darcy
$\mu\text{m}$	Micrometer
(")	Inch

## References

1. Aas, B., Sørbø, J., Stokka, S. et al. 2016. Cement Placement with Tubing Left in Hole During Plug and Abandonment Operations. Paper presented at the SPE - International Association of Drilling Contractors, 2016 March (Straume 2014).  
<https://doi.org/10.2118/0517-0085-jpt>
2. Ahmed, R., Shah S., Samuel O. et al. 2015. Effect of H<sub>2</sub>S and CO<sub>2</sub> in HPHT Wells on Tubulars and Cement final report Authors: Prepared under BSEE Project # E12PC00035.
3. Aïtcin, P. C. 2016a. Portland cement. In Science and Technology of Concrete Admixtures. Elsevier Ltd. <https://doi.org/10.1016/B978-0-08-100693-1.00003-5>
4. Aïtcin, P. C. 2016b. Water and its role on concrete performance. In Science and Technology of Concrete Admixtures. Elsevier Ltd. <https://doi.org/10.1016/B978-0-08-100693-1.00005-9>
5. Al Ramadan, M., Salehi, S. and Teodoriu, C. 2019. Robust Leakage Modeling For Plug & Abandonment Applications. ASME 2019 38th International Conference on Ocean, Offshore and Arctic Engineering, Glasgow, Scotland, UK. 9-14 June 2019. 8, 1–9.  
<https://doi.org/10.1115/OMAE2019-95612>
6. Al Ramadan, M., Salehi, S., Ezeakacha, C. et al. 2019. Analytical and Experimental Investigation of the Critical Length in Casing-Liner Overlap. Sustainability (Switzerland), 11(23), 1–17. 2 December 2019. <https://doi.org/10.3390/su11236861>

7. Al Ramis H, Teodoriu C, Bello O, Al Marhoon Z. High Definition Optical Method for Evaluation of Casing-Cement Microannulus (CCMA). *J Petrol Sci Eng.* 2020; 195:107719. <https://doi.org/10.1016/j.petrol.2020.107719>
8. Al Ramis H, Teodoriu Critical Leak Mechanism (A review) with Application to Oil, Gas and Geothermal Well Integrity. *Oil Gas European Magazine* 46 Edition, 2020 Issue 4/2020 26-32.
9. Al-Awad, M.N.J., 1997. A Laboratory Study of Factors Affecting Primary Cement Sheath Strength. *J. King Saud Univ. - Eng. Sci.* 9, 113–127. [https://doi.org/10.1016/s1018-3639\(18\)30670-6](https://doi.org/10.1016/s1018-3639(18)30670-6)
10. Albawi, A., De Andrade, J., Torsæter, M. et al. 2014. Experimental Set-Up for Testing Cement Sheath Integrity in Arctic Wells. *Society of Petroleum Engineers - Arctic Technology Conference 2014*, 375–385. <https://doi.org/10.4043/24587-ms>
11. Al-Tamimi, A., Al-Mansoori, S., Samad, S. et al. 2008. Design and Fabrication of a Low Rate Metering Skid to Measure Internal Leak Rates of Pressurized Annuli for Determining Well Integrity Status. *Society of Petroleum Engineers - 13th Abu Dhabi International Petroleum Exhibition and Conference, ADIPEC 2008*, 2, 1009–1015. <https://doi.org/10.2118/117961-ms>
12. API 14A, Specification for Subsurface Safety Valve Equipment, Tenth edition 2001. Washington DC: API
13. API 14B, Recommended Practice for Analysis, Design, Installation, and Testing of Basic Surface Safety Systems for Offshore Production Platforms, fourth edition .1996. Washington DC: API

14. API 14C, Recommended Practice for Analysis, Design, Installation, and Testing of Basic Surface Safety Systems for Offshore Production Platforms, fourth edition 1998. Washington DC: API <https://doi.org/10.1520/G0154-12A>
15. API 14D, Specification for Wellhead Surface Safety Valves and Underwater Safety Valves for Offshore Service, 1994. Washington DC: API
16. API 6DSS, Specification for Subsea Pipeline Valves Purchase, second edition. 2014. Washington, DC.: API
17. API BULL E3. 2019. In Wellbore Plugging and Abandonment Practices (2nd ed., Issue April 2018). API Publishing Services.
18. API RP 90 1993, Annular Casing Pressure Management for Offshore Wells. 1993. Washington, DC: API.
19. API SPEC 10. Specification for Cement and Materials for Well Cementing. twenty second edition. 1999, (October 1999). Washington, DC: API
20. API TR 10TR2, Shrinkage and Expansion in Oilwell Cements, first edition. 1997. Washington, DC: API.
21. Appleby, S. and Wilson, A. 1996. Permeability and Suction in Setting Cement. Chemical Engineering Science, Volume 51, Issue 2, January 1996, Pages 251-267 51(2), 251–267. [https://doi.org/10.1016/0009-2509\(95\)00260-X](https://doi.org/10.1016/0009-2509(95)00260-X)
22. Asala, H. I. and Gupta, I. 2019. Numerical Modeling Aspects of Fluid-driven Interface Debonding after Wellbore Plugging and Abandonment. 53rd U.S. Rock Mechanics/Geomechanics Symposium. New York, NY, USA, 23-26 June 2019.

23. Bachu, S. and Bennion, D.B., 2008. Experimental Assessment of Brine And/Or CO<sub>2</sub> Leakage Through Well Cement at Reservoir Conditions. *Int. J. Greenh. Gas Control* 3, 494–501. <https://doi.org/10.1016/j.ijggc.2008.11.002>
24. Backe, K. R., Lile, O. B., Lyomov, S. K. et al. 1999. Characterizing Curing-Cement Slurries By Permeability, Tensile Strength, And Shrinkage. *SPE Drilling and Completion*. 1997 SPE Western Regional Meeting. Long Beach, California 25-27 June 1997. 14(3), 162–167. <https://doi.org/10.2118/57712-PA>
25. Barajas, A. M., Walter D., and Buckingham J. 1999. “Allowable Leakage Rates and Reliability of Safety and Pollution Prevention Equipment.” Herndon, Virginia.
26. Bauer, S., Gronewald, P. Hamilton, J. et al. 2005. High-Temperature Plug Formation With Silicates. *SPE International Symposium on Oilfield Chemistry*, Houston, Texas, 2-4 February 2005. (1), 1–6. <https://doi.org/10.2523/92339-MS>
27. Baumgarte, C., Thiercelin, M., and Klaus, D. 1999. Case Studies of Expanding Cement to Prevent Microannular Formation. Paper SPE 56535 presented at the SPE Annual Technical Conference and Exhibition, Houston, 3–6 October. DOI: 10.2118/56535-MS.
28. Becker, H. and Peterson, G. (1963). Bond of Cement Compositions For Cementing Wells. *World Petroleum Congress Proceedings*, Frankfurt, Germany. 19-26 June. 1963, 313–328.
29. Bentur, A., Diamond, S. and Mindess, S. 1985. The Microstructure of The Steel Fibre-Cement Interface. October 1985. *Journal of Materials Science*, 20(10), 3610–3620. <https://doi.org/10.1007/BF01113768>
30. Bentz, D. P. 2014. A three-dimensional cement hydration and microstructure program. I. Hydration rate , heat of hydration and chemical shrinkage. June.

31. Bogaerts, M., Kanahuati, A., Khalilova, P., Moretti, F., Voon, E., & Dighe, S. 2012. Challenges in setting cement plugs in deep-water operations. Society of Petroleum Engineers - SPE Deepwater Drilling and Completions Conference 2012, June, 484–497. <https://doi.org/10.2118/155736-MS>
32. Bois, A. P., Vu, M. H., Noël, K. et al. 2018. Cement Plug Hydraulic Integrity - The ultimate Objective of Cement Plug Integrity. Society of Petroleum Engineers - SPE Norway One Day Seminar. Bergen, Norway. 18 April 2018, 576–596. <https://doi.org/10.2118/191335-ms>
33. Bosma, M., Ravi, K., van Driel, W., and Schreppers, G.J. 1999. Design Approach to Sealant Selection for the Life of the Well. Paper SPE 56536 presented at the SPE Annual Technical Conference and Exhibition, Houston, 3–6 October. <https://doi.org/10.2118/56536-MS>
34. Boukhelifa, L., Moroni, N., James, S. G. et al. 2005. Evaluation of Cement Systems For Oil and Gas Well Zonal Isolation in A Full-Scale Annular Geometry. Proceedings of the Drilling Conference, 825–839. March 2005. <https://doi.org/10.2523/87195-ms>
35. Brace, W.F., Walsh, J.B., and Frangos, W.T.: Permeability of Granite Under High Pressure, J. Geophys. Res. (1968) 73, 2225-36. <https://doi.org/10.1029/JB073i006p02225>
36. Buckingham, J. C. 1999. Allowable Leakage Rates for Safety and Pollution Prevention Equipment.
37. Carter, L. G. and Evans, G. W. 1964. A Study of Cement-Pipe Bonding. Journal of Petroleum Technology, 16(02), 157–160. February 1964. <https://doi.org/10.2118/764-pa>
38. Chatterji, A. K., and Rawat, R. S. 1965. Hydration of Portland cement. Nature, 207(4998), 713–715. <https://doi.org/10.1038/207713a0>

39. Chen, Y., Liang, T., Peng, X. et al. 2017. Calculation and Analysis of the First Interface Micro-gaps of the Thermal Production Wells. *Advances in Mechanical Engineering*, 9(2), 1–9. February 2017. <https://doi.org/10.1177/1687814016688586>
40. Chenevert, M.E. and Shrestha, B.K. 1991. Chemical Shrinkage Properties of Oilfield Cements. *SPEDE* 6 (1): 37–43. SPE-16654-PA. <https://doi.org/10.2118/16654-PA>
41. Chu, W., Shen, J., Yang, Y. et al. 2015. Calculation of Micro-Annulus Size In Casing-Cement Sheath-Formation System Under Continuous Internal Casing Pressure Change. *Petroleum Exploration and Development*, 42(3), 414–421. June 2015. [https://doi.org/10.1016/S1876-3804\(15\)30033-1](https://doi.org/10.1016/S1876-3804(15)30033-1)
42. Costeno, H., Mendoza, L. D., Djohor, M. et al. 2014. Optimized Well Plug & Abandonment Methodology Applied on A Brownfield Towards Future Development Offshore Malaysia. *International Petroleum Technology Conference*, Kuala Lumpur, Malaysia. 3, 2719–2730. 10 December 2014 <https://doi.org/10.2523/iptc-18013-ms>
43. Dastan Takhanov, 2011. Forchheimer Model for Non-Darcy Flow in Porous Media and Fractures. MSc Report, Imperial College London (September 2011).
44. Gray, Kenneth E., Podnos, Evgeny, and Eric Becker. "Finite-Element Studies of Near-Wellbore Region During Cementing Operations: Part I." *SPE Drill & Compl* 24 (2009): 127–136. doi: <https://doi.org/10.2118/106998-PA>
45. De Andrade, J. and Sangesland, S., 2015. Cement Sheath Failure Mechanisms: Numerical Estimates to Design for Long-Term Well Integrity. *J. Pet. Sci. Eng.* 147, 682–698. <https://doi.org/10.1016/j.petrol.2016.08.032>

46. De Andrade, J., Fagerås, S., and Sangesland, S. 2019. A Novel Mechanical Tool for Annular Cement Verification. SPE/IADC Drilling Conference, Proceedings, 2019-March, 5–7. <https://doi.org/10.2118/194135-ms>
47. De Andrade, J., Torsaeter, M., Todorovic, J. et al. 2014. Influence of Casing Centralization on Cement Sheath Integrity During Thermal Cycling. SPE/IADC Drilling Conference and Exhibition, Fort Worth, Texas, 4-6 March 2014. 2(1992), 870–879. <https://doi.org/10.2118/168012-ms>
48. Deremble L., Matteo L., Bruno H., Brice L., et al. 2011. Stability of a Leakage Pathway in a Cemented Annulus. Energy Procedia, Volume 4,2011, Pages 5283-5290, ISSN 1876-6102, <https://doi.org/10.1016/j.egypro.2011.02.508>.
49. Deshmukh, Viraj V. 2007. A Laboratory Analysis of Permeability of Typical Cement Mixtures Used in the Permian Basin. Ms.Thesis. Texas Tech University.
50. Double, D. D. and Hellowell, A. 1976. The hydration of Portland Cement. In Nature (Vol. 261, Issue 5560). <https://doi.org/10.1038/261486a0>
51. EIA, U.S. Energy Information Administration EIA .2019. U.S. Oil and Natural Gas Wells by Production Rate, <https://www.eia.gov/petroleum/wells/> (accessed April 1st, 2021)
52. Eijden, J., Cornelissen, E., Ruckert, F. et al. 2017. Development of Experimental Equipment and Procedures to Evaluate Zonal Isolation And Well Abandonment Materials. SPE/IADC Drilling Conference and Exhibition, The Hague, The Netherlands. 14-16 March 2017. Proceedings, 2017-March, 142–157. <https://doi.org/10.2118/184640-ms>
53. Evans, G. W., and Carter, L. G. 1962. Bonding studies of cementing compositions to pipe and formations. Drilling and Production Practice 1962, 72–79

54. Feng, R., Beck J., Buyuksagis A. et al. 2015. Electrochemical Corrosion Behavior of High Strength Carbon Steel in H<sub>2</sub>S-Containing Alkaline Brines. *ECS Transactions* 66 (17): 13–36. <https://doi.org/10.1149/06617.0013ecst>.
55. Fernandez, M. M. C. 2008. Effect of Particle Size on the Hydration Kinetics and Microstructural Development of Tricalcium Silicate. *Techniques*, 4102(7), 99–114. DOI:[10.5075/epfl-thesis-4102](https://doi.org/10.5075/epfl-thesis-4102)
56. Gardner, D., Volkov, M., and Greiss, R. M. 2019. Barrier verification during plug and abandonment using spectral noise logging technology, reference cells yard test. *SPE/IADC Drilling Conference, Proceedings*, 2019-March. <https://doi.org/10.2118/194075-ms>
57. Gasda, S. E., Bachu, S., Celia, M. A. 2004. Spatial Characterization of the Location of Potentially Leaky Wells Penetrating A Deep Saline Aquifer in A Mature Sedimentary Basin. *Environmental Geology*, 46(6–7), 707–720. 8 June 2004. <https://doi.org/10.1007/s00254-004-1073-5>
58. Glover, P. 2001. Chapter 10 - Relative Permeability. *Formation Evaluation M.Sc. Course Notes*, 104–30. <https://doi.org/10.1016/j.antiviral.2007.05.002>.
59. Goodwin, K.J., Crook, R.J., 1992. Cement Sheath Stress Failure. *SPE Drill. Eng.* 7, 291–296. <https://doi.org/10.2118/20453-PA>
60. Gray, K. E., Podnos, E., and Eric. 2009 Finite-Element Studies of Near-Wellbore Region During Cementing Operations: Part I.; *SPE Drill & Compl* 24:127–136. <https://doi.org/10.2118/106998-PA>
61. Halvorsen, C. 2016. Plug and Abandonment Technology Evaluation and Field Case Study. Ms Thesis, University of Stavanger

62. Herndon, J., and Smith, D. 1976. Plugging Wells for Abandonment. Union Carbide Corp., Nuclear Division, Office of Waste Isolation, Oak Ridge, TN, (September 1976).
63. IADC 2015. IADC Drilling Manual eBook Version (V.12).
64. IADC. 2000. IADC Drilling Manual eBook Version (V.11).
65. Ichim, A.-C. 2017. Experimental Determination of Oilfield Cement Properties and their Influence on Well Thesis, University of Oklahoma.
66. IOGP. 2017. Overview of International Offshore Decommissioning Regulations Wells Plugging & Abandonment Review Integrity. Second Edition. Vol. 2. Aberdeen. Report 585 International Association of Oil & Gas Producers
67. ISO 16530-1-2017 Petroleum and natural gas industries — Well integrity — Part 1: Life cycle governance
68. ISO. 2013. Well integrity — Part 2: Well integrity for the operational phase (Vol. 2013). ISO.
69. ISO/TS 16530-2:2014 Well integrity - Part 2: Well integrity for the operational phase. First edition 2014-08-15
70. Jackson, P. B. and Murphey, C. E. 1993. Effect of Casing Pressure on Gas Flow Through A Sheath of Set Cement. SPE/IADC Drilling Conference, Amsterdam, Netherlands. 22-25 February 1993. 215–224. <https://doi.org/10.2523/25698-ms>
71. James, S. and Boukhelifa, L. 2008. Zonal Isolation Modeling and Measurements—Past Myths and Today’s Realities. SPEDC 23 (1): 68–75. SPE-101310-PA. <https://doi.org/10.2118/101310-PA>

72. Kermani, B., Martin, J., and Esaklul, K. 2006. Materials Design Strategy: Effects of H<sub>2</sub>S/CO<sub>2</sub> Corrosion on Materials Selection. NACE International. Corrosion, San Diego, California. 12-16 March 2006. (06121), 1–18
73. Khalifeh, M. and Saasen, A. 2020. Introduction to Permanent Plug and Abandonment of Wells. Edited by Manhar R. Dhanak and Nikolas I. Xiros. Gewerbestrasse: company Springer Nature Switzerland
74. Khalifeh, M., and Saasen, A. 2013. OTC 23915 Techniques and Materials for North Sea Plug and Abandonment Operations. OTC. <https://doi.org/10.4043/23915-MS>
75. Khalifeh, M., Gardner, D., and Haddad, M. Y. 2017. Technology trends in cement job evaluation using logging tools. Society of Petroleum Engineers - SPE Abu Dhabi International Petroleum Exhibition and Conference 2017, 2017-Janua. <https://doi.org/10.2118/188274-ms>
76. Khandka, R. 2007. Leakage Behind Casing. Thesis work. NTNU. Norway
77. Kjølner, C., Torsæter, M., Lavrov, A. et al. 2016. Novel Experimental/Numerical Approach to Evaluate the Permeability of Cement-Caprock Systems. International Journal of Greenhouse Gas Control, 45, 86–93. February 2016. <https://doi.org/10.1016/j.ijggc.2015.12.017>
78. Kosinowski, C., Teodoriu, C., 2012. Study of class G cement fatigue using experimental investigations. Soc. Pet. Eng. - SPE/EAGE European Unconventional Resources and Exhibition, 2012 793–803. <https://doi.org/10.2118/153008-ms>.
79. Lavrov, A. and Torsæter, M. 2018. All Microannuli Are Not Created Equal: Role Of Uncertainty And Stochastic Properties In Well Leakage Prediction. International Journal

of Greenhouse Gas Control, 79. 323–328. December 2018.

<https://doi.org/10.1016/j.ijggc.2018.09.001>

80. Lavrov, A., and Torsæter, M. 2016. Physics and Mechanics of Primary Well Cementing (U. Dorrik Stow, Heriot-Watt University, Edinburgh, UK Mark Bentley, AGR TRACS Training Ltd, Aberdeen, UK Jebraeel Gholinezhad, University of Portsmouth, Portsmouth, UK Lateef Akanji, University of Aberdeen, Aberdeen, UK Khalik Mohamad Sabil, Heriot-Watt Univ (Ed.)). Springer International Publishing. <https://doi.org/10.1007/978-3-319-43165-9>
81. Lavrov, A., Panduro, E. A. C., Gawel, K. et al 2018. Electrophoresis-induced structural changes at cement-steel interface. AIMS Materials Science, 5(3), 414–421. <https://doi.org/10.3934/matensci.2018.3.414>
82. Lavrov, A., Todorovic, J. and Torsæter, M. 2016. Impact of Voids on Mechanical Stability of Well Cement. In Energy Procedia. Vol. 86, pp. 401–410. Elsevier Ltd. January 2016. <https://doi.org/10.1016/j.egypro.2016.01.041>
83. Li Juan, Su Donghua, Tang Shizhong, et al. 2021. Deformation and Damage of Cement Sheath in Gas Storage Wells Under Cyclic Loading. Energy Science & Eng. Volume 9 Issue 4 483-501. <https://doi.org/10.1002/ese3.869>
84. Li, Z., Zhang, K., Guo, X. et al. 2016. Study of the Failure Mechanisms of A Cement Sheath Based On An Equivalent Physical Experiment. Journal of Natural Gas Science and Engineering, 31, 331–339. April 2016. <https://doi.org/10.1016/j.jngse.2016.03.037>
85. Li, Zihao, Ripepi, Nino, and Cheng Chen. Comprehensive Laboratory Investigation and Model Fitting of Klinkenberg Effect and Its Role on Apparent Permeability in Various

U.S. Shale Formations. Paper presented at the 53rd U.S. Rock Mechanics/Geomechanics Symposium, New York City, New York, June 2019.

86. Liu, J. and Jia, Y. 2020. Experimental Investigation on Durability of Cement-Steel Pipe for Wellbores Under CO<sub>2</sub> Geological Storage Environment. *Construction and Building Materials*, 236, 117589. 10 March 2020.  
<https://doi.org/10.1016/j.conbuildmat.2019.117589>
87. Liu, K., Gao, D. and Taleghani, A. D. 2018. Analysis on Integrity of Cement Sheath in The Vertical Section of Wells During Hydraulic Fracturing. *Journal of Petroleum Science and Engineering*, 168, 370–379. September 2018.  
<https://doi.org/10.1016/j.petrol.2018.05.016>
88. Liu, S., Li, D., Yuan, J. et al. 2018. Cement Sheath Integrity of Shale Gas Wells: A Case Study from The Sichuan Basin. *Natural Gas Industry B*, 5(1), 22–28. February 2018.  
<https://doi.org/10.1016/j.ngib.2017.11.004>
89. Liu, X., Nair, S. D., Cowan, M. et al. 2015. A Novel Method to Evaluate Cement-Shale Bond Strength. *Proceedings - SPE International Symposium on Oilfield Chemistry*, The Woodlands, Texas, USA, 13-15 April 2015. 1282–1301. <https://doi.org/10.2118/173802-ms>
90. Michaux, M. 2012. Cement Chemistry & additives. In *Cement Chemistry & additives* (Vol. 5, Issue 1, pp. 2–8).
91. N.J. Welch, L.P. Frash, D.H. Harp, J.W. Carey. Shear strength and permeability of the cement-casing interface. *International Journal of Greenhouse Gas Control*, Volume 95, 2020,102977, ISSN 1750-5836. <https://doi.org/10.1016/j.ijggc.2020.102977>.

92. Nagelhout, A. C. G., Bosma, M. G. R., Mul, P. J. et al. 2010. Laboratory and Field Validation of a Sealant System for Critical Plug-And-Abandon Situations. *SPE Drilling and Completion*, 25(3), 314–321. September 2010. <https://doi.org/10.2118/97347-pa>
93. Neslon, E. B., and Dominique, G. 2006. Well Cementing. In J. Smith (Ed.), *Schlumberger (Second Edi, Vol. 53, Issue 2)*. Schlumberger. <https://doi.org/10.1017/CBO9781107415324.004>
94. NORSOK Standard D-010, 2012. Well integrity in drilling and well operation. 224 (rev. 4): 1–224. OP071
95. NORSOK Standard D-010. 2004. Well Integrity in Drilling and Well Operations. (Rev. August 3, 2004) <http://www.standard.no/pagefiles/1315/d-010r3.pdf>
96. NORSOK Standard, 2016. Norwegian Oil and Gas Recommended Guidelines For Well Integrity. Stavanger.
97. NORSOK, Oil Federation Industry 2013. Norsok Standard 1–244.
98. NORSOK. 2004. Well Integrity in Drilling and Well Operations. NORSOK Standard D-010, August, 157.
99. Nygard, R., Gutierrez, M., and K. Hoeg. "Shear Failure And Shear Fracturing In Shales." Paper presented at the 1st Canada - U.S. Rock Mechanics Symposium, Vancouver, Canada, May 2007.
100. Nygaard, R., Lavoie, R.G., 2011. Well Integrity and Workover Candidates for Existing Wells in the Wabamun Area CO2 Sequestration Project (WASP). Society of Petroleum Engineers (SPE). <https://doi.org/10.2118/137007-ms>
101. Oil & Gas UK, 2020. Decommissioning Insight Report 2020. Oil & Gas UK.

102. Oil & Gas UK. 2012. Guidelines on Qualification of Materials For the Suspension and Abandonment Of Wells. 90 (1): 1–90.
103. Opedal, N., Corina A., and Vrålstad T. 2018. Laboratory Test on Cement Plug Integrity. In ASME 2018 37th International Conference on Ocean, Offshore and Arctic Engineering, 1–5. Madrid: ASME. <https://doi.org/10.1115/OMAE2018-78347>
104. Parcevaux, P.A. and Sault, P.H. 1984. Cement Shrinkage and Elasticity: A New Approach to a Good Zonal Isolation. Paper SPE 13176 prepared for presentation at the SPE Annual Technical Conference and Exhibi[1]tion, Houston, 16–19 September. <https://doi.org/10.2118/13176-MS>
105. Parrott, L. J., Geiker, M., Gutteridge, W. A. et al. 1990. Monitoring Portland Cement Hydration: Comparison of Methods. Volume 20, Issue 6 919–926. [https://doi.org/10.1016/0008-8846\(90\)90054-2](https://doi.org/10.1016/0008-8846(90)90054-2)
106. Plee, D., Lebedenko, F., Obrecht, F. et al. 1990. Microstructure, Permeability and Rheology of Bentonite - Cement Slurries. Cement and Concrete Research, 20(1), 45–61. January 1990. [https://doi.org/10.1016/0008-8846\(90\)90115-E](https://doi.org/10.1016/0008-8846(90)90115-E)
107. Raj, M. 2014. Well Integrity - Christmas Tree Acceptable Leakage Rate and Sustained Casing Pressure. In Institution of Chemical Engineers Symposium Series, 1–13. Aberdeen: Atkins Ltd.
108. Randhol, P. C. 2008. CO<sub>2</sub> Injection Well Integrity. 7465, 1–50.
109. Rassenfoss, S., Emerging, J. P. T., and Senior, T. 2014. Permanently Plugging Deepwater Wells Challenges Standard Operating Procedures. December.

110. Rossum G. van, Python tutorial, Technical Report CS-R9526, Centrum voor Wiskunde en Informatica (CWI), Amsterdam, May 1995
111. Ruivo, Fabio & Morooka, Celso. 2001. Decommissioning Offshore Oil and Gas Fields. 10.2118/71748-MS. Rystad Energy
112. Saidin, S., Sonny, I., and Nuruddin, M. F. 2008. A New Approach for Optimizing Cement Design to Eliminate Microannulus in Steam Injection Wells. International Petroleum Technology Conference, IPTC 2008, 3, 1527–1541. <https://doi.org/10.2523/iptc-12407-ms>
113. Sant, G., Lura, P., and Weiss, J. 2006. Measurement of Volume Change in Cementitious Materials at Early Ages Review of Testing Protocols and Interpretation of Results. Transportation Research Record, C (1979), 21–29. <https://doi.org/10.3141/1979-05>
114. Saphir Software/DDA book Manual.  
<https://www.kappaeng.com/documents/flip/dda530/files/assets/basic-html/page-1.html>
115. Sasaki, T., Soga, K., and Abuhaikal, M., 2018. Water Absorption and Shrinkage Behaviour of Early-Age Cement in Wellbore Annulus. J. Pet. Sci. Eng. 169, 205–219. <https://doi.org/10.1016/j.petrol.2018.05.065>
116. Schreppers, G., 2015. A Framework for Wellbore Cement Integrity Analysis. 49th US Rock Mech. / Geomech. Symp. 2015 4, 2469–2477.
117. Seidel, F. A. and Greene, T. G. 1985. Use of Expanding Cement Improves Bonding And Aids In Eliminating Annular Gas Migration In Hobbs Grayburg-San Andres Wells. SPE Annual Technical Conference and Exhibition, Las Vegas, Nevada, 22-26 September 1985. <https://doi.org/10.2523/14434-ms>
118. SIMULIA. Abaqus/CAE User's Manual. <http://www.simulia.com/support/>

119. Smith, G. 2011. “Misconceptions and Misapplication of Production Valve Test Standards.”
120. Stormont, J. C., Fernandez, S. G., Taha, M. R. et al. 2018. Gas Flow Through Cement-Casing Microannuli Under Varying Stress Conditions. *Geomechanics for Energy and the Environment*, 13, 1–13. March 2018. <https://doi.org/10.1016/j.gete.2017.12.001>
121. Sutton, D. L., Sabins, F. L. 1991. Interrelationship Between Critical Cement Properties and Volume Changes During Cement Setting. *SPE Drilling Engineering*. 6(02), 88-94. June 1991. <https://doi.org/10.2118/20451-PA>
122. Takhanov, D. Forchheimer Model for Non-Darcy Flow in Porous Media and Fractures. (2011).
123. Teodoriu, C., Amani M., Yuan Z. et al. 2012. Investigation of the Mechanical Properties of Class G Cement and Their Effect on Well Integrity. *International Journal of Engineering* 3 (2): 1–7.
124. Teodoriu, C., Reinicke, K.M., Fichter, C., et al. 2010. Investigations on Casing-Cement Interaction with Application to Gas and CO<sub>2</sub> Storage Wells, SPE EUROPEC/EAGE Annual Conference and Exhibition, Barcelona, Spain, June 14-17. <https://doi.org/10.2118/131336-MS>
125. The [Statistical Analysis] for this paper was generated using SAS software. Copyright © [2021] SAS Institute Inc. SAS and all other SAS Institute Inc. product or service names are registered trademarks or trademarks of SAS Institute Inc., Cary, NC, USA.
126. Valvtechnologies. 2015. Valve Testings Standards. Houston.

127. Varshney, A., Gohil, S., Chalke, B. A. et al. 2017. Rheology of Hydrating Cement Paste: Crossover Between two Aging Processes. *Cement and Concrete Research*, 95, 226–231. <https://doi.org/10.1016/j.cemconres.2017.02.034>
128. Vijn, P., and B. Fraboulet. 2001. Improved Cement Formulations for Well Abandonment. In *Offshore Mediterranean Conference and Exhibition 2001*, OMC 2001.
129. Waite, M. B., and O'Brien, S. M. 2010. Air leakage: Difficulties in Measurement, Quantification, and Energy Simulation. - *Building Envelope Science and Technology Conference*.
130. Watson, T. L., Bachu, S. et al. U. 2007. Evaluation of the Potential for Gas and CO<sub>2</sub> Leakage Along Wellbores. <https://doi.org/10.2118/106817-PA>
131. Williams, S.M., Carlsen T., Constable, K. et al. Identification and Qualification of Shale Annular Barriers Using Wireline Logs During Plug and Abandonment Operations. Paper presented at the SPE/IADC Drilling Conference and Exhibition, Amsterdam, The Netherlands, March 2009. doi: <https://doi.org/10.2118/119321-MS>
132. Xueyu P., Dale P., Christian M., et al. 2013. A Comparison Study of Portland Cement Hydration Kinetics as Measured by Chemical Shrinkage and Isothermal Calorimetry. *Cement and Concrete Composites*, Volume 39,2013, Pages 23-32, ISSN 0958-9465, <https://doi.org/10.1016/j.cemconcomp.2013.03.007>.
133. Yang, H., Fu, Q., Wu, J. et al. 2020. Experimental Study of Shear and Hydraulic Bonding Strength Between Casing and Cement Under Complex Temperature and Pressure Conditions. *Royal Society Open Science*. 7. 192115. 10.1098/rsos.192115. <https://doi.org/10.1098/rsos.192115>

134. YI, M. 2019. An Experimental Study of the Wellbore Cement Bonding and Shear Stress. Ms Thesis, University of Oklahoma (Vol. 51, Issue 7).
135. Zeng, Y., Liu, R., Li, X. et al. 2019. Cement Sheath Sealing Integrity Evaluation Under Cyclic Loading Using Large-Scale Sealing Evaluation Equipment for Complex Subsurface Settings. *Journal of Petroleum Science and Engineering*, 176, 811–820. May 2019. <https://doi.org/10.1016/j.petrol.2019.02.014>
136. Zhang, M. and Bachu, S., 2011. Review of Integrity of Existing Wells in Relation to CO<sub>2</sub> Geological Storage:What do we know? *Int. J. Greenh. Gas Control* 5, 826–840. <https://doi.org/10.1016/j.ijggc.2010.11.006>
137. H&SE UK Report and Mineral Management System Report, OGUK, 2020. <https://oilandgasuk.co.uk/wp-content/uploads/2020/11/Health-Safety-and-Environment-Report-2020.pdf>
138. 2<sup>nd</sup> Well Bore Integrity Network Meeting, 2006/12, September 2006. Vol. 2<sup>nd</sup>. UK. [https://doi.org/IEA Greenhouse Gas R&D Programme \(IEA GHG\).](https://doi.org/IEA%20Greenhouse%20Gas%20R&D%20Programme%20(IEA%20GHG))
139. 30 CFR § 250, Subpart Q, Pub. L. No. 1700

## **Appendix A: Cement Field Evaluation**

### **A.1 Barrier Evaluation Review**

After being placed, plugs or barriers should hold all fluid and prevent any of them from reaching the surface. In addition to isolating pressure from the wellbore, the barrier should be strong enough to withstand against any conditions to which the well might be exposed. In the field, the conditions in which the cement or the barrier is installed may in response to one or more of many factors even at the early stage.

Any barrier between the casing and formation, such as the cement sheath, can be evaluated by temperature, acoustic, and/or passive noise logging. Also, hydraulic pressure is the test most commonly used on the well barriers (Khalifeh and Saasen 2020).

#### **A. 1.1 Acoustic Logging**

Acoustic logging is the primary verification method used in the industry. It is a sound wave science that can be described as working via waves of various lengths sent through a transmitter across the media through the casing and then reflected from the barrier and the formation back to the receiver. The technology, referred to as the cement bond log/variable density log (CBL/VDL), has been used to evaluate cement since 1950. The log should go through quality control to ensure that it has achieved a high level of reliability. The frequency of the tool is usually between 10 and 60 hertz. However, the sonic tool is a more accurate measurement with a frequency of 10–30 kHz. With this tool, an electrical signal is transmitted to the transducer to produce an omnidirectional acoustic signal.

Shear and compression waves are the two types of waves in the acoustic log. A shear wave type can propagate in solid media, but not in the liquid. On the other hand, compression waves move more rapidly than shear waves and can transfer through all the media. Plate waves transfer in the solid plate, although the transfer takes place slowly in steel. Usually, the acoustic log is run with a casing collar locator (CCL) and gamma rays to identify the formation and the location of the casing coupling.

The results obtained via logging are not consistent, could change with time, and are subject to more than one interpretation. The cement's properties change with time, and hydration could account for 20% of the acoustic log effect.

By 1980, a new tool, Ultrasonic, was introduced with a high-resolution frequency of 200–700 kHz, which is used for the casing–cement bond (Khalifeh et al. al7). The 3-ft receiver transmits information about the wave through the casing but not the formation or the cement, whereas the 5-ft receiver (VDL) transmits information about the cement and the casing (Halvorsen 2016).

### **A.1.2 Spectral Noise Logging (SNL)**

Spectral Noise Logging (SNL) is a logging tool that utilizes passive noise recording to evaluate the cement barrier. The tool is useful whenever there is a small channel or gap that the CBL/VDL does not record, and the flow is laminar in the channel with minimal noise. A large lab experiment has conducted with cement simulated inside 9 5/8 inches × 7 inches and then a different flow rate from nitrogen gas and water injected. The fluid is pumped at 1–1300 ml/min for water and at 1–30 l/min for gas. The results showed a very good response to the fracture reading for a fracture of 0.5 mm or more (Gardner et al. 2019).

### **A.1.3 Annulus Verification Tool (AVT)**

Ensuring accurate results with the logging tool is challenging. The existence of a microannulus might not be accurately shown in the logging. De Andrade et al. 2019 proposed the Annulus Verification Tool (AVT), a new machine concept for cement evaluation that helps to identify and measure the microannulus. A radial mechanical force is applied to the casing wall and the displacement is recorded. The stiffness of the casing and the materials behind are measured through this concept. When the cement is not behind the casing, the stiffness is less than when the casing is surrounded by cement. This tool has a limitation in relation to noise and stiffness, as well as in relation to whether it records casing displacement accurately. A test has been performed on the prototype version on 9 5/8 inches with a microannulus in class G cement at 0.44 W/C (De Andrade et al. 2019).

### **A.1.4 Temperature Logging**

Temperature logging is used to measure cement hydration around the casing. The hydration of the cement is an exothermal reaction, which generates significant heat in the range of 6–12 hr after placement. Further, this logging tool can be used to identify the top of cement (TOC). The challenge with this logging tool, however, is that the temperature should be known during and after hydration (Khalifeh and Saasen 2020).

### **A.1.5 Hydraulic Pressure Testing**

The acoustic log cannot be utilized if two casings have been installed. The test is a combination tool and its working mechanism can be summarized by knowing the base of the plug, and then a plug (mechanical) is installed and the pressure tested. Next, a perforation is opened above the plug and another plug is installed at a distance and pressure-tested. Then, the packer and fluid are pumped as the leakage is monitored, and also the system is checked for any communication between the casings.

## Appendix B: Cement Bond Overview

### B.1 Introduction

Any barrier materials considered for use in long-term abandonment should be non-permeable and have sufficient resistance to withstand the downhole conditions. Usually, when leakage accrues in the barriers, it is from the high-pressure to the low-pressure side. The capillary pressure of the fluid or material is a governing factor that when insufficient make it possible for a leak to take place. And, for rigid material, the grain-size packing is a controlling factor in determining the properties of this kind of material. The design of the barriers should account for degradation due to pressure and temperature variance and chemical attack for the long term.

The capillary pressure is a function of the tension and the radius of the pores:

$$P_c = \frac{2\sigma(\cos\theta)}{r} \dots\dots\dots (B-1)$$

where

$\sigma$  Tension in  $\frac{\text{dynes}}{\text{cm}}$

$\theta$  Angle of Water and the Surface in Degree

r Radius of Pores in Microns

## B.2 Bonding

Bonding strength in relation to adherence to the formation or casing is an important criterion and limitation that should be considered in the selection of barriers. Shear bond and tensile strength are two important factors in evaluating bonding.

Evan and Carter published one of the first studies focused on the shear bond in the oil industry in 1962. The shear bond refers to the parallel force to the adjusted surface (casing) to move it across the seal materials:

$$\text{Shear Bond} = \frac{\text{Force}}{\text{Contact Area}} \dots\dots\dots (\text{B-2})$$

And, the force for the cement between or outside the casing (Eq. B-3):

$$\tau = \frac{\text{Force}}{\pi \cdot d \cdot L_c} \dots\dots\dots (\text{B-3})$$

where

F Failure Load

d Casing Diameter (Outside or Inside)

L Cement Length

Hydraulic bond is a measure of the extent to which cement and other materials to withstand a certain level of pressure under given conditions.

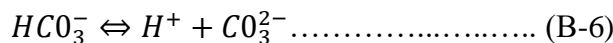
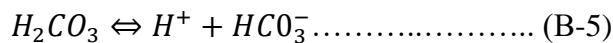
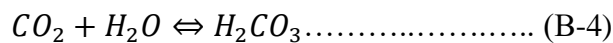
The hydraulic effect of class A cement at 80 °F was investigated by Evan and Carter, who found that for the first and second day of cement age the hydraulic bond of 300–700 psi and the shear bond of 79–422 psi depends on the casing shape (rusted or new).

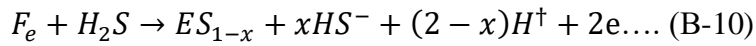
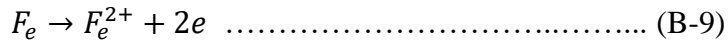
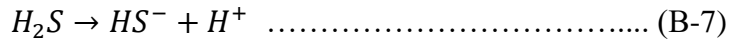
The cement might act differently by the time of hydration and the maturity depending on the temperature conditions. In other experiments, the bond stress was tested at multiple ages of class H cement, and the average for 1 day was 1.94 MPa (280 psi) to 14.48 MPa (2100 psi) in 147 days (Yi M. 2019).

**Table B-1—Shear test average value with curing days (Yi M. 2019).**

Curing days	Shear Stress (MPa)
<b>1day</b>	3.17
<b>3day</b>	7.28
<b>7day</b>	11.82
<b>14day</b>	16.36
<b>147day</b>	28.96

Bond strength is are greatly affected by chemical attacks and high-pressure and -temperature conditions. Sour gas such as H<sub>2</sub>S and CO<sub>2</sub> or any corrosion in the casing will damage the cement–casing contact. CO<sub>2</sub> has been a focus of many research studies in which the sustainability of the CO<sub>2</sub> sequestration project is considered (Zhang and Bachu 2011, Ahmed R et al. 2015, Kermani B et al. 2006). The CO<sub>2</sub> reaction with water creates acidity in the solution, which then corrodes the casing and cement. The reaction of CO<sub>2</sub> and H<sub>2</sub>S can be written as shown in Eqs. (B-4, B-5, B-6, B-7, B-8, B-9, and B-10:





Zhang et al. (2011) experimented with class H cement in the environment with H<sub>2</sub>S and CO<sub>2</sub> and found that more corrosion occurs in the liquid phase than in the gas phase and that debonding is, therefore, affected. Lavrov studied Class G cement for 1 day at 85 °C in a CO<sub>2</sub> environment and found that cement strength decreased to 58 psi (Lavrov et al. 2018).

Cement reacts in a CO<sub>2</sub> environment in the area where it is in contact with the formation. The calcium in the cement reacts with the CO<sub>2</sub> to create calcite, which has the effect of dissolving CO<sub>2</sub> (Deremble et al., 2011; Ahmed et al., 2015).

### **B.3 Cement Failure**

Cement is mainly designed in P&A operations to prevent fluid migration, fluid corrosion, gap and to withstand stress. But as the cement is hydrated and develops its strength, the gas might migrate through the cement body. The poor bonding between the cement and the formation opens a channel through which the gas travels across the cement body (Khandka 2007). The bonding can be categorized as intramolecular bonding, chemical bonding, and mechanical bonding.

The failure of shear between the casing and the cement does not represent a fracture according to Nygard (2007). However, no standard has been published to measure the bond strength or the shear stress between the cement and casing.

Numerous studies have been published with a focus on the cement sheath, especially after the development of the fracture technique and the possibility of cement fracture and the CO<sub>2</sub> project and sequestration. The stress mechanically and hydraulically causes a cement sheath to crack or create a void in the cement.

Casing-to-casing pressure exists in 60% of the production wells in the Gulf of Mexico. In China, several studies have concluded that fracking increases the sustained casing pressure (SCP) from 22.301 to 55.8% (Liu et al. 2018). Unconventional drilling is not an exception to casing annulus pressure (CCA) issues, with 25% of the wells in the Marcellus Shale showing evidence of this issue (2<sup>nd</sup> Well Bore Integrity Workshop, 2006).

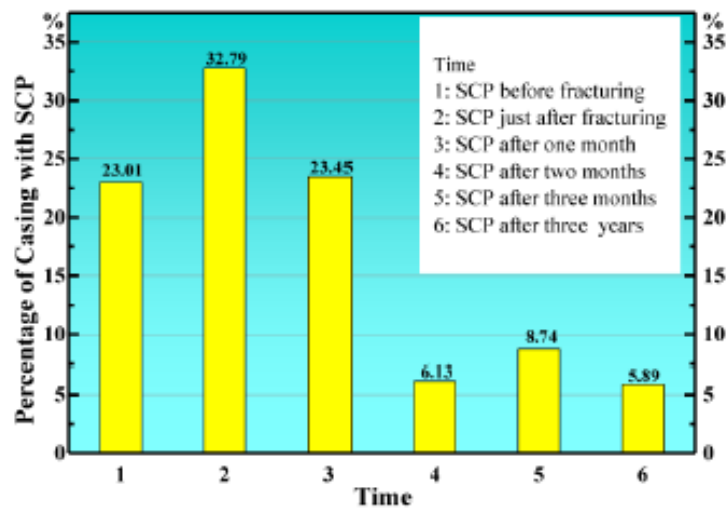


Fig. B-1—Shale gas sustaining casing pressure (SCP) in China (Liu et al. 2018).

Cement is classified as non-Newtonian fluid when the cement hydrate and the calcium hydroxide might increase the porosity, as it stayed in the void especially at the interface with the casing (Neslon and Dominique 2006).

Failure in the cement body can occur because of several strength failures that lead to microannuli or gas in the cement body.

### **B.3.1 Tensile Strength**

Maximum tensile stress is the maximum amount of pressure that a cement body can bear before any cracks in it occur. It refers to the tensile strength of the cement, the pressure it can withstand inside the casing.

### **B.3.2 Mechanical Property Failure**

The stress-strain and elasticity of the cement are measured by the Poisson ratio and Young's modulus.

To reduce the stress-induced in the cement sheath, Young's modulus should be decreased and the Poisson ratio increased. It had been found that cracks travel across the cement-casing contact at a magnitude of 10  $\mu\text{m}$ .

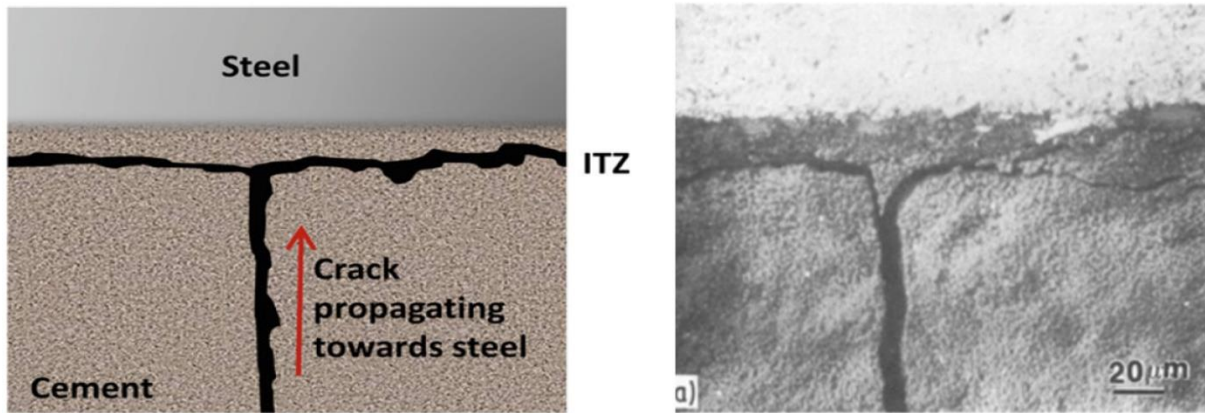


Fig. B-2—Crack propagation toward casing (Bentur et al. 1985).

### B.3.3 Radial and Hoop Stress Failure

The failure around the circumference of the cement radial stress and in the axial direction referred to as “hoop stress shrinkage,” can be categorized as radial stress failure. It is especially likely to occur during the hardening process where the hydrostatic pressure of the cement is lost, which thereby decreases the radial stress and increases the tangential stress (Liu et al. 2015).

### B.3.4 Shrinkage

Shrinkage could be a major mechanism in the formation of cracks in the body of the cement. Any stress that exceeds the tensile strength of the cement will lead to cracks. According to Nelson, shrinkage in the cement body occurs because of changes in porosity (Nelson and Dominique 2006). Saidin et al. (2008) showed that 100–300  $\mu\text{m}$  of the outer microannulus can be attributed to shrinkage. Bentz (2014) and Parrott et al. (1990) related the degree of hydration to chemical shrinkage. Further, Parcevaux et al. showed that shrinkage causes discrete pores, which create the microannulus (Parcevaux and Sault 1984). Cement properties such as compressive strength do not

influence the sheath bond or the hydraulic bond, as these are physical properties of the cement with the pipe.

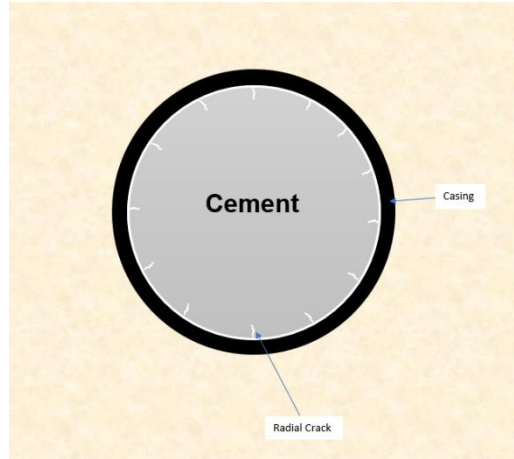


**Fig. B-3—Radial cracking.**

### B.3.5 Shear Failure

When cement is in the liquid phase, hydrostatic pressure is exerted on the surrounding area. However, once the cement is hydrated, shear stress is exerted on the cement, and during shrinkage the shear stress of the cement increases. The relationship between cement hydrostatic pressure and its yield ignoring the effect of pressure and temperature can be expressed as follows:

$$P_{BHP} = P_{BHP,0} - \frac{2\tau_Y L}{R_\omega - R_C} \dots\dots\dots (11)$$

$P_{BHP,0}$  Initial Pressure Downhole at Initial Condition (Cement Pumped)

$P_{BHP}$  Final Pressure Downhole

$\tau_Y$  Cement Yield Stress

L Cement Interval Length

$R_\omega$  Wellbore Radius

$R_C$  Casing Radius

$$S = \frac{P}{\pi D H}$$

S Shear Bond Strength

P Maximum Load (Compressibility)

D Inner Diameter

H Cement Sheath Height

### **B.3.5 Cyclic Pressure and Temperature Variation Failure**

Stress variations and geological movement can cause huge cracks and significant failure in cement due to the expansion and shrinkage of the cement under such conditions. Any pressure increments in the casing or the formation from testing the casing or formation overpressure might increase or decrease hoop stress and decrease tensile stress. During a negative test, casing pressure decreases the radial movement of the cement toward the casing, which has the potential to create a crack.

The temperature change during the well-flowing or mud circulation will expand the casing, which might, therefore, cause the cement to fail in tension.

Different simulations and lab experiments have been performed to study the effects of pressure and temperature on cement. Lavrov and Torsæter simulated a temperature increase of 1 °C with Young's modulus of the cement lower than that of the rock. Cement becomes more compressed when the temperature increases, and with decreasing temperature the tensile stress increases, which may lead to debonding. (Lavrov and Torsæter 2016). The eccentricity was studied also and found to be a cause for the debonding (Lavrov and Torsæter 2016).

The cement shear bond could decrease by 50% if the temperature increases even that the shear bond increase at the early stage (Parcevaux Sault 1984).

### B.3.6 Hydraulic Bond Failure

As described, hydraulic failure refers to the permeability of the microannuli caused by fluid pressure. It has been found that the hydraulic bond is much stronger than the cement shear bond (Khandka 2007).

Hydraulic fracturing creates radial stress on the cement sheath, which causes elastic deformation in the casing. This deformation might eventually reach the plastic deformation after the operation is finished (Chu et al. 2015).

Yang et al. (2020) experimented with class G cement and found that the hydraulic bond does not change with casing roughness whereas the shear bond does change with casing roughness and increases rapidly. Also, the researchers found the hydraulic bond increment with the temperature change to be insignificant in comparison with the shear bond in the same conditions. In addition to that, their experiment showed that hydraulic bonding had a very little effect within 30 days of cement curing time. The cement additive included ed latex, defoamer, retarder, dispersant, and silica fume (Yang et al. 2020).

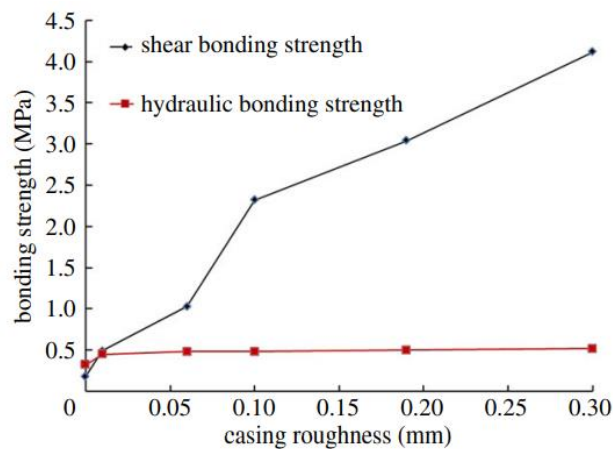


Fig. B-4—Bond strength and roughness of casing effect (Yang et al. 2020).

## **Appendix C: Numerical Modeling of Cement Debonding**

### **C.1 Introduction**

In this appendix, a discussion of numerical modeling for the cement–casing bonding contact is presented as future work to simulate the debonding and the microannulus.

### **C.2 Model Assumption**

Numerical modeling is utilized in this section in support of the experimental results showing the initiation of de-bonded regions between the cement matrix and the pipe metal. The model created for this purpose is largely based on Gray et al.'s (2009) well-regarded study focused on describing the effect of different events on the bonding strength of cement. That study shows that a finite element modeling software program can be used to simulate the debonding process between the cement and the casing occurs under stress conditions. The modeling work in the study relies on several simplifying assumptions, among which the main one relates to the application of cement shrinkage and its contribution to the debonding process. The assumption is based on published data according to which conventional oil and gas well cement shows volume shrinkage from 0.5 to 7% (Parcevaux and Sault 1984; Chenevert and Shrestha 1991; API TR 10TR2 1997; Becke et al. 1997; Baumgarte et al. 1999). The role of shrinkage in these studies is manifested by creating additional stress on both the formation rock and the casing metal rather than by directly creating gaps. The additional stress caused by cement shrinkage is assumed to induce plastic strain within the cement body. When this is induced, the strain is high enough, eventually leading to initiating channels and gaps in the interface area. Within this methodology, the cement matrix shrinkage is accounted for although it is not the direct cause of debonding. It should also be mentioned that the

shrinkage process itself is not modeled. Instead, volume shrinkage is simply introduced as a step in the model. Gray et al. used a 5% volume shrinkage assumption and estimated that the width of the debonding zone due to the combined effect of all relevant processes can be as large as  $1.5 \times 10^{-6}$  meters (Fig. C-1). This falls within the range of micro-channels observed in the experimental work discussed in this study.

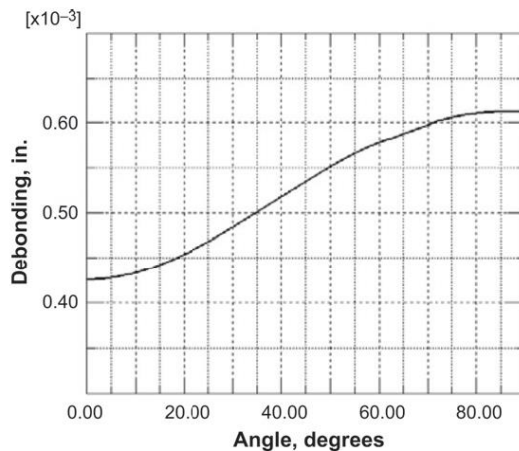


**Fig. C-1—Size of debonding region between cement and casing along the circumferential angle of the wellbore after subjecting the model to effects of cement hardening, cement shrinkage, stimulation, and production (Gray et al. 2009).**

### C.3 Model Construction

To create a similar model to simulate the debonding process in lab experiments, the Abaqus finite-element package (SIMULIA) student version was used. This model uses SI units, which means that the distance is measured in meters, pressure in Pascal (Pa), and density in  $\text{kg/m}^3$ . As the model requires several mechanical properties of the used cement, which are not available through this work, the cement mechanical properties as described in other published studies are used (Table C-1) (Bosma et al. 1999; James and Boukhelifa 2008).

**Table C-1—List of mechanical properties used for modeling cement behavior (Bosma et al. 1999; James and Boukhelifa 2008).**

Property	Unit	Model	Value
Density (measured)	kg/m <sup>3</sup>	Linear Elasticity	1941
Young's Modulus	Pa	Linear Elasticity	$7.5 \times 10^9$
Poisson's Ratio	Fraction	Linear Elasticity	0.09
Cohesion	Pa	Mohr-Coulomb Plasticity	$2.16 \times 10^7$
Friction Angle	Degrees	Mohr-Coulomb Plasticity	17.1

The lab experimental setup is replicated in the modeling environment by creating a mesh of each component within the experiment, including the cement matrix and the pipe body (Fig. C-2). The 6-inch specimen experiment is used as the basis for this model, and the two components are assembled to produce a single structure (Fig. C-2). Boundary conditions are another consideration in the model setup. In general, the role of boundary conditions is to reflect non-allowed movements and failures within certain components of the model and certain directions. The definition of these conditions serves to reduce several unknown variables, which the finite-element solver will determine. To satisfy this requirement, three boundary conditions are applied to the model:

1. The pipe body does not rotate and is not displaced in any direction.
2. Deformation is not allowed along the z-axis at pipe cross-section, which is the axis along with the pipe opening.
3. Deformation is not allowed along the z-axis at the cement face, which is the axis along with the pipe opening.

The element for the model is continuum 3D 4 nodes and 8 nodes. The pressure applied to the cement face is added at a value of  $3.45 \times 10^5$  Pa, which equates to the 50 psi applied during the

actual experiment. These boundary conditions and loading are shown in Fig. C-2. The boundary conditions applied are boundary 1, which does not allow the outer surface of the pipe to move or rotate in any direction as signified by the orange markers; boundary condition 2, which does not allow the outer surface of the cement to move in the z-direction, but does allow it to move in the x- and y-directions; and boundary condition 3, which does not allow the outer surface of the cement to move in the z-direction, but does allow it to move in the x- and y-directions. The pressure load on the cement face is represented by the pink arrow in Fig. C-3.

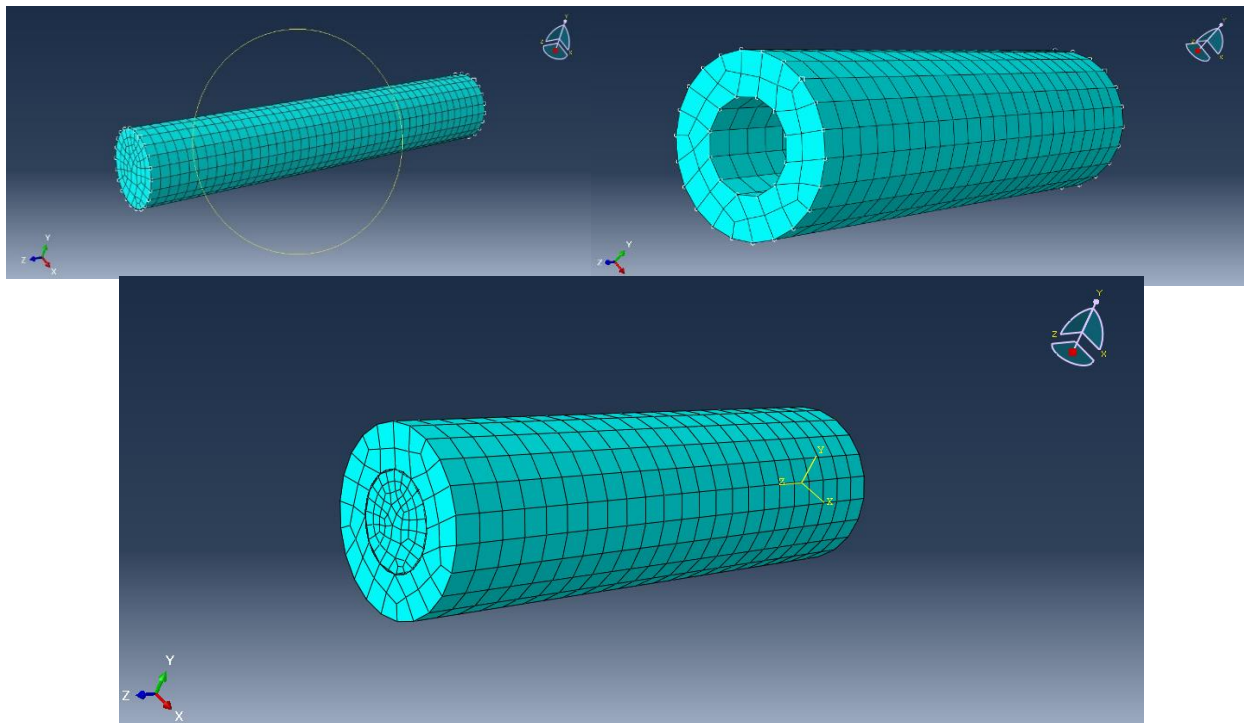


**Fig. C-2—Top left: mesh of the cement matrix geometry; top right: mesh of the 6-inch-length pipe; bottom: assembled structure of cement within the 6-inch-length pipe.**

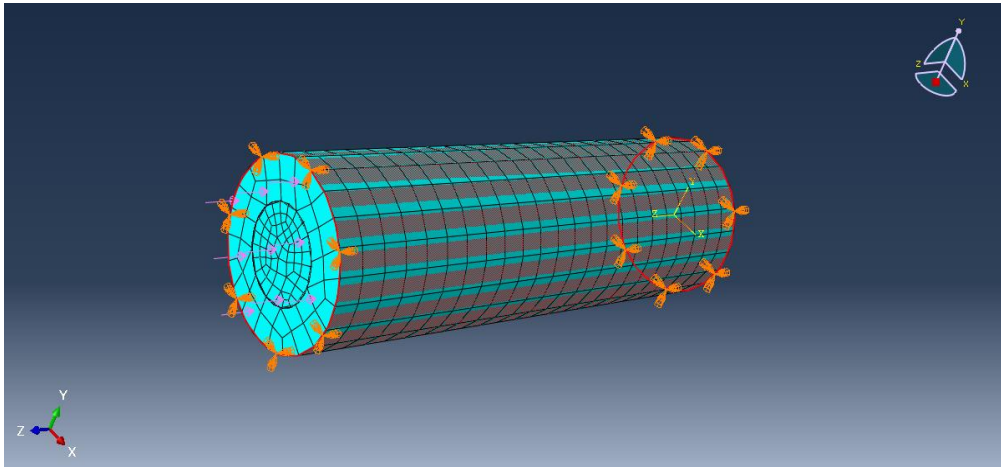


**Fig. C-3—Illustration of boundary conditions and loading.**

In order to model the bonding area between the pipe and cement, a contact condition is defined. This condition follows the procedure outlined by Gray et al. (2009). The contact condition defines the area between the cement and pipe as a cohesive contact area that does not allow for the intersection of the two materials. However, under sufficient loading, the contact condition can allow for separation between the two parts. Modeling this separation is the main tool for replicating the initiation of micro-channels.

As stated previously, the shrinkage process itself was not modeled by Gray et al. (2009), but is simply introduced as a step in the model. In the model constructed for this work, no shrinkage is introduced as the purpose is to assess the standalone action of the pressure loading on the process through which micro-channels develop.

## C.4 Model Results

The deformation resulting from the loading process is initially observed as displacements at the cement–pipe steel interface. These displacements are the main output from the mechanical finite-element analysis. The value for the displacements is then used to determine the strain, which is consequently used to evaluate stresses based on the corresponding constitutive stress-strain model and the elastic-plastic properties listed in Table C-1. Node displacements in the 6-inch pipe model are shown in Fig. C-4, where U1 is the displacement in the x-axis direction and U2 is the displacement in the y-axis direction. The sign for these values shows the direction of the node displacement along its corresponding axis. There is no U3 value, as it is constrained by the boundary conditions at zero.

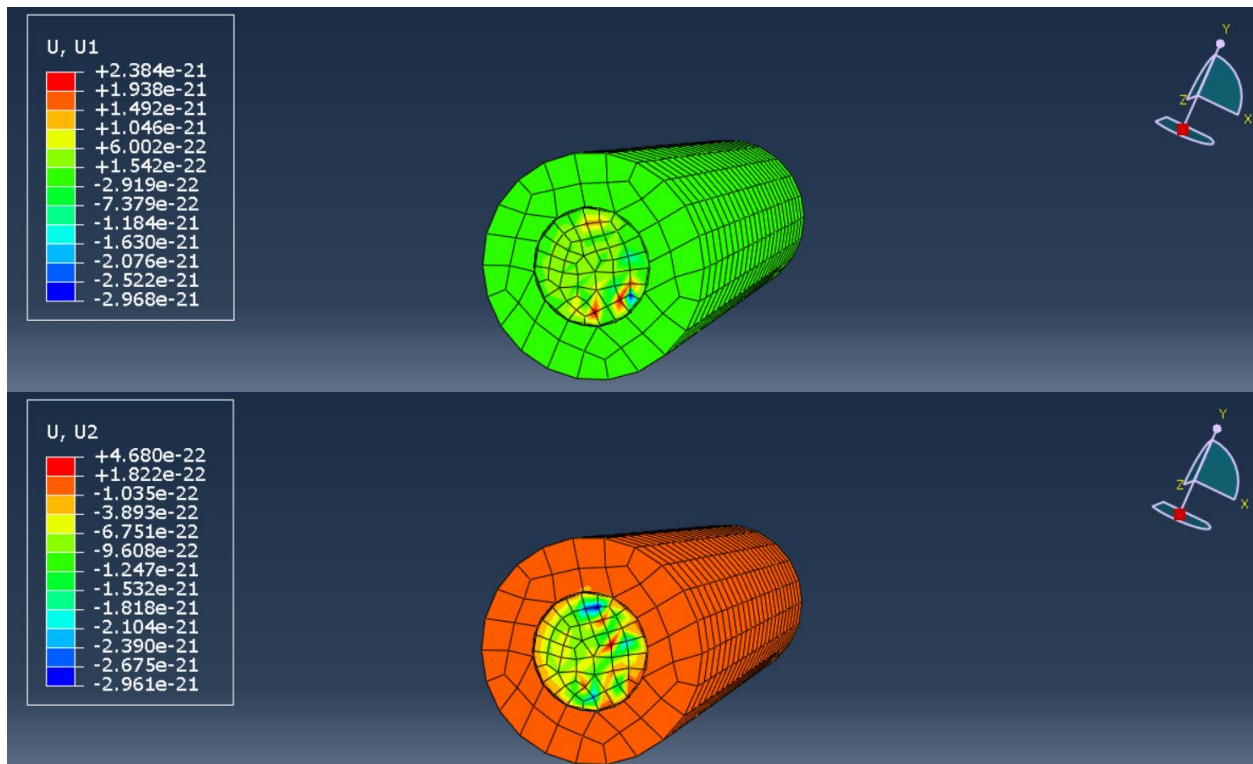


**Fig. C-4—Node displacements in the 6-inch-length pipe model; top: displacement in the x-axis direction; bottom: displacement in the y-axis direction.**

To show the output in terms of debonding, the contact-opening variable is used (Fig. C-5). This variable indicates the clearance between two surfaces due to the failure of the bonding between them under the action of the specified load. The areas with positive values, highlighted by the green-, yellow-, and red-color gradients, are allowed in order to initiate a gap at the interface. It should also be noted that these values are in meters. The maximum gap width is predicted as  $5.6 \times 10^{-17}$  m, which is quite different from the actual gap area observed by Gray et al. (2009). The results of the model indicate the extent to which the applied load initiates gaps at the interface region and also show the limitations of the simplified modeling approach followed here. The model described in this section is purely mechanical, as it does not consider the influence of a multitude of potentially relevant phenomena. These considerations were not included in the model because of the lack of lab-determined properties, which are essential to determining the effects of these phenomena. Here is a list of some of the relevant considerations that were not included due to lack of data and/or a lack of available modeling capabilities:

- Cohesive porous medium response to loading
- Actual linear elastic and plastic properties of the cement
- The efficiency of cement placement and displacement within the pipe opening (gaps and bubbles created while placing the cement can propagate further debonding when subjected to loading)

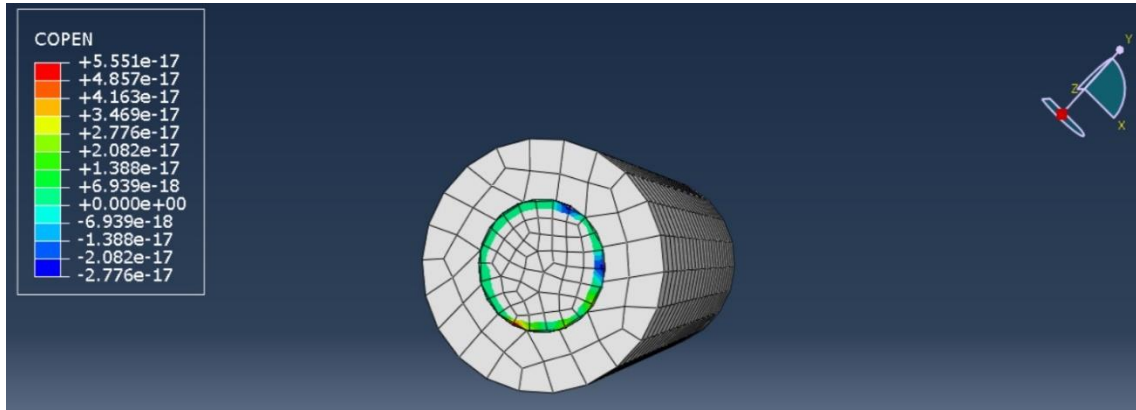


**Fig. C-5—Illustration of the contact-opening variable at the cohesive cement and pipe interface.**